Prediction of the characteristics of a tsunami wave near the Tohoku coastline

Jochem J. Roubos[a]*, Toni Glasbergen[a], Bas Hofland[a], Jeremy D. Bricker[a], Marcel Zijlema[a], Miguel Esteban[b] and Marion F. S. Tissier[a]

[a]*Dept. of Hydraulic Engineering, Faculty of Civil Engineering and Geosciences, Delft University of Technology, Delft, The Netherlands, jochemroubos@gmail.com;*

[b]*Dept. of Civil and Environmental Engineering, Waseda University, Tokyo, Japan.*

To calculate tsunami forces on coastal structures, the wave type in front of the coast is of great importance. Hence this paper aims to find ways to predict the type of tsunami wave breaking. Based on literature review, video footage, analytical reasoning and numerical modelling (SWASH) it can be concluded that both the continental shelf slope (α_2) and the bay geometry (β) have a significant influence on the transformation of a tsunami wave near the coastline. After conducting 1D and 2DH wave simulations, a distinction is made in three types of tsunami waves; a non-breaking front (surging), a breaking front (plunging) and an undular bore breaking front (spilling). Tsunami waves transform into these three wave types for a steep continental shelf, an intermediate sloped continental shelf, and a gentle sloped continental shelf respectively. A new tsunami breaker parameter ($\xi_{tsunami}$) is proposed to predict the type of wave at the coastline in a quantitative way.

Keywords: tsunami; breaker parameter; undular bore; wavefront breaking; surging; classification; continental shelf; bay geometry

1. Introduction

1.1 Problem description

On the 11th of March 2011, a magnitude-9 undersea earthquake occurred in the north-western Pacific Ocean near the Tohoku region of Japan. The epicenter of the earthquake was around 70 kilometers east of the coast of Tohoku and the depth of the hypocenter was approximately 32 km. The earthquake triggered a tsunami which was one of the most destructive tsunamis in known history, causing 15,853 casualties, 3,282 people missing, 6,023 injured, and over 220 billion dollars of damage along the coastline (Wei et al. 2012).

A large variation in inundation and run-up heights was observed along the east coast of Japan during this tsunami event. The tsunami behavior showed a clear regional dependence on the bathymetry and topography along the coastline. This research focusses on the Tohoku coastline, which mainly consists of the Sendai Plain and the Sanriku coastline, Figure 1. The Sanriku coast is attacked several times throughout history, where the 1896 Meji Sanriku tsunami is the last comparable event before 2011. Where the Sendai Plain features a fluvial lowland and a flat coastal plain, the Sanriku coast is known as a ‘ria-coast’, a coastal inlet formed by a river valley which is characterized by an indented coastline that consists of numerous small bays of variable geometry. During a tsunami event like 2011, the waves were amplified in the narrow bays and resulted in destructive flows into coastal towns situated along the inner coasts

(Shimonzono et al. 2012).

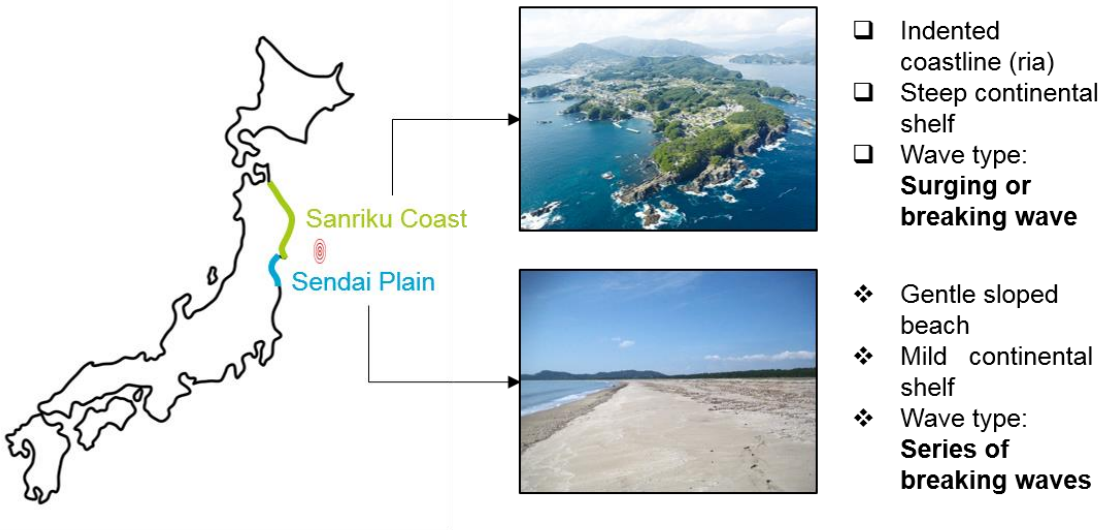

Figure 1: Characteristics of the Tohoku coastline. The red symbol indicates the location of the epicentre of the 2011 Tohoku Earthquake. Top: (ENV, sd). Bottom: (Rita, 2008).

Even with the constructed seawalls and sea dykes up to 10 m or more, the 2011 tsunami led to many deaths and a lot of damage. New implemented design rules by the Japanese government led to the construction of higher seawalls and sea dykes (Figure 2). There are still a lot off uncertainties in wave types and wave loads along the coastline during a tsunami event, which makes the impact on the coastal structure unpredictable. The breaking of tsunami waves, as they approach the shore, depends on the local bathymetry and the type of coastline. Figure 3 provides several snapshots of video footage made along the Tohoku coastline during the tsunami in 2011. The wavefront can be broken (breaking wavefront or series of bores) or non-broken (surging/rising water level). Since the Sendai Plain has a gentle sloped continental shelf, a series of tsunami bores can develop in front of the coastline (Figure 3c). Along the Sanriku coastline, where the slope of the continental shelf is much steeper, different tsunami wave types were observed. Figure 3a shows a broken wavefront that has been observed in the Kuji Bay, and Figure 3b shows a non-broken surging wave that propagates into the Miyako Bay.

Figure 2: Left: Otsuchi Town (Sanriku coast), the yellow line indicates the location of the planned sea dyke. Right: Sea dyke under construction, height is 14.5 m. Photos: (Roubos 2018)

The velocities near the coast differ for breaking tsunami waves compared to non-breaking tsunami waves. The velocity near the coastline is an important factor to obtain the dimensionless Froude number (Fr) or the maximum momentum flux $(hu^2)_{max}$ near the coastal structure. Several design standards that deal with tsunami loads on coastal structures have been proposed by the American Society of Civil Engineers (ASCE 2017) and the Federal Emergency Management Agency (FEMA 2012). FEMA (2012) classifies the coastal inundation along the Tohoku coastline, given by Figure 4. This classification shows that tsunami waves will approach the shoreline in a different way, but it is not quantitative. Therefore, a more quantitative understanding of tsunami wave transformation is needed to predict the attack on coastal defence systems along the Tohoku coastline.

Figure 3: Real-life observation from different tsunami wave types at several location along the Thoku coastline during the 2011 Tohoku Earthquake Tsunami. Left to right: Kuji Bay (Topics 2016), Miyako Bay (Topics 2017), Sendai coast (Topics 2018).

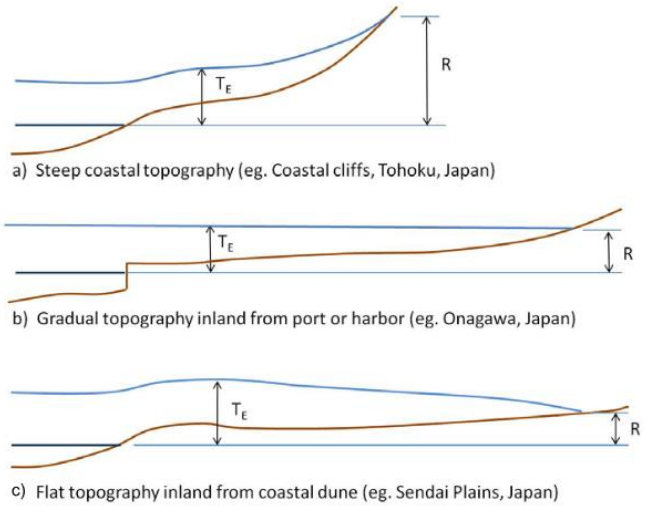

Figure 4: Classification of coastal inundation, where TE is the tsunami elevation and R the run-up elevation (FEMA 2012).

1.2 Literature review

Tsunami wave frequency dispersion is represented by the depth-to-wavelength ratio, $\mu^2 = d/L$, and the nonlinearity by the amplitude-to-depth ratio, $\varepsilon = A/d$ (Liu 2009). Tsunami waves in the open ocean are mostly non-dispersive long waves because the wavelength is much larger than the water depth. When they propagate to the nearshore area, dispersive effects can become significant (Dalrymple et al. 2015). Madsen et al. (2008) investigated the phenomenon of the disintegration of long waves into shorter waves, typically of the order 10-15 s, which is called undular bore formation. The further transition of these undular bores into completely separated solitons, a self-reinforcing wave that maintains its shape while propagating at a constant velocity, rarely happens due to geophysical constraints (Madsen et al. 2008). During tsunami events (Thailand 2004, Japan 2011), observed tsunami waves were sometimes described as a series of breaking waves in front of the coastline. However, it is most likely that these are short breaking waves riding on top of the main wave (undular bore). In the nearshore area, the front of a tsunami wave can evolve into a large range of bore types, from an undular non-breaking bore to purely breaking bore (Tissier et al. 2011).

The existence of bore formation at the front of a tsunami wave is of influence for the wave speed and thus for the impulsive impact on the seawall. ASCE (2016) assumes that the Froude number at the coastline is 1.0 for situations without bore formation and 1.3 for situations with bore formation, which results in a bigger impact on the structure for tsunamis with bore formation since the velocity is calibrated to the Froude number.

The most important wave forces on a seawall or dyke are the hydrostatic F_h, the hydrodynamic forces F_d and impulsive forces F_s according to FEMA (2012). Impulsive forces are important for the design of a seawall or sea dyke since the force during initial impact can be approximately 50% higher than the resistance force during the bore passing, according to the experiments of Árnason (2015).

$$F_d = \frac{1}{2}\rho_s C_d B (hu^2)_{max} \tag{1}$$

$$F_s = 1.5 F_d \tag{2}$$

The Iribarren number ξ from (Battjes 1974), equation 3, gives an expression for the relation between non-breaking and breaking progressive waves on a slope. This parameter expresses the type of breaking - a spilling wave, a plunging wave or a surging wave - which will occur for certain wave characteristics and a given slope of the bathymetry. ASCE (2016) proposed a surf similarity parameter to calculate the run-up. However, this surf similarity parameter is not valid in case wave focusing is expected, such as in V-shaped bays along the Sanriku coast. Therefore, an improved parameter is needed to predict wave types in wave focussing bays.

$$\xi = \frac{\tan(\alpha)}{\sqrt{H/L_o}} \tag{3}$$

Tsunami transformation in a bay along the Sanriku coast can be compared with the investigations of Bonneton et al. (2015) regarding the formation and dynamics of tidal bores in funnel-shaped estuaries. They showed that tidal bore formation is mainly

113 governed by a dissipative parameter $\mathcal{D}$, which characterizes the amount of nonlinearity.
114 $\mathcal{D}$ depends on bottom friction, wave characteristics and estuary geometry. The
115 dissipation parameter is enhanced by the increase of the tidal range, friction coefficient,
116 converging length and bathymetry slope. When $\mathcal{D}$ is large, the dissipative character of
117 the estuaries is large, and the conditions are favorable for bore formation.
118 Shimonzono et al. (2012) studied the tsunami wave behavior of the 2011
119 tsunami event along the central Sanriku coast. Observed was that the tsunami wave
120 types were different along the coastline. The waves exhibit breaking progressive wave
121 crests over gentle slopes while they have features of standing waves over steep slopes.

122 ***1.3 Objectives and Outline***

123 More insight is needed in the characteristics and the transformation of a tsunami wave
124 approaching a ria coast to increase the safety of flood defense systems in the future. The
125 difference in wave types along the Tohoku coastline will be investigated, where the
126 steep ria coast of Sanriku is compared to the gentle sloped Sendai Plain (Figure 1). The
127 main focus in this research is wave breaking since the impact on the coastal structure
128 differs for a broken or a non-broken tsunami wave. The main question to be answered is
129 how the characteristics of a tsunami wave can be predicted along the Tohoku coastline.
130 The paper is split up in four chapters; Introduction, Nearshore tsunami
131 transformation, Discussion and Conclusions. Chapter 2 is the main chapter, where a
132 new tsunami breaker parameter $\xi_{tsunami}$ is proposed based on depth-averaged SWASH
133 simulations. In Chapter 3, the Green's Law approximation of tsunami wave
134 transformation before breaking is discussed.

135 **2. Nearshore tsunami transformation**

136 The goal of this chapter is to give more insight into the differences of tsunami wave

behaviour for the different characteristics of the Tohoku coastline. The main focus is the tsunami wave transformation near a ria, a bay in the indented coastline. The results will be compared with the simulations of tsunami wave transformation over a gently sloping beach without bays (straight coastline) near the Sendai Plain.

Table 1 gives an overview of the geometries of the bays along the Sanriku coastline and the bathymetry along the Sendai Plain, obtained by Navionics (2018) and survey results of Shimonzono et al. (2012). The bathymetry parameters (α_2, W_b and W_h) are explained in Figure 8.

Table 1: Classification of the Tohoku coastline (Navionics 2018; Shimonzono et al. 2012).

Area	**Nr.**	**Location**	**Coast type**	**Observed wave type**	**Continental shelf slope (α_2)**	**Bay depth (d_b) [m]**	**Bay mouth width (W_b) [km]**	**Bay head width (W_h) [km]**
North Sanriku	1	Kuji Bay	Ria coast	Breaking	1/160	40-60	5.5	2.5
	2	Noda Bay	Ria coast	Breaking	1/150	40-60	9.6	4.5
	3	Miyako Bay	Ria coast	Surging	1/145	60	3.5	1.4
Central Sanriku	4	Yamada Bay	Ria coast	Surging	1/90	80	3.0	3.0
	5	Otsuchi Bay	Ria coast	Surging	1/110	60	3	2.5
	6	Toni Bay	Ria coast	Surging	1/66	80	3.3	1.8
	7	Yoshima Bay	Ria coast	Surging	1/75	80	7.3	1.2
	8	Ryori Bay	Ria coast	Surging	1/88	60	3	1

South Sanriku	9	Hirota Bay	Ria coast	Surging	1/140	60	5.7	2.6
	10	Oppa Bay	Ria coast	Surging	1/104	60	6.5	6.5
	11	Onagawa Bay	Ria coast	Surging	1/120	60	5.0	5.0
Sendai Plain	12	Yuriage	Gentle sloped beach	Series of bores	1/590	-	-	-

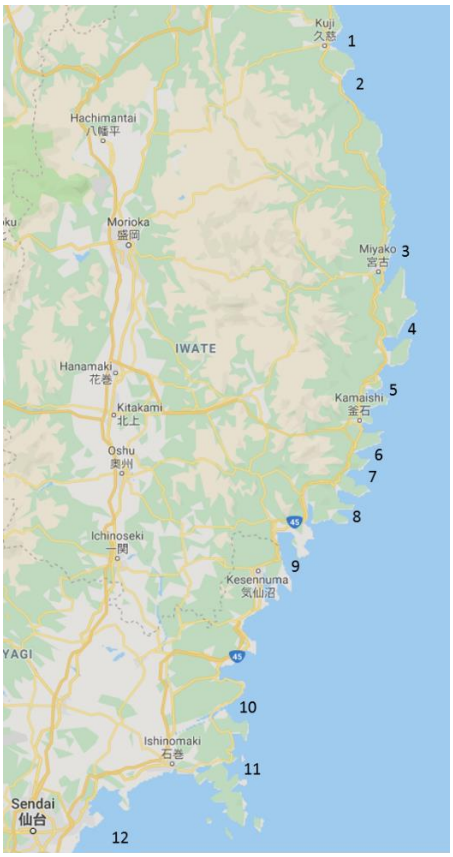

Figure 5: Sanriku + Sendai coast with numbered locations (Google 2019).

2.1 Methodology

As described by ASCE (2016), it is important to know if the front of a tsunami wave breaks, due to the difference in impact on a coastal structures and other infrastructure. To improve the classification in tsunami waves approaching the shore, a new tsunami

153 breaker parameter $\xi_{tsunami,}$ based on the Iribarren number ξ, is considered (equation 4).
154 Parameters describing the bay geometry will be included to predict the breaker type of
155 the tsunami wave.

$$\xi_{tsunami} = \frac{\tan(\alpha_s)}{\sqrt{\frac{H_\xi}{L_\xi}}}\beta \quad (4)$$

156 where αs is the slope of the continental shelf, Hξ and Lξ are the wave height and the
157 wavefront length at a depth of 100 m (see figure 6), and β is a new proposed bay
158 geometry factor. In case the coast can be schematized as a 1D model, β will be equal to
159 1. For cases where 2D effects become important β will describe the shape of the bay.
160 To obtain $\xi_{tsunami}$, simulations have been performed with the numerical program
161 SWASH (Simulating WAves till SHore). To simulate large-scale wave evolution and
162 shallow water flows efficiently, an approach is adopted where the free-surface motion is
163 tracked using a single-valued function of the horizontal plane. This makes SWASH a
164 more suitable program than Volume-of-Fluid (VOF) and Smoothed Particle
165 Hydrodynamics (SPH), which can describe fluids in a more detailed but more time-
166 consuming way. SWASH is a phase-resolving non-hydrostatic model which is based on
167 vertically integrated, time-independent mass and momentum balance equations. The
168 governing equations are the NLSW (NonLinear Shallow water) equations, including the
169 non-hydrostatic pressure (Zijlema, Stelling, and Smit 2011).
170 SWASH simulations are used to investigate the influence of the initial wave
171 characteristics and the bathymetry characteristics on the transformation of a tsunami
172 wave. The wave characteristics are the wave height *H*, wavelength *L* and the wave
173 steepness *H*/*L*. Glasbergen (2017) conducted several simulations to investigate the
174 important parameters for wavefront breaking. He concluded that only the front part L_{front}
175 of the wave is of interest for breaking. Therefore, the tsunami wavefront can be

described by the tsunami wave height H_ξ and the tsunami wavefront length L_ξ, both at a depth of 100 m. When the wave is approximately symmetric, L_ξ is equal to half the wavelength.

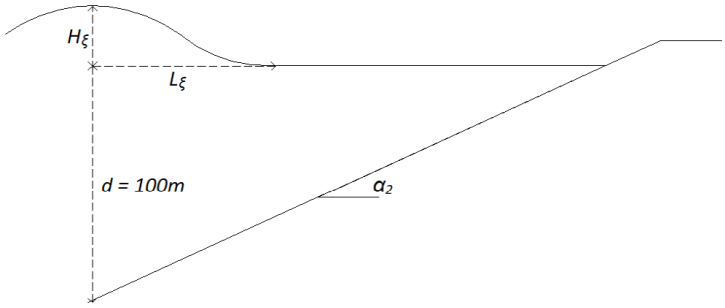

Figure 6: Characteristics to describe a tsunami wave (Glasbergen 2017).

In this research, a depth-integrated 1D and 2DH ('H' for horizontal plane) model is used to find the influence of the continental shelf slope and the bay geometry respectively. For all simulations, a timeseries of a sinusoidal wave is used as a boundary condition, where the wave is situated above sea mean level (equation 5).

$$\eta_{B.C.} = H_\xi * \sin\left(\frac{\omega t}{2}\right)^2 \quad (5)$$

where ω is the angular frequency given by $\omega = 2\pi/T$, H_ξ is the wave height which varies between 4, 6 and 8 meters and T is the wave period which varies between 600 and 1200 seconds. H_ξ and T are based on wave buoy observations along the Tohoku coastline during the 2011 Tohoku Earthquake Tsunami (Shimonzono et al. 2012).

The parameters of the bathymetry are drawn in Figure 8. The most important bathymetry parameter for the 1D simulations is the slope of the continental shelf (α_2), which is assumed to be equal to the slope of the bay (α_3) and the inland topography (α_4). The continental slope varies along the Tohoku coastline from 1/50 to 1/500.

Another important parameter is bay geometry, which is included in the 2DH simulations. These 2DH simulations are conducted for a continental slope in the rage of 1/50 to 1/100 since that is the averaged slope along the Sanriku coastline. The depth at

the bay mouth (d_b) stays constant at a depth of 100 m during the simulations. It is assumed that the narrowing of the bay, given by W_b/W_h, is a leading parameter in the transformation of a tsunami wave and is expressed by a single bay geometry factor β. The parameters of the schematic bay can be changed one by one to see the influence on the characteristics of the tsunami wave. Based on the given bathymetry and geometry in Table 1, and the wave buoy observations (Shimonzono et al. 2012), the parameters in Table 2 are used to simulate different tsunami waves along the Tohoku coastline.

*Table 2: Parameters used for the SWASH simulations in this research. *The slopes are based on the range of continental shelf slopes along the Sendai Plain (1D) and the Sanriku coast (2DH).*

Parameter	**1D model**	**2DH model**
Wave height H_ξ [m]	4,6 and 8	4,6 and 8
Wavelength L_ξ [s]	300 and 600	300 and 600
*Continental shelf slope α_s [-]	1/50, 1/75, 1/100, 1/150, 1/200, 1/300 and 1/500	1/50, 1/75 and 1/100
Bay mouth width W_b [m]	-	2000, 3000, 4000, 5000 and 6000
Bay head width W_h [m]	-	500, 1000, 1500, 2000, 2500 and 3000

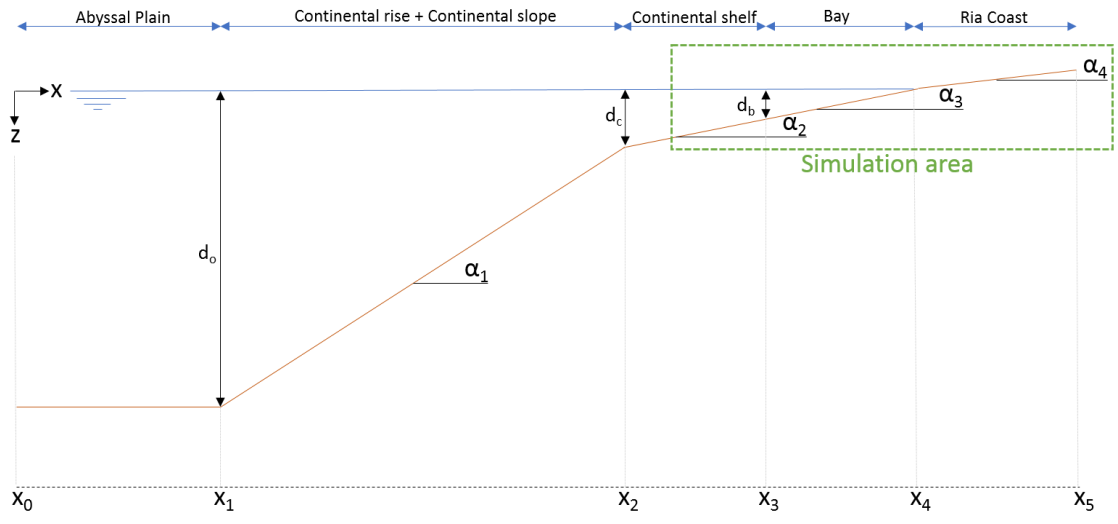

Figure 7: Schematization of the ocean bathymetry, where d_o, d_c and d_b are the depth offshore, at the edge of the continental shelf and at the bay mouth. α_1, α_2, α_3 and α_4 are the slopes of the continental rise, continental shelf, bay and inland topography.

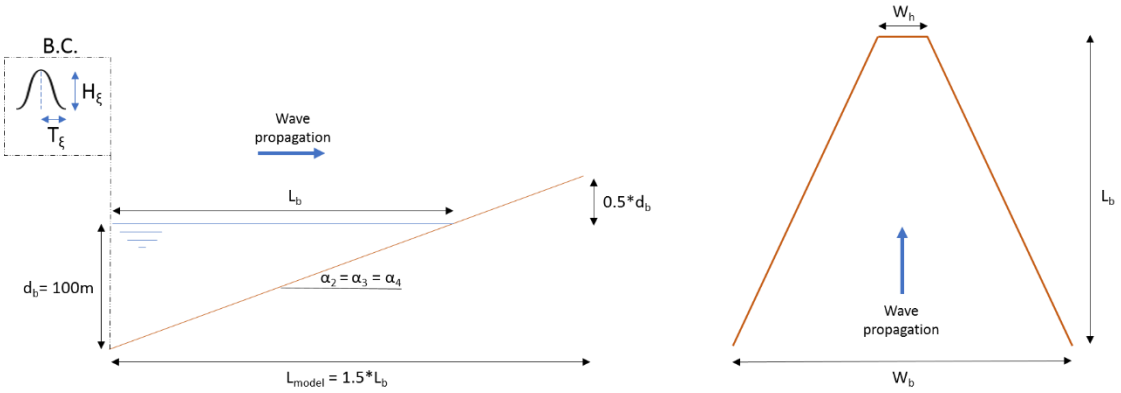

Figure 8: Simulation area: The schematization of a bay along the Sanriku coast, where d_b is the depth at the bay mouth, L_b the length of the bay, W_b the width of the bay mouth, W_h the width of the bay head and α_3 the slope of the bay.

To analyze different kind of tsunami types at the coastline, a local Froude number Fr_{coast} is used, given by equation 6, where $u_{max,coast}$ is the maximum velocity at the coastline during inundation and h_{coast} is the water level at this moment of maximum velocity at the coastline. Another important value is the maximum momentum flux $(hu^2)_{max}$ at the coastline during inundation, since this is an important parameter for the hydrodynamic and impulsive forces on the coastal structure (FEMA 2012).

$$Fr_{coast} = \frac{u_{max,coast}}{\sqrt{g h_{coast}}} \tag{6}$$

2.2 Validation

An important process during this research is breaking. However, SWASH is a non-hydrostatic model which cannot be directly applied to details of breaking waves, since essential processes such as overturning, air-entrainment and wave generated turbulence, are absent. But, if only the macro scale is important, the conservation of mass and momentum can be used to treat discontinuities in flow variables (free surface, velocities) in a proper way, to determine energy dissipation of waves (Smit, Zijlema, and Stelling 2013). SWASH uses a hydrostatic front approximation which is an effective and efficient method to approximate wave-breaking phenomenon's in the non-hydrostatic phase resolving model. The hydrostatic pressure is assumed at the front of

the wave when it exceeds a certain threshold of the steepness of the wave, equation 7. The range of maximum steepness (α_s) varies in literature, from 0.3 (Schäffer, Madsen, and Deigaard 1993) to 0.6 (Lynett 2006). The threshold used in SWASH is based on simulations of flume experiments, an α_s of 0.6 is advised, which correspond to a local front slope of 25° (Smit et al. 2013). There is no need to calibrate this value since it seems to work well for all test cases carried out to validate the model (INCLUDE REFERENCES). The energy dissipation due to breaking is accounted for by ensuring that mass and momentum are conserved once the wavefront is transferred into a bore-like shape.

$$\frac{\partial \zeta}{\partial t} = \alpha_s \sqrt{gd} \tag{7}$$

An extra validation is carried out by comparing wave breaking in SWASH to the results of Grilli et al. (1997), where the breaking criterion of solitary waves is investigated. By using an experimentally validated fully nonlinear wave model, Grilli et al. (1997) performed tests where shoaling and breaking of solitary waves were computed on slopes of 1/100 to 1/8 and wave heights of 0.2, 0.4 and 0.6 m at a water depth of 1m, see Figure 9.

Nine SWASH simulations were conducted with varying continental shelf slopes, varying wave heights, a time step of 0.01 s and a grid size of 0.1 m. Table 3 shows the results of the SWASH model versus the results of Grilli et al. (1997), where the breaking height (H_b), the breaking depth (h_b) and the breaking location (x_b) are given.

Table 3: Breaker height (H_b), breaker depth (h_b) and breaker location (x_b) for the test by Grilli et al. (1997) and the SWASH simulations.

		Tests (Grilli et al. 1997)			**SWASH**			**Difference**
Slope	*H_0 [m]*	*H_b [m]*	*h_b [m]*	*x_b [m]*	*H_b [m]*	*h_b [m]*	*x_b [m]*	*x_b [%]*
1/100	0.2	0.36	0.34	66	0.32	0.45	55.4	16.1
	0.4	0.63	0.60	39	0.48	0.66	33.8	13.3

	0.6	0.78	0.76	24	0.60	0.81	18.9	21.30
1/35	0.2	0.36	0.25	26	0.28	0.36	22.4	13.9
	0.4	0.59	0.43	20	0.46	0.58	14.6	27.0
	0.6	0.75	0.57	15	0.58	0.74	9	40.0
1/8	0.2	-	-	-	0.23	0.18	6.6	-
	0.4	0.41	0.08	7.4	0.41	0.41	4.7	36.5
	0.6	0.59	0.13	7	0.55	0.56	3.5	50.0

The results of the SWASH simulations give a rather good match to the tests of Grilli et al. (1997), see Figure 9 for a test with a slope of 1/35 and H_0 is 0.2m. Up to x/h_o = 22.5, the results for SWASH and Grilli et al. (1997) are the same. After that, the wave in SWASH starts to dissipate energy and drops in wave height in contrast to Grilli et al. (1997) where the wave starts its plunging breaking process, which is not explicitly modelled in SWASH.

The waves of the SWASH simulations break earlier/in deeper water, compared to Grilli et al. (1997). This difference is larger for steeper slopes. For the 1/8 slope, the location of wave breaking in SWASH is quite far off and for the mild slopes, the SWASH simulations results are a rather good match to the tests of Grilli et al. (1997). The mismatch in the location of breaking can be explained by the fact that the location of breaking in SWASH is when the slope of the free surface is larger than the factor α = 0.6, as explained earlier. The breaking by Grilli et al. (1997) starts when a vertical tangent is reached, which is never the case in SWASH. To see the effect of bottom friction, a simulation is conducted where the default value of 0.019 $m^{-1/3}s$ was decreased to 0.01 $m^{-1/3}s$. However, there was no significant effect on the breaking location is SWASH.

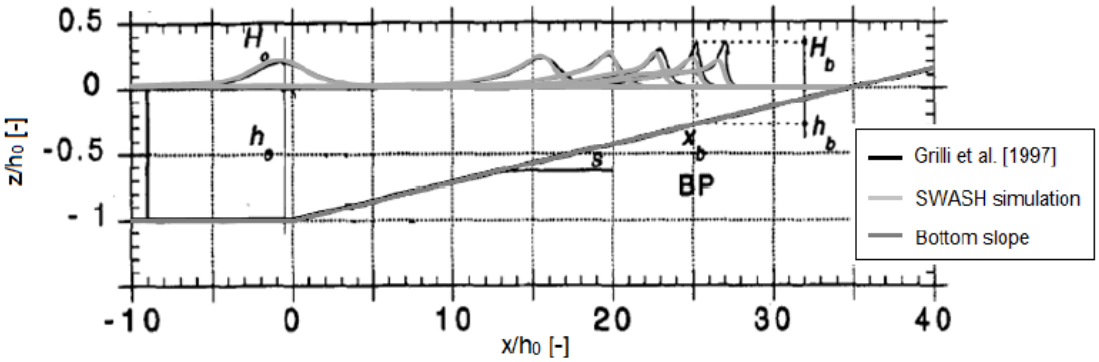

Figure 9: Solitary wave breaking tests: Results of Grilli et al. (1997) vs SWASH simulations. H_o is the offshore wave height, ho is the offshore depth, H_b is the breaker height, h_b is the breaker depth, x_b is location of breaking and s is the slope.

2.3 Results

Bonneton et al. (2015) showed that bore formation for tidal waves is mainly governed by dissipation of energy. The dissipation depends on the bottom friction, wave characteristics and estuary geometry. Tidal waves and tsunami waves are both long waves, therefore the theory of Bonneton (2015) is applicable. Bottom friction becomes important for run-up of tsunami waves (Dao and Tkalich 2007). Since the focus of this research is the transformation in front of the coast, the influence of bottom friction is assumed to be negligible. First the influence of wave characteristics on the transformation of a tsunami wave is described. Subsequently the influence of the bay geometry along the Sanriku coast on the transformation of a tsunami wave is explained.

2.3.1 Wave characteristics

When analyzing the wave characteristics H_ξ and L_ξ on varies slopes, a relation was found between the maximum momentum flux at the coastline and the slope, see Figure 10. For an increasing wave height, $(hu^2)_{max}$ increases. For the wavelength, the opposite relation applies. When the wavelength increases, $(hu^2)_{max}$ coastline decreases, except for the mildest slope 1/500. An interesting result is that the maximum momentum flux depends on the slope and the wave period. For simulations with T_ξ = 300 s, the

maximum momentum flux is reached for a slope of 1/300. When T_ξ is increased to 600 s, the maximum occurs for slopes for a smaller slope (1/500 for this input parameters). This can be explained by the fact that shorter waves, with similar wave heights and similar slopes, break earlier than longer waves. The type of tsunami wave with corresponding momentum flux is investigated in the following sections.

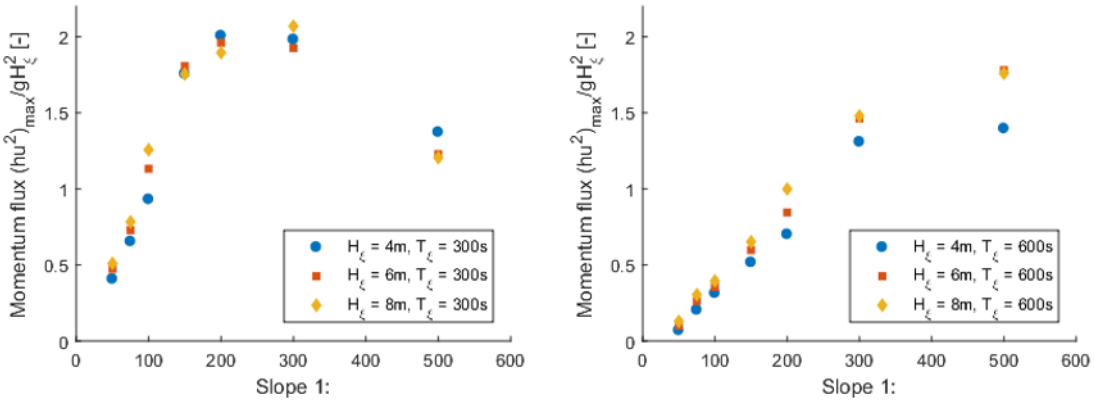

Figure 10: The slope of the continental shelf (α_2) vs. the maximum momentum flux at the coastline $(hu^2)_{max}$ divided by (gH_ξ^2) for three different wave heights (H_ξ) and two different wavefront periods (L_ξ) at a depth of 100 m. Left: T_ξ = 300 s. Right: T_ξ = 600 s.

2.3.2 Continental shelf (1D model)

To obtain a clear classification in tsunami wave types, several simulations are conducted for different continental shelf slopes. In this research, it is suggested to classify tsunami wavefronts into three different types; non-breaking wave (surging), breaking wavefront and undular bore breaking. Figure 11 shows this clear distinction in wave types.

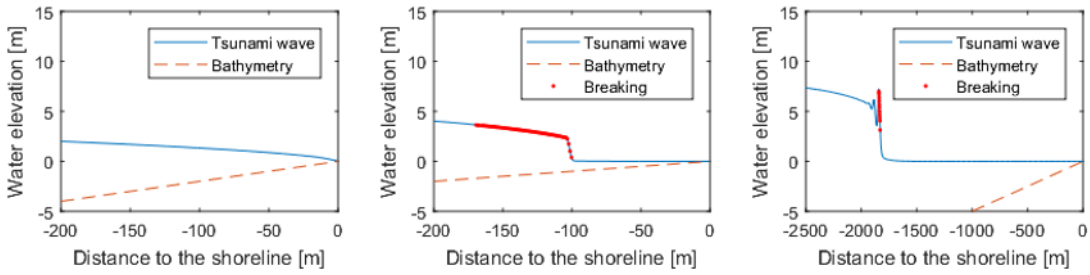

Figure 11: Three simulations with three different wavefront types. B.C.: timeseries H_ξ = 6 m and T_ξ = 300 s. Left to right: Continental shelf slope (α_2) 1/50: Non-breaking (surging) wave, 1/100: Breaking wavefront, 1/200: Undular bore breaking.

Several SWASH simulations are conducted to propose the tsunami breaker parameter $\xi_{tsunami}$, given by equation 4. For the 1D simulations, without the influence of the bay geometry ($\beta=1$), this parameter is plotted against the Froude number at the coastline Fr_{coast} in Figure 12a and the maximum momentum flux at the coastline in Figure 12b. A clear distinction can be seen for the three different wave types. The boundary between a surging wave and a breaking front is $\xi_{tsunami} = 0.54$ and between a breaking front an undular bore breaking $\xi_{tsunami} = 0.27$. It can also be observed that the Froude number (Fr_{coast}) and the maximum momentum flux $(hu^2)_{max}$ at the coastline increases when tsunami waves break and even more when undular bore breaking occurs, which is related to a decreasing $\xi_{tsunami}$.

$\xi_{tsunami} < 0.27$: Undular bore breaking

(1D: $\beta = 1$) $0.27 < \xi_{tsunami} < 0.54$: Breaking wavefront

$\xi_{tsunami} > 0.54$: Non-breaking wavefront (surging)

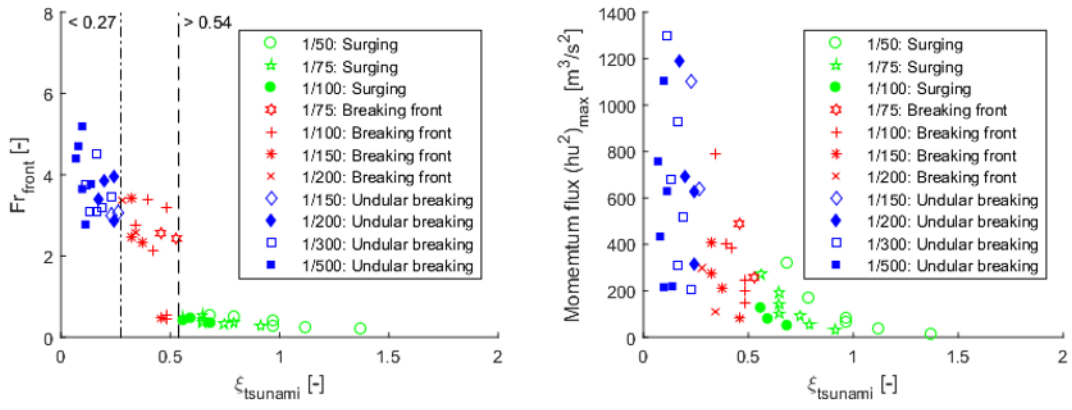

Figure 12: Breaker parameter $\xi_{tsunami}$ vs maximum Froude number F_{rcoast} and maximum momentum flux $(hu^2)_{max}$ at the coastline.

Figure 13 shows a scatter plot of the simulation results and the trend lines for the location of undular bore formation, undular bore breaking and purely wavefront breaking. The coefficient of determination R^2 is a statistical measure that indicates the coherence between the data and the trendline. The closer R^2 to 1.00, the better the

correlation. Equation 8, 9 and 10 are the empirical equations that describe the trend line for the different tsunami types. The correlation of the trend lines for undular bore formation and undular bore breaking is quite good in contrast to the trend line for the wavefront breaking.

$$Undular\ bore\ formation: \quad x = 34.7\xi_{tsunami}^{-2.46}\ [m] \tag{8}$$

$$Undular\ bore\ breaking: \quad x = 60.7\xi_{tsunami}^{-2.03}\ [m] \tag{9}$$

$$Wavefront\ breaking: \quad x = 1.97\xi_{tsunami}^{-4.13}\ [m] \tag{10}$$

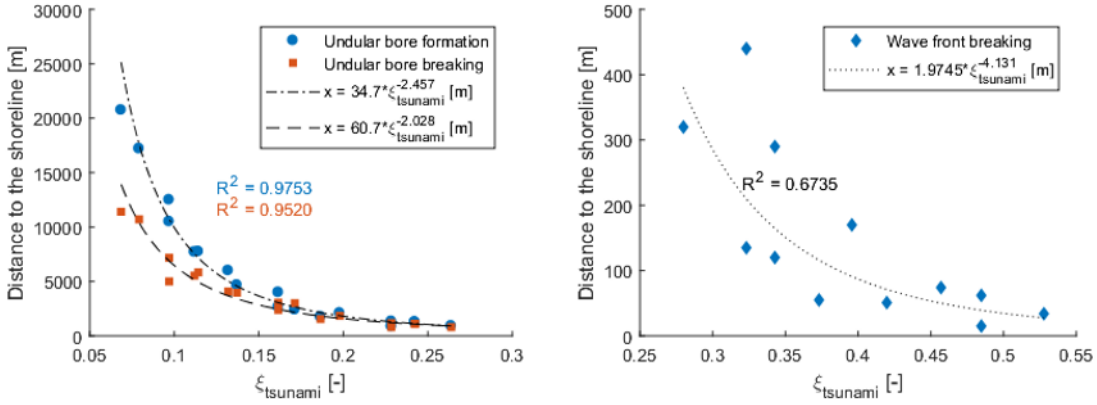

Figure 13: Empirical fitting to obtain formulas to predict the location of undular bore formation, undular bore breaking and purely wavefront breaking. R2 is the coefficient of Determination.

2.3.3 Bay geometry (2DH model)

The indented coastline along the Sanriku coast ensures that 2D effects become important in the nearshore area. 2DH simulations are performed to provide more insight into the influence of different bay geometries on the transformation of a tsunami wavefront. Figure 14 gives an example of a simulation where α_2 = 1/100, W_b = 3000 m, W_h = 1500 m, H_ξ = 6m and T_ξ = 300s. In Figure 15 a slightly curved wave crest can be seen near the boundaries of the bay, due to the stepwise angular grid. However, the wave crest in the middle of the bay remains rather straight. Therefore, the obtained results in the following simulations are based on the output values in the middle of the bay, given by the red line in Figure 14a.

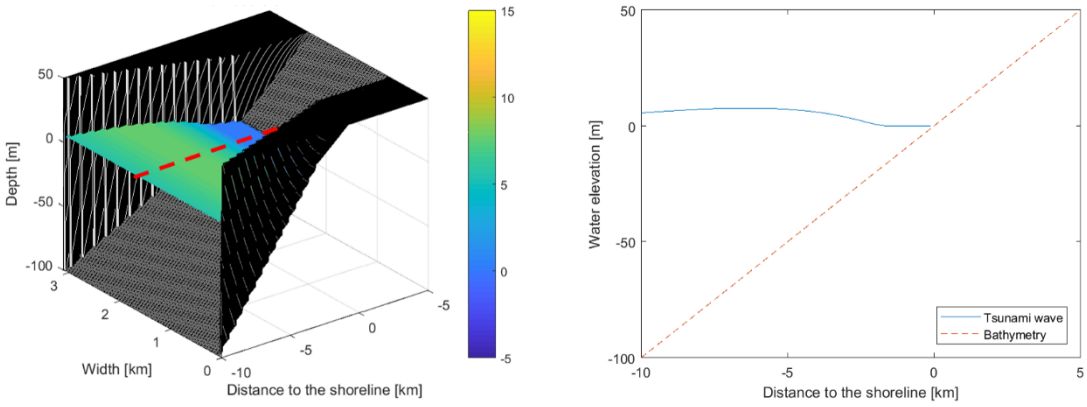

Figure 14: Example of a 2DH SWASH simulation. Left: 3D animation, red dashed line indicates the section of the 1D plot. Right: Plot of the section indicated by the red dashed line, which is used as a comparison between simulations.

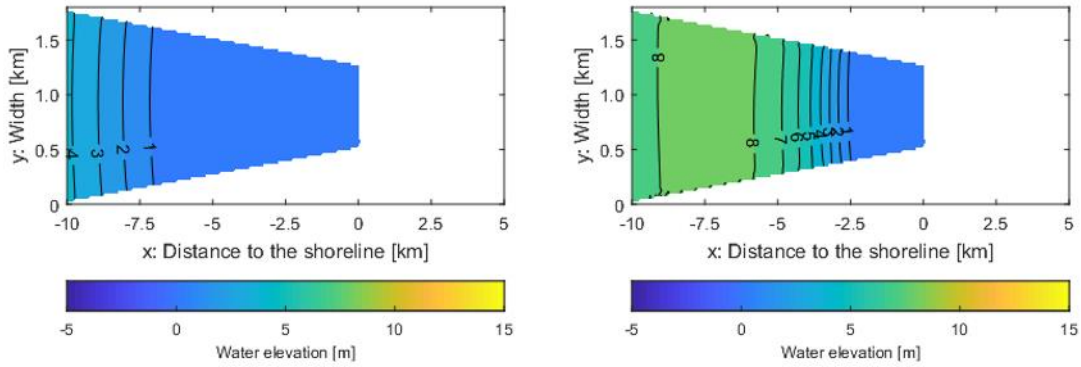

Figure 15: Top view of a 2DH simulation, where the 2D effects near the boundaries are visible. Left: At t = 1550.3 s. Right: At t = 1750.5 s.

Since the narrowing of the bay influences the amplification of the wave, and therefore the breaking, the following hypothesis is established:

The narrowing of the bay, averaged over the length of the bay, is the most important 2D parameter in the transformation of a tsunami wave in a bay.

To test the validity of this hypothesis several 2DH simulations are conducted with varying bay geometries, where some of them are given in Table 4. Since the depth at the bay mouth is set constant at a depth of 100 m, the bathymetry parameters that change along the Sanriku coast are the width of the bay mouth (W_b) and the width of the bay head (W_h).

Simulations 8, 10, 11 and 12 show the influence of a change in W_b. The funnelled shaped geometry of the bay will amplify the tsunami wave and therefore the steepness of the wave increases. The larger the bay mouth opening, with a constant bay head width, the larger this amplification factor becomes. This ensures that the wavefront breaks earlier when the bay mouth increases. The wave height, velocity and momentum flux at the coastline increases when W_b increases.

The effect of a changing W_h is the same but opposite to the change in W_b. Simulations 8 (1D: $W_b = W_h$), 9, 11, 13 and 14 show the influence of a change in W_h. When W_h increases, the amplification of the wave decreases and therefore the steepness decreases. The tsunami wave will break in a later stage. The wave height, velocity and momentum flux at the coastline decreases when W_h increases.

Simulation 11, 15 and 16 have the same bay shape factor β, which is defined as the W_b/W_h-ratio. The point of breaking, the Froude number and the maximum momentum flux at the coastline are approximately equal for these simulations. This corroborates the hypothesis that β is one of the most important parameters for tsunami wave transformation in bays. An interesting conclusion can be made when comparing simulations 6 and 7, where the only changing parameter is β. Simulation 6 is a 1D simulation ($\beta = 1$) and simulation 7 is 2DH simulation where bay geometry is included ($\beta = 2$). The wave type at the coastline is different for the simulations, a surging wave for a simulation without the influence of bay geometry and a breaking wave for a simulation including bay geometry. This indicates that bay geometry influences the type of tsunami wave along the Tohoku coastline and that a shape factor β needs to be included in the tsunami breaker parameter $\xi_{tsunami}$.

382 *Table 4: 2DH simulations: Influence of the bay geometry (β) on the tsunami wave transformation. *1D simulations,*
383 *without the influence of bay geometry.*

Simulation nr.	**α_2**	**L_{front} [m]**	**H_ξ [m]**	**W_b [m]**	**W_h [m]**	**β [-]**	**Wave type**	**Breakpoint [m]**	**Fr_{coast} [-]**	**$(hu^2)_{max}$ [m^3/s^2]**
6*	1/75	9396.28	4	-	-	1.00	Surging	x	0.54	102.61
7	1/75	9396.28	4	3000	1500	2.00	Breaking front	60	1.28	142.12
8*	1/75	9396.28	6	-	-	1.00	Breaking front	34	2.43	257.15
9	1/75	9396.28	6	3000	2000	1.50	Breaking front	61	1.36	387.10
10	1/75	9396.28	6	2000	1500	1.33	Breaking front	58	1.19	332.05
11	1/75	9396.28	6	3000	1500	2.00	Breaking front	85	1.36	490.87
12	1/75	9396.28	6	4000	1500	3.00	Breaking front	88	1.23	654.05
13	1/75	9396.28	6	3000	1000	3.00	Breaking front	105	1.40	675.55
14	1/75	9396.28	6	3000	500	6.00	Breaking front	125	1.37	678.19
15	1/75	9396.28	6	4000	2000	2.00	Breaking front	75	1.38	488.05
16	1/75	9396.28	6	5000	2500	2.00	Breaking front	80	1.21	501.32

384

$$H = K_r K_s H_o \qquad with: K_s = \sqrt[4]{\frac{d_o}{d_i}} \; ; \; K_r = \sqrt{\frac{b_o}{b_i}} \tag{11}$$

385 A tsunami parameter $\xi_{tsunami}$, including 2D effects, is proposed by including the
386 bay geometry factor β. To include the influence of a converging geometry of the bay, it
387 is assumed that the wave height in the bay will increase by the refraction factor K_r from
388 the Green's Law formula, equation 11. Green's Law describes the increase in wave

height due to a varying width by a factor $\sqrt{b_o/b_i}$. When applying this factor to a varying bay width, the refraction factor becomes $\sqrt{W_b/W_h} = \sqrt{\beta}$. Figure 16 compares the position of β. The best fit is obtained by including β in the denominator, in front of the wave height. The final tsunami breaker parameter is therefore given by equation 12.

$$\xi_{tsunami} = \frac{\tan(\alpha_s)}{\sqrt{\frac{\beta H_\xi}{L_\xi}}} \qquad where \begin{cases} \beta = 1 \; for \; straight \; coastlines \\ \beta = \frac{W_b}{W_h} \; for \; indented \; coastlines \end{cases} \tag{12}$$

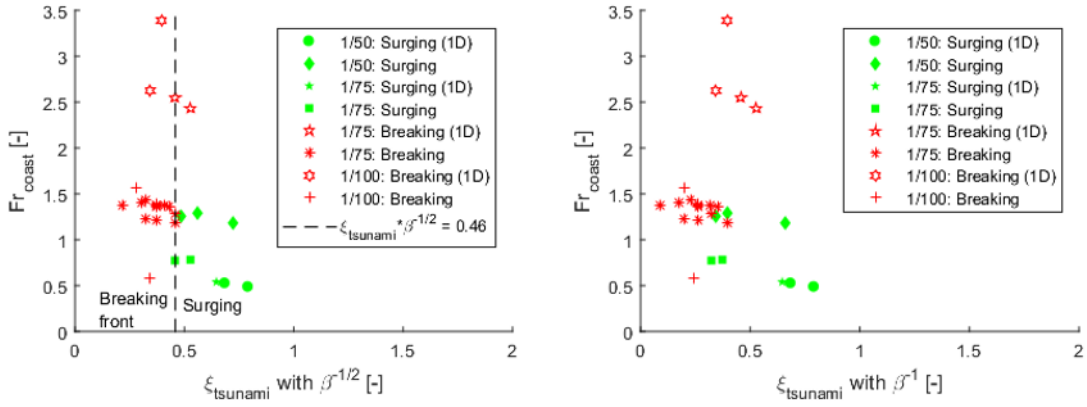

Figure 16: Comparison bay geometry factor (β) in tsunami parameter ($\xi_{tsunami}$) vs. Froude number at the coastline (Fr_{coast}).

The final proposed parameter $\xi_{tsunami}$ is plotted against the Froude number and the maximum momentum flux at the coastline in Figure 17. A clear distinction between a surging wave and a breaking wavefront is obtained. One simulation, for a slope of 1/75, does not meet this boundary for an unknown reason. Therefore, the boundary of breaking for $\xi_{tsunami}$ = 0.46 is a good approximation but not 100% reliable.

(2DH: $1 < \beta < 6$) $\xi_{tsunami} \leq 0.46$: Breaking wavefront

$\xi_{tsunami} > 0.46$: Non-breaking wavefront (surging)

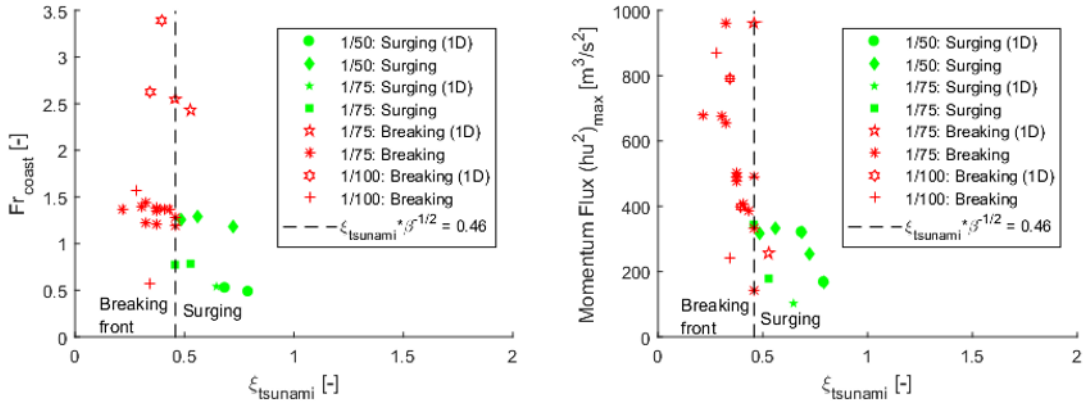

402

403 *Figure 17: Final tsunami breaker parameter ($\xi t_{tsunami}$) vs. Froude number (Fr_{coast}) and maximum momentum flux*
404 *$(hu^2)_{max}$ at the coastline.*

405 *2.3.4 Effectivity of the tsunami breaker parameter*

406 To check if the proposed method can be used for real-life prediction of tsunami
407 wave types along the Tohoku coastline, a efficiency study is done with the observations
408 of the tsunami in 2011. 12 different locations, as shown in Figure 5, are used to see if
409 the wave type along the coastline can be predicted with $\xi_{tsunami}$, with or without the bay
410 shape factor β. The results can be seen in Table 5.

411 For the 1D prediction, four out of 12 locations are predicted incorrectly. An
412 interesting observation is that only two out of 12 predictions were incorrect when using
413 the new proposed parameter including β. This can be due to the bay geometry that is
414 considered, which influences the steepness of the wave and therefore the wave
415 breaking. The incorrect prediction in Miyako Bay can probably be explained by the fact
416 that the direction of the incoming tsunami wave was very different in comparison to
417 other bays. Figure 5 shows that the opening of the Miyako Bay is directed to the north-
418 east, where the tsunami wave is coming from the south-east. It is therefore
419 recommended to include the incoming wave angle in the tsunami breaker parameter as
420 well. There is no clear explanation for the incorrect prediction in the Hirota Bay. Since
421 the bay slope is gentle and the narrowing effect of the bay is small a breaking wavefront

is expected, in contrast to the observations during the 2011 Tohoku Earthquake Tsunami.

*Table 5: Case study 2011 Tohoku Earthquake Tsunami. Red: Wrong predictions. Green: Good predictions due to bay geometry influence, after a wrong prediction without bay geometry influence. *Yuriage is characterized by a gentle sloped beach without 2D effects, which is the reason for the missing 2DH model results.*

Nr.	**Location**	β	H_ξ	T_ξ	L_ξ	$\xi_{tsunami}$	**Prediction 1D**	$\xi_{tsunami}*\sqrt{\beta}$	**Prediction 2DH**	**Observed wave type**
1	Kuji Bay	2.20	4.20	300	9396	0.30	Breaking front	0.20	Breaking front	Breaking front
2	Noda Bay	2.13	4.20	300	9396	0.32	Breaking front	0.22	Breaking front	Breaking front
3	Miyako Bay	2.50	4.20	300	9396	0.33	Breaking front	0.21	Breaking front	Surging
4	Yamada Bay	1.00	6.80	900	28189	0.72	Surging	0.72	Surging	Surging
5	Otsuchi Bay	1.20	6.80	900	28189	0.59	Surging	0.53	Surging	Surging
6	Toni Bay	1.83	6.80	900	28189	0.98	Surging	0.72	Surging	Surging
7	Yoshima Bay	6.08	6.80	900	28189	0.86	Surging	0.35	Breaking front	Breaking front
8	Ryori Bay	3.00	6.80	900	28189	0.73	Surging	0.42	Breaking front	Breaking front
9	Hirota Bay	2.19	6.40	900	28189	0.47	Breaking front	0.32	Breaking front	Surging
10	Oppa Bay	1.00	6.40	900	28189	0.62	Surging	0.62	Surging	Surging
11	Onagawa Bay	1.00	6.40	900	28189	0.55	Surging	0.55	Surging	Surging
12	Yuriage*	-	6.00	900	28189	0.12	Undular breaking	-	-	Undular breaking (series of bores)

3. Discussion

For most tsunami events, both the frequency dispersion and the nonlinearity effects are small and could be neglected for offshore propagation (Liu 2009). Therefore, the linear theory can be used as a first approximation to calculate changes in tsunami wave height as the wave moves across an ocean (Bryant 2014). A classic linear theory for shoaling is called Green's Law, equation 11, and applies for cases where the depth varies slowly (Lipa et al. 2016). Glasbergen (2017) compared wave buoy measurements near Sendai, during the 2011 Tohoku Earthquake Tsunami, with the results of a 1D SWASH model and with a Green's Law approximation. In this research, similar simulations were conducted to compare the SWASH results with a Green's Law approximation and buoy observations near the Kamaishi Bay. Before the point of breaking, Green's Law and the SWASH model gave a rather good match with the buoy observations. However, when the fault plane is elongated like the one of the 2011 Tohoku Earthquake, the initial free surface profile is almost uniform over the fault line and the tsunami propagates mainly in perpendicular direction of the fault line. It seems unlikely that Green's Law, which is a 1D analytical solution, is valid for all locations along the Tohoku coast. Therefore, for coastal regions near the epicenter of the earthquake a first approximation of the offshore wave height can be made by the Green's Law. This approximated wave height can be used predict the tsunami wave type near the coastline with the proposed tsunami parameter $\xi_{tsunami}$.

The wave characteristics in the proposed tsunami breaker parameter $\xi_{tsunami}$, H_ξ and L_ξ, are the wave height and wavelength at a depth of 100 meter. Since the transformation of tsunami waves can be approximated by Green's Law, these wave characteristics can be converted to parameters without a fixed depth. By substituting offshore parameters in equation 11 and applying $\frac{L}{\sqrt{gd}} = constant$ (Green's Law), the

tsunami parameters can be described by equation 13 and 14. The input parameters for the breaker parameter, H_ξ and L_ξ, can be obtained by any offshore depth d_o, offshore wave height H_o and offshore wavelength L_o. Investigation of the accuracy of this approach can be part of a further study.

$$H_\xi = \sqrt[4]{\frac{d_o}{100}} H_o \tag{13}$$

$$L_\xi = \frac{1}{2} L_0 \frac{\sqrt{g * 100}}{\sqrt{g * d_o}} = L_0 \frac{5}{\sqrt{d_o}} \tag{14}$$

The results for the 2DH simulations with $\beta = 1$ should be similar to the results of the 1D simulations. However, the results do not overlap exactly, where the boundary between a surging and a breaking waverfront is $\xi_{tsunami} = 0.54$ for the 1D and $\xi_{tsunami} = 0.46$ for 2DH simulations. This can be due to the difference in the way the simulations are performed. For a 2DH model with $\beta = 1$, the wave propagation is simulated in a bay without convergence, which is similar to wave propagation in an open channel. Apparently, the breaking of waves is slightly different for waves propagating in a channel versus waves propagating in open water (1D).

4. Conclusions

Several depth-integrated numerical simulations are conducted to find a relation between wave characteristics, bathymetry parameters and the type of tsunami wave breaking. A breaker parameter for tsunamis $\xi_{tsunami}$, given by equation 15, can be used to obtain more insight in tsunami wave transformation. The parameter describes the steepness of the front of the wave and includes the relative horizontal contraction of the bay. The tsunami breaker parameter shows a distinction in three different tsunami wave types; undular bore breaking, a breaking wavefront and a non-breaking (surging) wavefront. These wave types occur for a gentle, an intermediate and a steep continental shelf

473 respectively. The first classification is based on 1D simulations where there is no bay
474 forming along the coast (β = 1), with a continental slope (α_s) in the range of 1/50 to
475 1/500. The second classification is based on 2DH simulations where bay geometry plays
476 a role along the coastline (1<β <6), with a continental slope in the range of 1/50 to
477 1/100.
478

$$\xi_{tsunami} = \frac{\tan(\alpha_s)}{\sqrt{\frac{\beta H_\xi}{L_\xi}}} \qquad where \begin{cases} \beta = 1 \; for \; straight \; coastlines \\ \beta = \frac{W_b}{W_h} \; for \; indented \; coastlines \end{cases} \qquad (15)$$

$\xi_{tsunami}$ < 0.27: Undular bore breaking

(1D: β = 1) 0.27 < $\xi_{tsunami}$ < 0.54: Breaking wavefront

$\xi_{tsunami}$ > 0.54: Non-breaking wavefront (surging)

(2DH: 1 < β < 6) $\xi_{tsunami} \leq$ 0.46: Breaking wavefront

$\xi_{tsunami}$ > 0.46: Non-breaking wavefront (surging)

479 **Acknowledgements**

480 We would like to express sincere gratitude to the Delft Deltas, Infrastructures & Mobility
481 Initiative (DIMI) who made it possible to do research in Japan. A multidisciplinary group from
482 the Delft University of Technology and the University of Tokyo and Waseda visited Otsuchi
483 Town to learn lessons from the reconstruction of the Japanese coasts destroyed by the tsunami
484 in 2011. A special thanks to the Delft University of Technology and the Waseda University who
485 contributed to this research and offered the research facilities.

References

Árnason, H. (2005). *Interactions between an Incident Bore and a Free-Standin Coastal Structure.* Washington: Doctoral dissertation.

ASCE. (2016). Chapter 6: Tsunami Loads and effects. In ASCE, *ASCE 7 Standard, Minimum Design Loads and Associated Criteria for Buildings and Other Structures* (pp. 25-50). Reston: American Society of Civil Engineers.

Battjes, J. A. (1974). Surf Similarity. *Coastal Engineering Proceedings*.

Bonneton, P., Bonneton, N., Parisot, J.-P., & Castelle, B. (2015). Tidal bore dynamics in funnel-shaped estuaries. *Journal of Geophysical Research: Oceans*, 923-940.

Bryant, E. (2014). *Tsunami - The Underrated Hazard.* Chichester: Springer International.

Dalrymple, R. A., Grilli, S. T., & Kirby, J. T. (2015). Tsunamis and Challanges for Accurate Modeling. *Oceanography*, 142-151.

Dao, M. H., & Tkalich, P. (2007). Tsunami propagation modelling - a sensitivity study. *Natural Hazards and Earth System Sciences*, 741-754.

FEMA. (2012). *Guidelines for Design of Structures for Vertical Evacuation from Tsunamis.* California.

Glasbergen, T. (2017). *Characteristics of incoming tsunamis for the design of coastal structures.* Delft: Delft University of Technology.

Google. (2019, June 19). *Japan*. Retrieved from Google Maps: https://www.google.com/maps/place/Japan/@39.2940583,141.6539264,8.75z/data=!4m5!3m4!1s0x34674e0fd77f192f:0xf54275d47c665244!8m2!3d36.204824!4d138.252924

Grilli, S. T., Member ASCE, Svendsen, I. A., Member ASCE, & Subramanya, R. (1997). Breaking criterion and characteristics for solitary waves on slopes. *Journal of Waterway Port Coastal and Ocean Engineering*, 102-112.

512 Liu, P. L.-F. (2009). Tsunami. In J. H. Steele, *Encyclopedia of Ocean Sciences* (pp.
513 127-140). Massachusetts.
514 Lynett, P. (2006). Nearshore Wave Modelling with High-Order Boussinesq-Type
515 Equations. *Journal of Waterway, Port, Coastal and Ocean Engineering* , 348-
516 357.
517 Madsen, P. A., Fuhrman, D. R., & Schäffer, H. A. (2008). On the solitary wave
518 paradigm for tsunamis. *Journal of Geophysical Research*, 22.
519 Navionics. (n.d.). *Chart Viewer*. Retrieved from Navionics:
520 https://webapp.navionics.com/?lang=en#boating@5&key=oaioFuwg%7BY
521 Ramsden, J. D. (1993). *Tsunamis: forces on a verticall wall caused by long waves,*
522 *bores, and surges on a dry bed.* California: Doctoral dissertation.
523 Schäffer, H. A., Madsen, P. A., & Deigaard, R. (1993). A Boussinesq model for waves
524 breaking in shallow water. *Coastal Engineering*, 185-202.
525 Shimonzono, T., Sato, S., Okayasu, A., Tajima, Y., Fritz, H. M., Liu, H., & Takagawa,
526 T. (2012). Propagation and inundation characteristics of the 2011 Tohoku
527 Tsunami on the central Sanriku coast. *Coastal Engineering Journal* , 17.
528 Smit, P., Zijlema, M., & Stelling, G. (2013). Depth-induced wave breaking in a non-
529 hydrostatic, near-shore wave model. *Coastal Engineering*, 1-16.
530 Tissier, M., Bonneton, P., Marche, F., Chazel, F., & Lannes, D. (2011). Nearshore
531 Dynamics of Tsunami-like Undular Bores using a Fully Nonlinear Boussinesq
532 Model. *Journal of Coastal Research*, 1-6.
533 Topics, T. (2016, November 25). *Kuji Tsunami Compilation - Japan 2011*. Retrieved
534 from Youtube: https://www.youtube.com/watch?v=ob28xxKT6uE&t=433s

Topics, T. (2017, May 9). *Giant Tsunami in Miyako - Final Documentary - Japan 2011*. Retrieved from Youtube: https://www.youtube.com/watch?v=xtd6xUuul1s&t=578s

Topics, T. (2018, March 6). *Sendai Tsunami Final Edition - Japan 2011 seventh Anniversary*. Retrieved from Youtube: https://www.youtube.com/watch?v=spmTTNInXx8&t=342s

Wei, Y., Chamberlin, C., Titov, V. V., Tang, L., & Bernard, E. N. (2012). Modeling of the 2011 Japan Tsunami: Lessons for Near-Field Forecast. *Pure and Applied Geophysics*, 24.

Yeh, H. (2006). Maximum Fluid Forces in the Tsunami Runup Zone. *Journal of Waterway, Port, Coastal, and Ocean Engineering*, 496-500.

Zijlema, M., Stelling, G. S., & Smit, P. (2011). SWASH: an operational public domain code for simulating wave fields and rapidly varied flows in coastal waters. *Coastal Engineering* , 77.

558

559

Table 1. Classification of the Tohoku coastline (Navionics 2018; Shimonzono et al. 2012).

Table 2. Parameters used for the SWASH simulations in this research. *The slopes are based on the range of continental shelf slopes along the Sendai Plain (1D) and the Sanriku coast (2DH).

Table 3. Breaker height (H_b), breaker depth (h_b) and breaker location (x_b) for the test by Grilli et al. (1997) and the SWASH simulations (Glasbergen 2017).

Table 4. 2DH simulations: Influence of the bay geometry (β) on the tsunami wave transformation. *1D simulations, without the influence of bay geometry.

Table 5. Case study 2011 Tohoku Earthquake Tsunami. Red: Wrong predictions. Green: Good predictions due to bay geometry influence, after a wrong prediction without bay geometry influence.

Figure 1. Characteristics of the Tohoku coastline. The red symbol indicates the location of the epicentre of the 2011 Tohoku Earthquake.

Figure 2. Left: Otsuchi Town (Sanriku coast), the yellow line indicates the location of the planned sea dyke. Right: Sea dyke under construction, height is 14.5 m.

Figure 3. Real-life observation from different tsunami wave types at several location along the Thoku coastline during the 2011 Tohoku Earthquake Tsuanmi. Left to right: Kuji Bay (Topics 2016), Miyako Bay (Topics 2017), Sendai coast (Topics 2018).

Figure 4. Classification of coastal inundation, where T_E is the tsunami elevation and R the run-up elevation (FEMA 2012).

Figure 5. Sanriku + Sendai coast with numbered locations (Google 2019).

Figure 6. Characteristics to describe a tsunami wave front (Glasbergen 2017).

Figure 7. Schematization of the ocean bathymetry, where d_o, d_c and d_b are the depth offshore, at the edge of the continental shelf and at the bay mouth. α_1, α_2, α_3 and α_4 are the slopes of the continental rise, continental shelf, bay and inland topography.

Figure 8. Simulation area: The schematization of a bay along the Sanriku coast, where d_b is the depth at the bay mouth, L_b the length of the bay, W_b the width of the bay mouth, W_h the width of the bay head and α_3 the slope of the bay.

Figure 9. Solitary wave breaking tests: Results of Grilli et al. (1997) vs SWASH simulations. H_o is the offshore wave height, h_o is the offshore depth, H_b is the breaker height, h_b is the breaker depth, x_b is location of breaking and s is the slope.

Figure 10. The slope of the continental shelf (α_2) vs. the maximum momentum flux at the coastline $(hu^2)_{max}$ divided by (gH_ξ^2) for three different wave heights (H_ξ) and two different wavefront periods (L_ξ) at a depth of 100 m. Left: T_ξ = 300 s. Right: T_ξ = 600 s.

Figure 11. Three simulations with three different wavefront types. B.C.: timeseries H_ξ = 6 m and T_ξ = 300 s. Left to right: Continental shelf slope (α_2) 1/50: Non-breaking (surging) wave, 1/100: Breaking wavefront, 1/200: Undular bore breaking.

Figure 12. Breaker parameter $\xi_{tsunami}$ vs maximum Froude number F_{rcoast} and maximum momentum flux $(hu^2)_{max}$ at the coastline.

Figure 13. Empirical fitting to obtain formulas to predict the location of undular bore formation, undular bore breaking and purely wavefront breaking. R^2 is the coefficient of Determination.

Figure 14. Example of a 2DH SWASH simulation. Left: 3D animation, red dashed line indicates the section of the 1D plot. Right: Plot of the section indicated by the red dashed line, which is used as a comparison between simulations.

Figure 15. Top view of a 2DH simulation, where the 2D effects near the boundaries are visible. Left: At t = 1550.3 s. Right: At t = 1750.5 s.

Figure 16. Comparison bay geometry factor (β) in tsunami parameter ($\xi_{tsunami}$) vs. Froude number at the coastline (Fr_{coast}).

Figure 17. Final tsunami breaker parameter (ξt_{sunami}) vs. Froude number (Fr_{coast}) and maximum momentum flux $(hu^2)_{max}$ at the coastline.

Prediction of the characteristics of a tsunami wave near the Tohoku coastline

Numerical SWASH modelling

J. J. (Jochem) Roubos

Section of Hydraulic Engineering
Faculty of Civil Engineering & Geosciences
Delft University of Technology

TU Delft

Prediction of the characteristics of a tsunami wave near the Tohoku coastline

Numerical SWASH modelling

by

J. J. (Jochem) Roubos

in partial fulfilment of the requirements for the degree of Master of Science at the Delft University of Technology, to be defended publicly on Tuesday July 2, 2019 at 02:00 PM.

Student number:	4162803	
Project duration:	September 3, 2018 – July 2, 2019	
Charmain:	Dr. ir. B. Hofland,	TU Delft
Thesis committee:	Dr. ir. J. D. Bricker,	TU Delft
	Dr. ir. M. Zijlema,	TU Delft
	Dr. M. Esteban,	Waseda University (Tokyo)

An electronic version of this thesis is available at `http://repository.tudelft.nl/`.

TU Delft

Abstract

On the 11th of March 2011, a magnitude-9 undersea earthquake occurred in the north-western Pacific Ocean near the Tohoku region of Japan. The earthquake triggered a tsunami which was one of the most destructive tsunamis in history, causing 15,853 casualties, 3,282 missing, 6,023 injured, and over 220 billion dollars of damage along the coastline.

Even with the constructed seawalls and sea dykes up to 10 m or more, the 2011 tsunami led to many deaths and damage. New design rules are accepted to build higher and/or more overtopping resistant seawalls and sea dykes, but there are still a lot off uncertainties in impacting wave types and wave loads. The front of the wave can be bore like or non-broken (surging/rising water level), and depends on the local bathymetry and the type of coastline. To obtain the impacting forces on the coastal structure, the need for quantitative classification of tsunami waves in front of the coastline has been increased.

This research focussed on the Tohoku coastline, which mainly consists of the Sendai Plain and the Sanriku coastline, with a gentle and a steep sloping continental shelf respectively. A schematized model of a bay is used to represent reality. This model helps to understand the role of different parameters in the transformation of tsunami waves. Based on this model, detailed calculations are performed by using the numerical program SWASH (Simulating WAves till SHore).

The research is divided into offshore and nearshore modelling. A 1D model is used to show the characteristics of the offshore tsunami propagation from the origin up to the continental shelf. Another 1D model showed the effect of the continental shelf slope, which is one of the most important nearshore parameters for wave transformation. Along the Sanriku coast, which is characterized by an indented coastline, 2D effects become important. In order to include the effect of bay geometry, 2DH simulations have been performed.

It is shown that nonlinear effects can be neglected for long wave propagation in the deep ocean. The main propagation path of a tsunami wave is perpendicular to the fault lane, which is typically parallel to the coastline in the northern part of Japan. Green's Law, an analytical solution, appeared to give a good approximation of the offshore propagation to locations with an angle of 0-33°relative to the perpendicular propagation path. This model can be used for a first assessment of tsunami impact. To accurately include all the effects on wave transformation, a 2D or 3D model would have to be used.

The nearshore transformation of tsunami waves is affected by two sets of parameters: wave characteristics and geophysical properties. The wave characteristic parameters, wave height H_ξ and wavelength L_ξ at a depth of 100 m, are important because the wave skewness H_ξ/L_ξ is the ultimate cause of breaking. The change in wave characteristics is influenced by geophysical properties like the continental shelf α_2 and bay geometries (W_b, W_h, d_b and L_b).

It turned out that an increase in wave height H_ξ is related to an increase in the Froude number and the momentum flux (hu^2) at the coastline. An increase in wavelength L_ξ is related to a decrease in the Froude number and momentum flux. The slope of the continental shelf turned out to be one of the most important nearshore parameters. A classification of the tsunami wave front is obtained, based on the wave characteristics and the slope of the continental shelf ranging from 1/50 to 1/500. Undular bore formation, accompanying with undular breaking, occurs for mildly sloping shelves. A purely breaking wavefront can be observed when tsunami waves propagate over intermediate shelf slopes and non-broken wavefronts (surging) are visible along steep coastlines. Based on several 1D numerical simulations, empirical equations are proposed for the location of undular bore formation and undular bore breaking.

A bay shape factor β is introduced that describes the amount of narrowing over the length of the bay. The point of breaking is affected by the geometry of the bay, where the wave breaks more offshore when β increases. The Froude number and the momentum flux at the coastline increases when β increases.

Finally, the tsunami breaker parameter $\xi_{tsunami}$ is improved by including the 2D bay geometry effects (β) in the formula. A distinction for a tsunami wavefront is found in breaking and non-breaking (surging) wave-

fronts along the Sanriku coastline (range slope: 1/50 - 1/100) and can be used to predict the impact loads on the coastal structures in a more reliable way.

The proposed bay shape factor β and tsunami breaker parameter $\xi_{tsunami}$ contribute to a first prediction of the present tsunami wave type along a coastline, with which the forces on the coastal structure can be predicted in a more reliable way.

Acknowledgements

This thesis is written to fulfil the requirements of the Master of Science program 'Hydraulic Engineering' at the Delft University of Technology. The research is part of the interdisciplinary project 'Tsunami reconstruction Otsuchi' and was carried out at the Delft University of Technology and the Waseda University in Tokyo.

I would like to express my gratitude to my thesis committee who always provided me with some good advice. Bas, thanks for your daily supervision. In our first conversation, you made me very enthusiastic about the thesis subject and during the project you were there to keep me on track and keep me motivated. Jeremy, thanks for giving me all the substantive and practical advises during the thesis. I appreciated you for always put me at ease and having time for a chat. Marcel, thanks for joining the committee and for helping me out when I struggled with modelling issues. Miguel, last but not least, thanks for helping me and Jesse during the experiments in Tokyo. We successfully finished all the tests in only two weeks, and we could not have done it without your preparations before our arrival and the help during these weeks. Also thanks to all the Japanese students who helped us during the execution of the experiments.

A special thanks to the 'Delft Deltas, Infrastructures & Mobility Initiative' (DIMI) for funding the trip to Japan, which made this thesis project a wonderful experience.

Finally, I want to thank the people who supported me during my whole study period. My friends, who were always there for me to spend my free time with. And in particular, thanks to my parents, Cor and Anja, who supported me mentally and financially during my whole study. I really appreciate it and I could not have done this without you.

J. J. (Jochem) Roubos
Delft, June 2019

Contents

Abstract iii

Acknowledgements v

List of Figures ix

List of Tables xi

Nomenclature xiii

1 Introduction 1
- 1.1 Problem description . . . 1
- 1.2 Objectives . . . 3
- 1.3 Approach . . . 3
  - 1.3.1 Simulations SWASH . . . 5
  - 1.3.2 Schematized model . . . 5
  - 1.3.3 Definition Froude number . . . 6
- 1.4 Outline of the report . . . 6

2 Background theory 7
- 2.1 Cause of a tsunami . . . 7
- 2.2 Tsunami characteristics . . . 8
  - 2.2.1 Tsunami waves . . . 8
- 2.3 Tsunami wave propagation . . . 8
  - 2.3.1 Shoaling and refraction . . . 8
  - 2.3.2 Reflection . . . 9
  - 2.3.3 Breaking . . . 10
- 2.4 Tsunami wave theory . . . 10
  - 2.4.1 Offshore behaviour . . . 10
  - 2.4.2 Shallow water limit . . . 11

3 Previous studies and Standards 13
- 3.1 ASCE 7-16: Design for Tsunami Loads and Effects . . . 13
- 3.2 FEMA - Loads on vertical structures . . . 13
- 3.3 Sensitivity of offshore tsunami parameters . . . 14
- 3.4 Bore simulations . . . 15
- 3.5 Tsunami breaker parameter . . . 15
- 3.6 Classification of the Tohoku coastline . . . 16
  - 3.6.1 Type of tsunami wave . . . 16
  - 3.6.2 Bathymetry . . . 16
  - 3.6.3 Sanriku Ria coast . . . 17
- 3.7 Converging estuaries . . . 18
- 3.8 The 2011 Tohoku Earthquake Tsunami . . . 18
  - 3.8.1 Numerical simulations . . . 18
  - 3.8.2 Real-life observations . . . 19
- 3.9 Design of defence systems . . . 19
  - 3.9.1 Seawalls and sea dykes . . . 20
  - 3.9.2 Warning system and evacuation plan . . . 21
- 3.10 Summary and discussion . . . 21

4 Offshore modelling 23
- 4.1 Approach . . . 23

4.2 Validation . . . 23
4.2.1 Input . . . 23
4.2.2 Output . . . 24
4.2.3 Calibration . . . 26
4.3 Green's law . . . 27
4.4 Behaviour along Tohoku coastline . . . 28

5 Nearshore modelling 31
5.1 Introduction . . . 31
5.2 Approach . . . 32
5.3 Input . . . 32
5.4 Simulations: 1D model . . . 33
5.4.1 Wave characteristics . . . 33
5.4.2 Continental shelf slope (α_2) . . . 34
5.4.3 Breaker parameter for 1D approximations . . . 34
5.4.4 Empirical formulas for 1D tsunami wave breaking . . . 35
5.5 Simulations: 2DH model . . . 36
5.5.1 Bay geometry . . . 37
5.5.2 Breaker parameter for 2DH approximations . . . 40
5.6 Application of the results . . . 41

6 Discussion 43
6.1 Offshore modelling . . . 43
6.2 1D nearshore model . . . 44
6.3 2DH nearshore model . . . 45

7 Conclusions and recommendations 47
7.1 Conclusions . . . 47
7.2 Recommendations . . . 50
7.2.1 Simulations . . . 50
7.2.2 Green's Law approximation . . . 50
7.2.3 Tsunami breaker parameter . . . 50

Bibliography 50

A Physical modelling 55
A.1 Introduction . . . 55
A.2 Wave flume set-up . . . 55
A.3 Results . . . 56

B Command files SWASH 59
B.1 1D model: offshore - nearshore . . . 59
B.2 1D and 2DH model: nearshore . . . 61

C Background of SWASH 65
C.1 Different models . . . 65
C.2 Derivation of the Shallow Water Equations . . . 65

D 1D simulations: Results 69

E 2DH simulations: Results 73

F Extra Tsunami Theory Details 75
F.1 Green's law . . . 75
F.2 N-waves . . . 75
F.3 Run-up and Inundation . . . 76
F.4 Inland penetration and velocity . . . 76
F.5 Resonance and Mach-Stem waves . . . 76

G Extra figures 77

List of Figures

1.1 Destroyed Government building in Otsuchi Town during the 2011 Tohoku Earthquake Tsunami [pictures: J.J. Roubos] . . . 1
1.2 Characteristics of the Tohoku coastline. The red symbol indicates the location of the epicentre of the 2011 Tohoku Eartquake . . . 2
1.3 Otsuchi Town [pictures: J.J. Roubos] . . . 2
1.4 Youtube footage from different tsunami wave types at several locations along the Tohoku coastline . . . 3
1.5 Classification of coastal inundation where T_E is the tsunami elevation and R the run-up elevation. 4
1.6 Modelling steps . . . 4
1.7 Schematic ocean topography with parameters (1D) . . . 6
1.8 Schematic ria bay at the Sanriku coast . . . 6

2.1 Submarine earthquake, cause of a tsunami (Atwater et al., 1999) . . . 7
2.2 Basic wave parameters (James, 2016) . . . 8
2.3 Tsunami wave propagation and shoaling (Irwanto, 2015) . . . 9
2.4 Schematization of refraction (Bryant, 2014) . . . 9
2.5 Breaking wave types (Wikimedia, 2016) . . . 10
2.6 Blue line: solitary wave theory with frequency dispersion; Red line: SWE without frequency dispersion (Wikipedia, 2018) . . . 11
2.7 Bore shapes for varying Froude numbers (Tissier et al., 2011) . . . 12

3.1 Sketch of a bore with their characteristics (Glasbergen, 2018) . . . 15
3.2 Sketch of parameters for Tsunami breaker parameter (Glasbergen, 2018) . . . 16
3.3 Froude number at maxiumum velocity vs breaking parameter. Relation between the Froude number and the breaker parameter for slopes steeper than 1:200 (dotted line). Breaker relation equation 3.7 (black line). Empty markers are surging breakers. (Glasbergen, 2018) . . . 16
3.4 Bathymetry perpendicular to the coast; data obtained from 'Navionics' . . . 17
3.5 Classification Ria coast (Shimozono et al., 2012) . . . 17
3.6 Location of the Sanriku coast and the offshore tsunami recordings (Shimozono et al., 2012) . . . 19
3.7 Tsunami height, topographic slope and local coastline orientation of the study area (rectangle in figure 3.6) (a) Relationship between the tsunami heights and topographic slopes. (b) Classification of the data points by the local coastline orientation. (Shimozono et al., 2012) . . . 20
3.8 Results of the numerical simulations of Shimozono et al. (2012) . . . 21

4.1 2011 Tohoku Earthquake Tsunami water elevation . . . 24
4.2 Splitting of a tsunami wave . . . 24
4.3 Tsunami propagation and transformation from the origin of the tsunami to the nearshore area . 25
4.4 SWASH results vs. GPS buoy GB802 on March 11, 2011 . . . 26
4.5 Tests 1D model . . . 27
4.6 Green's Law approximation for Kamaishi . . . 28
4.7 Wave buoy observations along the Tohoku coastline . . . 28
4.8 Locations buoy observations relative to the highest initial water elevation. θ gives the angle relative to the perpendicular propagation path of the tsunami wave. θ_1 is 7.7°, θ_2 is 32.7°and θ_3 is 46.9°. . . . 29

5.1 Boundary condition: timeseries of the water level coming in to the bay . . . 32
5.2 The slope of the continental shelf (α_2) vs the Froude number of the wavefront (Fr_{coast}) at the coastline for 3 different wave heights (H_ξ) and 2 different wavefront periods (T_ξ) at a depth of 100 m. . . . 33

5.3 The slope of the continental shelf (α_2) vs the maximum momentum flux at the coastline $(hu^2)_{max}$ divided by (gH_ξ^2) for 3 different wave heights (H_ξ) and 2 different wavefront periods (T_ξ) at a depth of 100 m. . . . 34
5.4 1D simulations of tsunami transformation for different slopes. BC: sinusoidal wave H = 6m and T = 600s . . . 35
5.5 4 simulations with 4 different wavefront types. BC: sinusoidal wave H = 6m and T = 600s . . . 36
5.6 Breaker parameter ($\xi_{tsunami}$) vs Froude number (Fr_{coast}) and Momentum flux (hu^2). . . . 37
5.7 Empirical fitting to obtain formulas to predict the location of undular bore formation, undular bore breaking and purely wavefront breaking. R^2 is the coefficient of Determination. . . . 37
5.8 Example of a 2DH SWASH simulation . . . 38
5.9 Top view simulation with 2D effects . . . 38
5.10 $\xi_{tsunami}{}^*\beta^{-1/2}$ vs Froude number (Fr_{coast}) and Momentum flux ($(hu^2)_{max}$). . . . 40
5.11 Comparison tsunami parameters vs Froude number (Fr_{coast}). . . . 41
5.12 Sanriku coast with numbered bays which are used for the case study. . . . 42

7.1 Schematic ria bay at the Sanriku coast . . . 48

A.1 Setup wave flume . . . 55
A.2 Comparison of the Froude numbers of a rough and a smooth bed for the range of experiments provided in table A.1 . . . 57

B.1 Input file 1D model SWASH . . . 59
B.2 Input file 1D nearshore model SWASH . . . 62
B.3 Input file 2DH nearshore model SWASH . . . 63

C.1 Averaged models derived from Navier-Stokes equations (Sainte-Marie and Bristeau, 2008) . . . 65

G.1 (a) Map of the study area along the central Sanriku coast. (b) Topography and bathymetry of the study area. (c) Distribution of the measured tsunami heights and topographic slopes along the x-axis. (Shimozono et al., 2012) . . . 77

List of Tables

2.1 Wind waves vs. Tsunami waves 8

3.1 Coastal Classification (ExtremePlanet, 2014) 19

5.1 Classification of the Sanriku coastal bays (Navionics, 2018; Shimozono et al., 2012) 31
5.2 2DH simulations: Influence of a changing bay mouth width W_b. *1D simulations, without influence of bay geometry. 39
5.3 2DH simulations: Influence of a changing bay headwidth W_h. *1D simulations, without influence of bay geometry. 39
5.4 2DH simulations: Influence of the bay geometry (β). *1D simulations, without influence of bay geometry. 40
5.5 Case study 2011 Tohoku Earthquake Tsunami 42

A.1 Results of the experiments with a rough bed compared to the experiments with a smooth bed (Esteban et al., 2017). Including the Froude numbers of the wavefront. 56

D.1 1D simulations: point of breaking with corresponding breaker parameter 70
D.2 1D simulations: characteristics tsunami wavefront with corresponding Froude numbers. 71

E.1 2DH simulations: Slope continental shelf, wave characteristics, bay dimensions, wave type and the tsunami breaker parameters for each simulation. *Test 1,4,7,20,23 and 25 are 1D simulations to compare 73
E.2 2DH simulations: point of breaking, Froude number at the coastline and the maximum momentum flux at the coastline for all simulations. *Test 1,4,7,20,23 and 25 are 1D simulations to compare 74

Nomenclature

Name	Description
Bathymetry	The study of underwater depth of lake or ocean floors. In other words, bathymetry is the underwater equivalent to topography.
Inundation height	The maximum water level of the tsunami in a reasonably flat area, measured from mean sea level.
Run-up height	The maximum water level the tsunami reaches due to run-up, measured from mean sea level.
Run-up length	The maximum length of the inland run-up, measured from the coastline.
Shoaling	The effect by which the wave height increases when a wave enters shallow water, caused by a decrease in group velocity.
Topography	The study of the shape and features of land surfaces.
Tsunami	A Japanese word for "harbour wave", where "tsu" means "harbour" and "nami" means "wave". In this research the word Tsunami refers to a wave caused by an underwater earthquake.
Tsunami bore	A steep and turbulent broken wavefront generated on the front edge of a long-period tsunami wave, which occurs when shoaling over a mild continental shelf or abrupt seabed discontinuities.
Tsunami height	The height of the wave until it reaches the shoreline, measured from sea level.

Abbreviation	Full Name
ASCE	American Society of Civil Engineers
B.C.	Boundary Condition
FEMA	Federal Emergency Management Agency
KdV	Korteweg-de Vries
LSW	Linear Shallow Water
NLSW	Non Linear Shallow Water
SWASH	Simulating WAves till SHore
SWE	Shallow Water Equations
T.P.	Tokyo Peil (T.P. datum corresponds to mean sea level of Tokyo Bay)
VM	Velocity Meter
WG	Wave Gauge

Symbol	[Units]	Description
A	$[m]$	Wave amplitude
b_i	$[m]$	Distance between wave orthogonals at any shoreward point in the Green's Law formula
b_o	$[m]$	Distance between wave orthogonals at a source point water in the Green's Law formula
c	$[m/s]$	Wave celerity
c_b	$[m/s]$	Bore celerity
C_{f0}	[-]	Friction coefficient
Cr	[-]	Courant number
$\mathfrak{D}$	[-]	Dimensionless dissipative parameter
d	$[m]$	Water depth
D_0	$[m]$	Characteristic water depth
d_1	$[m]$	Water depth ahead of the bore
d_b	$[m]$	Water depth the bay mouth
d_c	$[m]$	Water depth at continental shelf edge
d_i	$[m]$	Water depth at any shoreward point in the Green's Law formula
d_o	$[m]$	Water depth offshore
E_i	[]	Total energy head (experiments)
Fr	[-]	Froude number, a dimensionless number defined as the ratio of the flow inertia to the external field
Fr_{coast}	[-]	Froude number of the wavefront, used in this thesis
g	$[m/s^2]$	Gravitational constant on earth = 9.81
H	$[m]$	Wave height
H_b	$[m]$	Wave height behind the structure (experiments)
H_f	$[m]$	Wave height in front of the structure (experiments)
H_i	$[m]$	Incident wave height
H_o	$[m]$	Offshore wave height
H_o	$[m]$	Overtopping wave height (experiments)
H_T	$[m]$	Offshore tsunami amplitude
H_w	$[m]$	Height structure (experiments)
H_ξ	$[m]$	Wave height at d = 100 m
K_r	[-]	Refraction coefficient
K_s	[-]	Shoaling coefficient
L	$[m]$	wavelength
L_b	$[m]$	Length bay
L_o	$[m]$	Deep-water wavelength
L_ξ	$[m]$	Wavelength at d = 100 m
R^2	[-]	Coefficient of Determination used to measure how close the date are fitted to the regression line.
S_o	[-]	Slope parameter
t	$[s]$	Time
T	$[s]$	Wave period
T_{TSU}	$[s]$	Wave period of the tsunami at 100 m water depth
u	$[m/s]$	Velocity in x-direction
u_1	$[m/s]$	Cross-sectionally averaged velocity
v	$[m/s]$	Velocity in y-direction
V_i	$[m/s]$	Bore velocity
w	$[m/s]$	Velocity in z-direction
W_b	$[m]$	Width bay
x	$[m]$	Distance
x_0	$[m]$	Start location of the model
x_1	$[m]$	Location of the continental rise
x_2	$[m]$	Location of the continental slope
x_3	$[m]$	Location of bay mouth
x_4	$[m]$	Location of the coastline
x_5	$[m]$	End location of the model

Symbol	[Units]	Description
α_s	[-]	Breaking coefficient SWASH
α_1	[deg]	Continental slope
α_2	[deg]	Continental shelf slope
α_3	[deg]	Slope of the bay
α_4	[deg]	Inland slope
η	[m]	Water level
Φ	[deg]	Mean slope angle of the nearshore profile from the 100 m depth to the Mean High Water elevation
θ	[deg]	Angle of bay convergence
β	[-]	Bay shape coefficient
ϵ	[-]	Nonlinearity ratio (A/d)
μ^2	[-]	Dispersion ratio (d/L)
ξ	[-]	Iribarren number
$\xi_{tsunami}$	[-]	Tsunami breaker parameter (Glasbergen, 2018)
ξ_{100}	[-]	Surf similarity parameter (ASCE, 2016)

1 Introduction

This chapter provides an introduction to the research of the prediction of the characteristics of a tsunami wave near the Tohoku coastline. First, a brief problem description is given in which the relevance of this research emerges. After that, the research objective and multiple research questions are outlined in section 1.2, followed by the approach in section 1.3 and the outline of the report in section 1.4.

1.1. Problem description

On the 11th of March 2011, a magnitude-9 undersea earthquake occurred in the north-western Pacific Ocean near the Tohoku region of Japan. The epicentre of the earthquake was around 70 kilometres east of the coast of Tohoku and the depth of the hypo centre was around 32 km. The earthquake triggered a tsunami which was one of the most destructive tsunamis in history, causing 15,853 casualties, 3,282 missing, 6,023 injured, and over 220 billion dollars of damage along the coastline (Wei et al., 2012). Figure 1.1 shows the destroyed government building in Otsuchi, Iwate prefecture, which was fully inundated by the tsunami wave. Most of the other buildings were washed away. The government building has been preserved to remind the people of the danger of a tsunami event.

Figure 1.1: Destroyed Government building in Otsuchi Town during the 2011 Tohoku Earthquake Tsunami [pictures: J.J. Roubos]

A large variation in inundation and run-up heights was observed along the east coast of Japan during this tsunami event. The tsunami behaviour showed a clear regional dependence on the bathymetry and topography along the coastline. This research focusses on the Tohoku coastline, which mainly consists of the Sendai Plain and the Sanriku coastline, figure 1.2. The vulnerable Sanriku coast is attacked several times throughout history, where the 1896 Meji Sanriku tsunami is the last comparable event before 2011. The Sanriku coastline extends from southern Aomori prefecture, through Iwate prefecture and northern Miyagi prefecture. Sendai is the capital of the Miyagi prefecture. Where the Sendai Plain features a fluvial lowland and a flat coastal plain, the Sanriku coast is known as a "ria-coast" and is a rugged coastline that consists of numerous small bays of variable geometry. A ria coast, with deep bays, is an attractive place to establish a harbour. The fish-

ery industry had become the most important source of income in this area. The human settlement happened near the shoreline, in the bottom of narrow bays, due to the limited flatland at the ria coast. During a tsunami event like in 2011, the waves were amplified in the narrow bays and resulted in destructive flows into coastal towns situated along the inner coasts (Shimozono et al., 2012).

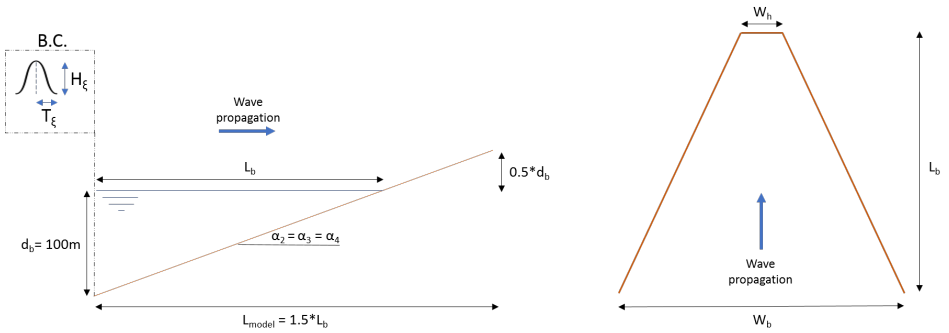

Figure 1.2: Characteristics of the Tohoku coastline. The red symbol indicates the location of the epicentre of the 2011 Tohoku Eartquake

Even with the constructed seawalls and sea dykes up to 10 m or more, the 2011 tsunami led to many deaths and damage. New design rules are accepted to built higher seawalls and sea dykes (figure 1.3), but there are still a lot off uncertainties in wave types and wave loads. The breaking of tsunami waves, as they approach the shore, depends on the local bathymetry and the type of coastline. Figure 1.4 provides several snapshots of Youtube footage along the Tohoku coastline. The wave front can be broken (bore forming) or non-broken (surging/rising water level). Since the Sendai Plain has a gentle sloped continental shelf, tsunami bores will develop in front of the coastline (figure 1.4c). Along the Sanriku coastline, where the slope of the continental shelf is much steeper, different wave types were observed. Figure 1.4a shows wave breaking that has been observed in the Kuji Bay, and figure 1.4b shows a surging wave that propagated into the Miyako Bay. The velocities near the seawalls differ for breaking tsunami waves compared to surging tsunami waves. The velocity near the coastline is an important factor to obtain the dimensionless Froude number or the momentum flux near the structure. Several Design Standards have been proposed that deal with tsunami loads on coastal structures, like the American Society of Civil Engineers (ASCE) and the Federal Emergency Management Agency (FEMA), discussed in chapter 3. FEMA (2012) came up with a classification of coastal inundation in figure 1.5. This classification shows that tsunami waves will attack the shoreline in a different way, but it is not quantitative in the sense that it is not linked to real values. Therefore, a more quantitative understanding of tsunami wave transformation is needed to predict the attack on coastal defence systems like a seawall or a sea dyke along the Tohoku coastline.

(a) Yellow line indicates the location of the planned sea dyke

(b) Sea dyke under construction, height = 14.6m

Figure 1.3: Otsuchi Town [pictures: J.J. Roubos]

Finally, tsunami behaviour is not the same for every observed event. Kato et al. (1961) compared the tsunami inundation heights of the 1933 Sanriku Tsunami and the 1960 Chile Tsunami in Ofunato Bay and Hirota Bay. During the 1933 event, the tsunami height decreased with distance from the bay mouth, and in 1960 the wave

(a) Kuji Bay (Clancy688, 2012)

(b) Miyako Bay (Youtube, 2011)

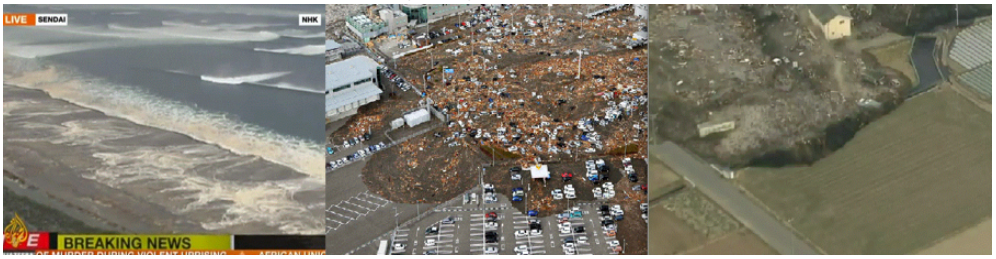

(c) Sendai (CNN, 2011) (Matuo, 2013)

Figure 1.4: Youtube footage from different tsunami wave types at several locations along the Tohoku coastline

height was 2-3 times larger at the bay head than at the bay mouth (Kato et al., 1961). These contrary results raise many questions about tsunami behaviour in a ria coast area.

1.2. Objectives

More insight is needed in the characteristics and the transformation of a tsunami wave approaching a ria coast to increase the safety of flood defence systems in the future. The steep ria coast of Sanriku will be compared to the gentle sloped Sendai Plain.

Main question
How can the characteristics of a tsunami wave be predicted along the Tohoku coastline?

Sub questions

- How can the Tohoku coast in Japan schematically be classified?
- What are the most important parameters to model tsunami waves propagating towards the coast?
- Which parameters influence the type of tsunami at the coastline?
- How to find a breaking parameter for a tsunami wave in a bay?

1.3. Approach

This research is part of an interdisciplinary project on the post-tsunami reconstruction in Japan, where the students visited Otsuchi (figure 1.3) to learn from the tsunami reconstruction processes after the 2011 Tohoku Earthquake Tsunami. Otsuchi is a small fishing village along the Sanriku coast and is characterized by a ria coast. During the 2011 Tohoku Earthquake Tsunami half of the city was inundated and more than 10% of the inhabitants lost their lives. The purpose of this thesis is to provide more insight into different wave types

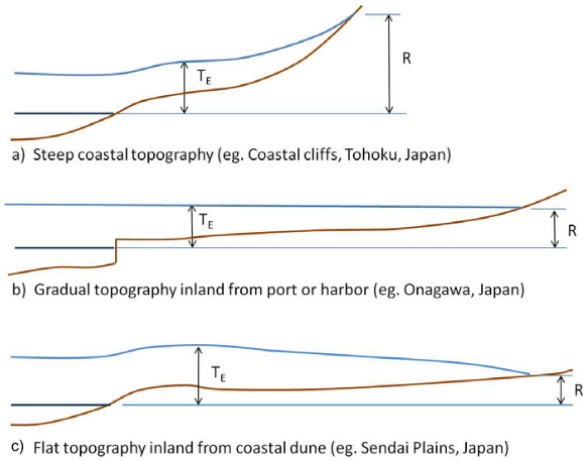

Figure 1.5: Classification of coastal inundation where T_E is the tsunami elevation and R the run-up elevation.

along the Sanriku coast, which can be used as a boundary condition in the multidisciplinary project.

To find the importance of surface roughness on the potential overtopping mechanisms of tsunami bores as they hit coastal structures, physical experiments have been conducted in the Waseda University wave flume by using a dam-break mechanism. The results and conclusions of the experiments are given in appendix A and are reported in (Esteban et al., 2019).

The first step in this research is to make a 1D model from the source of the 2011 Tohoku Earthquake Tsunami to the continental shelf to simulate the offshore propagation. This model will be validated with observed wave measurements of the GB802 wave buoy in front of the Otsuchi bay. The results of the model can be compared with the linear wave approximation Green's law. If nonlinear and 2D propagation effects are limited during the propagation to the continental shelf, a quick approximation of the wave elevation near the coast can be made which saves a lot of time.

The second step is to model the nearshore tsunami wave behaviour to obtain an improved tsunami breaker parameter. The nearshore wave behaviour can be modelled by using the nonlinear shallow water equations (SWE) in a 1D or a 2DH SWASH model.

A schematized model, based on model assumptions, is used to represent reality. This model helps to understand the role of different parameters in the transformation of tsunami waves. Based on this schematic model, detailed calculations are performed by using the numerical program SWASH (Simulating WAves till SHore).

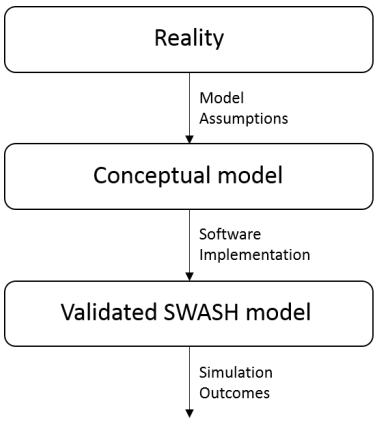

Figure 1.6: Modelling steps

1.3.1. Simulations SWASH

To simulate large-scale wave evolution and shallow water flows efficiently, an approach is adopted where the free-surface motion is tracked using a single-valued function of the horizontal plane. This makes SWASH a more suitable program than Volume-of-Fluid (VOF) and Smoothed Particle Hydrodynamics (SPH), which can describe fluids in a more detailed but more time-consuming way. SWASH is a phase-resolving model which is based on vertically integrated, time-dependent mass and momentum balance equations. The governing equations are the nonlinear shallow water (NLSW) equations, including the non-hydrostatic pressure. The SWASH model stands out in its ability to simulate complex nearshore processes, including wave breaking, nonlinear interaction, wave run-up and wave-induced circulation and can describe shallow water flows in coastal areas due to tsunamis. A further distinguishing feature is the numerical implementation of momentum conservation, which is a prerequisite for a plausible representation of hydraulic jumps and bores and is therefore important in this research. Mass and momentum are strictly conserved at a discrete level while the method only dissipates energy in the case of wave breaking (Stelling and Zijlema, 2009). Finally, the SWASH model requires just one tuning parameter for wave breaking, which in practice is relatively easy to estimate (Zijlema et al., 2011). This model is validated multiple times, and the computed results show a good agreement with analytical and laboratory data for wave propagation, transformation, breaking, and run-up within the surf zone (Stelling and Zijlema, 2009).

SWASH uses a hydrostatic front approximation which is an effective and efficient method to approximate wave-breaking phenomenons in the non-hydrostatic phase resolving model. The hydrostatic pressure is assumed at the front of the wave when it exceeds a certain threshold of the steepness of the wave, equation 1.1. The range of maximum steepness (α_s) varies in literature, from $\alpha_s = 0.3$ (Schäffer et al., 1993) to $\alpha_s = 0.6$ (Lynett, 2006). The threshold used in SWASH is based on simulations of flume experiments and a α_s of 0.6 is advised, which correspond to a local front slope of 25° (Smit et al., 2013). There is no need to calibrate this value since it seems to work well for all test cases carried out by the authors of SWASH. The energy dissipation due to breaking is accounted for by ensuring that mass and momentum are conserved once the wavefront is transferred into a bore-like shape.

The content of SWASH is described in more detail by Zijlema et al. (2011). The SWASH Manual (TeamSWASH, 2010) gives a good approach to start your own simulations. A quick overview of the most important equations is given in appendix C.

$$\frac{\partial \zeta}{\partial t} > \alpha_s \sqrt{gd} \tag{1.1}$$

1.3.2. Schematized model

The Tohoku coastline will be schematized to be able to apply the results and recommendations at different locations with similar coast characteristics. The advantage of a schematic model is that the influence of each characteristic parameter can be reviewed individually.

The parameters of the bathymetry are drawn in Figure 1.7. One important parameter in this research is the slope of the continental shelf α_2, which varies along the Tohoku coastline. The Sendai Plain is characterized by flat sandy beaches with a gentle sloped continental shelf. The Sanriku Coast is characterized by steeply formed bays (ria coast) and has a steep sloped continental shelf.

The other important parameter is bay geometry. Figure 1.8 shows the schematic ria bay along the Sanriku coast. The parameters of the schematic bay can be changed one by one to see the influence on the characteristics of the tsunami wave.

Glasbergen (2018) did research on the offshore tsunami wave parameters and concluded that the continental shelf is the most important factor of the bathymetry of the Sendai Plain. The wave characteristics, wavelength L and wave height H, are also very important. The main focus of this research is the tsunami wave characterization from the edge of the continental shelf up to the ria coastline of Sanriku. The goal of the research is to find a new breaking parameter for a tsunami wave approaching a ria coast. This breaking parameter is related to:

1. wave parameters (H and L);
2. slope of the continental shelf (α_1);

3. geometry of the ria bay (d_b,α_3,L_b, W_b and W_h)

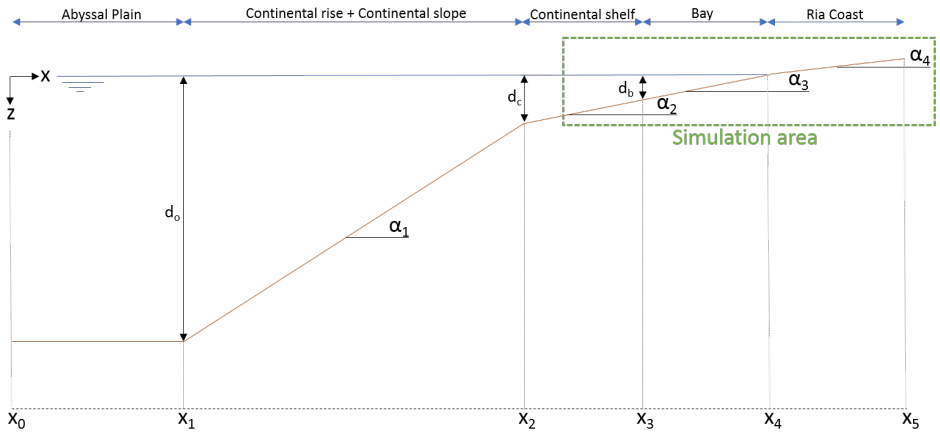

Figure 1.7: Schematic ocean topography with parameters (1D)

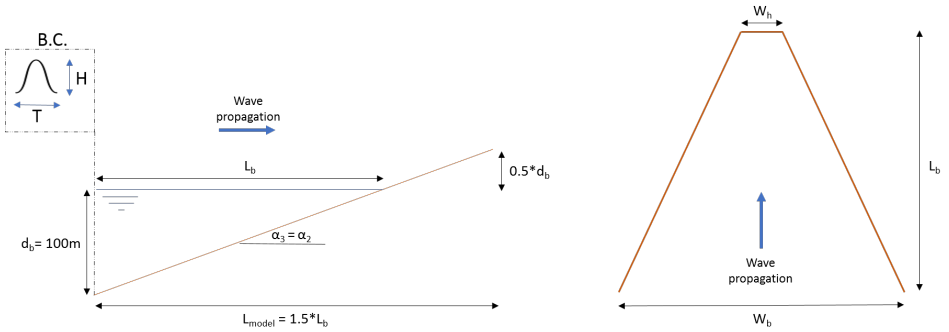

Figure 1.8: Schematic ria bay at the Sanriku coast

1.3.3. Definition Froude number

In this research, a Froude number at the coastline Fr_{coast} during maximum velocity is proposed. For every simulation, Fr_{coast} is obtained by using the characteristics of the wavefront when inundation of the coastline takes place. u_{max} is taken as the maximum flow velocity during inundation at the coastline x=0, averaged over the cross-section perpendicular to the flow direction. h_{front} is the water depth at the coastline during maximum velocity.

$$Fr_{coast} = \frac{u_{max,coast}}{\sqrt{(g h_{coast})}} \tag{1.2}$$

1.4. Outline of the report

In chapter 2, the most relevant background theory is given to understand the technical processes in this report. An overview of the studies carried out so far in this field of research are given in chapter 3, where the conclusions can be used as a guideline in this research. Chapter 4 describes the input and set-up of a 1D SWASH model describing the propagation of a tsunami wave from the source of the tsunami up to the continental shelf, followed by a discussion and the conclusions of the results. The nearshore tsunami wave transformation is investigated by a 1D and a 2DH SWASH model and is discussed in chapter 5. A discussion of the made assumptions and the obtained results are given in chapter 6. Finally, the conclusions and recommendations are outlined in chapter 7. The appendices are attached to give more background to different parts of the report, including the details of the performed physical modelling experiments in appendix A, carried out at the Waseda University in Tokyo.

2

Background theory

This chapter lines out the basic background theory needed to understand the rest of the research. First, a short introduction is given about tsunami generation in section 2.1. After that, tsunami characteristics and specific wave propagation processes are described in section 2.2 and 2.3. Finally, explanations are given about used theories to describe tsunami waves in section 2.4.

2.1. Cause of a tsunami

Tsunamis can have different causes; earthquakes, landslides, volcanic eruptions or even incoming comets. Tsunamis caused by point sources (landslides, volcanic eruptions and incoming comets) may be highly destructive locally. On the other hand, seismic action along a subduction zone (earthquakes) may cause a long length of fault to move, causing a longer wavefront which reduces less with distance than from a point source, causing potentially more damaging to coastlines (Allsop et al., 2014). Tsunamis caused by point sources are rare in comparison with tsunamis caused by undersea earthquakes. Therefore, this thesis is focussing on the tsunamis caused by an undersea earthquake (Figure 2.1). The surface of the Earth consists of tectonic plates which are continuously slowly moving from each other. Near tectonic plate boundaries (fault line) a phenomenon called 'tectonic subduction' occurs, where an oceanic plate is being forced down into the mantle by plate tectonic forces. Tectonic plates have large roughness coefficients, therefore moving tectonic plates can build up an enormous amount of energy during subduction which can be released after slipping, similar to the energy stored in a compressed spring. After slipping, the overriding plate snaps back into an unrestrained position. The leading edge of the overriding plate breaks free, springing seaward and upward (wave crest). Behind, the plate stretches and its surface falls (wave trough). This last phenomenon clarifies the observations of a rapid drawback of water at the coastline prior to the arrival of a tsunami wave crest. The initial free surface profile can be approximated as having the same shape as the seafloor deformation at the end of rupture (Liu, 2009). When the fault plane is elongated, the initial free surface profile is almost uniform over the fault line and the tsunami propagates mainly in a perpendicular direction of the fault line. These tsunami waves attempt to regain its equilibrium and consist of a series of water waves ("wave train") with an extremely long wavelength and long period (Liu, 2009).

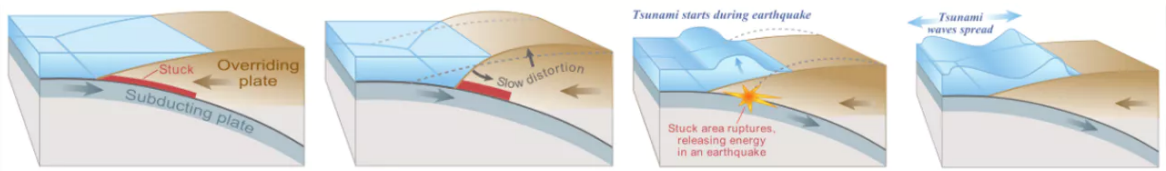

Figure 2.1: Submarine earthquake, cause of a tsunami (Atwater et al., 1999)

2.2. Tsunami characteristics

Figure 2.2 gives an overview of the characteristics of a schematic wave. These basic parameters can also be used to describe the characteristics of tsunami waves. The wave height (H) is the difference between the lowest point of a wave (trough) and the highest point of a wave (crest). The wave amplitude (A) is the distance from the centre of the wave to the crest or the trough. The wavelength (L) is the distance between adjacent maxima or minima of a wave. The wave period (T) is the time for one full wavelength to pass a given point.

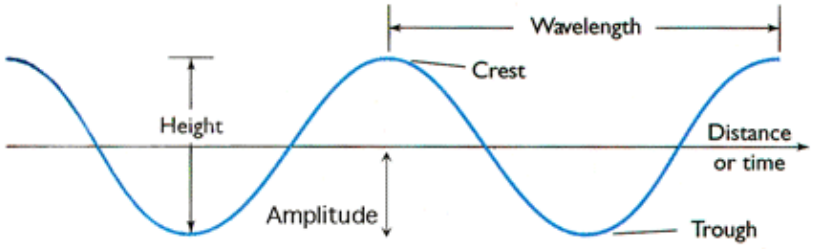

Figure 2.2: Basic wave parameters (James, 2016)

2.2.1. Tsunami waves

Tsunami waves are different from ordinary wind-generated waves but have some things in common. Both waves have a trough and a crest and consist not of moving water but the movement of energy through water. Tsunami and wind waves can undergo shoaling, refraction, reflection and diffraction. They differ in where the energy comes from. For wind-generated waves, it comes from wind blowing over the surface. Because it only affects the surface, the waves are limited in size and speed. Tsunamis are originated underwater (landslides, volcanic eruptions or earthquakes), where an enormous amount of energy is released and travels up to the water surface. A tsunami wave can have a wave period of ten minutes to two hours and wavelengths greater than 500 km (Bryant, 2014). Even in the open ocean, where the depth can be several kilometres, the tsunami wavelength (L) is much larger than the water depth (d). Therefore, tsunami waves can be described as shallow water waves and they influence the entire water depth of the ocean.

Table 2.1: Wind waves vs. Tsunami waves

	Wind Wave	**Tsunami Wave**
Wave period (T)	5 - 20 s	10 m - 2 h
wavelength (L)	100 - 200 m	100 - 500 km
Wave speed (c)	8 - 100 km/h	up to 1000 km/h

Another difference between wind and tsunami waves is the breaking of the waves and the storage of their energy. Wind waves break in shallow water and expend all their energy at the coastline. On the other hand, tsunami waves mostly come ashore as a 'rapid rising tide', where the energy pours all the water onto land for several minutes to an hour.

2.3. Tsunami wave propagation

2.3.1. Shoaling and refraction

Most people imagine a tsunami wave as a large breaking wave, but in the open ocean the wavelength is very long and the amplitude is quite small and therefore the tsunami can be unnoticed by sailing ships. When a wave travels to the coast and 'feels' the bottom it experiences a force from the seabed which will slow down the wave. As waves slow down they start bunching together and become shorter than in the open ocean. When the wavelength becomes smaller, the wave height must increase due to the conservation of energy. This phenomenon is called "shoaling".

Refraction is the change in direction which is caused by parts of the wave moving with different wave speed as the water depth along the wavefront varies. Since tsunami waves are shallow water waves, they always feel the bottom of the ocean and their crest undergo refraction around the topography. In the nearshore area,

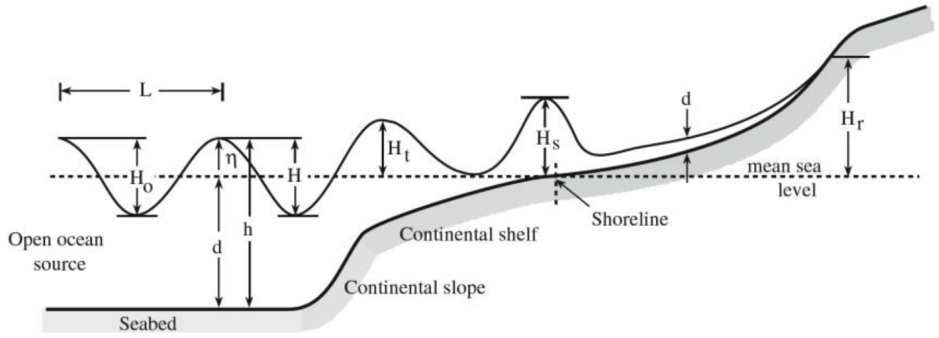

Figure 2.3: Tsunami wave propagation and shoaling (Irwanto, 2015)

refraction forces the wave to arrive perpendicular to the shoreline (figure 2.4).

Linear theory can be used as a first approximation to calculate changes in tsunami wave height as the wave moves across an ocean (Bryant, 2014). A classic linear theory for shoaling is called Green's Law and applies for cases where the depth varies slowly (Lipa et al., 2016). Green's law is given in equation 2.1 where K_s is the shoaling factor, K_r the refraction factor and H_o the offshore wave height. The shoaling factor depends on the offshore water depth (d_o) and the initial water depth (d_i). The important parameters for refraction are based on the distance between the two lines of the wave crests, offshore (b_o) and more nearshore (b_i), and is explained in figure 2.4.

$$H = K_r K_s H_o \qquad with: \quad K_s = (\frac{d_o}{d_i})^{0.25} \quad ; \quad K_r = (\frac{b_o}{b_i})^{0.5} \tag{2.1}$$

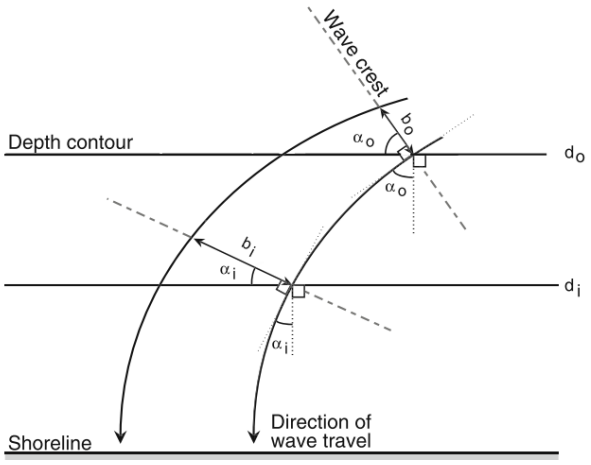

Figure 2.4: Schematization of refraction (Bryant, 2014)

2.3.2. Reflection

When a tsunami wave encounters an abrupt step in the bathymetry, a part of the wave will be reflected which will reduce the energy of the wave. In this research, the bathymetry is assumed to be linear and therefore the reflection due to changes in sea bottom is small.

The second or third wave in the tsunami wave train can be amplified due to reflection when the first wave interacts with shelf topography (Bryant, 2014). After run-up of the first tsunami wave, the receding wave holds tremendous energy. If this receding wave interacts with the second incoming wave and releases their kinematic energy, the incoming wave is forced to increase in size. In this research, single waves are analysed to disregard the influence of reflection between successive waves.

2.3.3. Breaking

When a tsunami reaches the shore, it may often appear as a rapidly rising or falling water. Sometimes it comes ashore as a series of breaking waves or even a bore.

The Iribarren number ξ from Battjes (1974) gives an expression for the relation between non-breaking and breaking progressive waves on a slope, in which α is the slope angle, H is the wave height at the toe of the slope and L_o is the deep-water wavelength.

$$\xi = \frac{tan\alpha}{\sqrt{H/L_o}} \tag{2.2}$$

Grilli et al. (2002) came up with a slope parameter S_o, equation 2.3, for solitary waves. This parameter shows the type of breaking which will occur for a given slope; a spilling wave, a plunging wave or a surging wave.

$$S_o = \frac{tan\alpha \cdot L_o}{h_o} = 1.521 \frac{tan\alpha}{\sqrt{H_o}} \tag{2.3}$$

Figure 2.5: Breaking wave types (Wikimedia, 2016)

- Spilling breaking: $S_o < 0.025$
- Plunging breaking: $0.025 < S_o < 0.30$
- Surging breaking: $0.3 < S_o < 0.37$

For tsunami waves, this classification is not that clear. Wave dissipation due to undular bore formation (section 2.4.2) can occur when propagating over a gentle slope, where the small amplitude waves can break eventually. Wavefront breaking can happen for steeper slopes. Once a tsunami wavefront has been broken, it can be considered as a bore because of its very long wavelength (FEMA, 2012).

2.4. Tsunami wave theory

The theory to describe tsunami wave propagation differs for the offshore and the nearshore case. In most cases, the offshore tsunami propagation can be described by the linear shallow water (LSW) equations and the nearshore propagation by the nonlinear shallow water (NLSW) equations.

2.4.1. Offshore behaviour

Section 2.1 explains the cause of an earthquake-generated tsunami. The wavelength is generally determined by the width of the fault plane (Liu, 2009). Tsunami wave dispersion is represented by the depth-to-wavelength ratio, $\mu^2 = d/L$, and the nonlinearity by the amplitude-to-depth ratio, $\epsilon = A/d$ (Liu, 2009). After the 2011 Tohoku Earthquake, the offshore wavelength of the first tsunami wave was approximately 360 km (Tang et al., 2012) and the wave amplitude was in the order of meters. For this tsunami event, both the frequency dispersion and the nonlinearity effects were small and could be neglected for offshore propagation. Liu (2009) discussed the applicability of linear and nonlinear shallow water equations for different ocean depths in the China Sea. There is a critical zone between 400 and 500 m depth for employing linear and nonlinear models. Therefore, the LSW equations are adequate relations to describe the initial stage of tsunami propagation in this case.

The wave speed (c) for LWS waves only depends on the water depth, see equation 2.4. Since the average water depth in the Pacific Ocean is 5km, a tsunami can travel at a speed of about 800 km/h, which is almost the same as the speed of a jet plane (Liu, 2009).

$$c = \sqrt{gd} \tag{2.4}$$

2.4.2. Shallow water limit

Due to the shoaling effect, the dimensions of tsunami waves change when propagating to the coastline. The wave height increases and the wavelength decreases and therefore nonlinearity and dispersive effects become more important.

The NLSW equations can be used to model coastal tsunami effects. Numerical modelling is used in this research to make 1D and 2DH nearshore models, which includes the NLSW equations. SWASH is proved to reproduce the main features of surf zone dynamics, such as nonlinear shoaling, wave breaking and wave run-up (TeamSWASH, 2010).

Soltion fission and solitary waves

As described in subsection 2.4.1, frequency dispersion and nonlinearity effects depend on the wavelength, wave amplitude and the water depth. Liu (2009) concluded that frequency dispersion effects might need to be considered if the initial wavelength is short and the distance of propagation is relatively large. In time, individually negligible nonlinear factors have a significant cumulative nonlinear effect that is balanced by dispersion to sustain waves of almost permanent form at sea, with the tsunami becoming a manifestation of solitons (soliton fission) (Constantin and Henry, 2009). The Korteweg-de Vries (KdV) equation, equation 2.5, represents the soliton theory. For the KdV equation, an initial waveform evolves existing of multiple solitons and an oscillatory tail. The taller solitons travel faster, while the oscillatory tail moves slower, disperses and spreads out in space (Constantin and Henry, 2009). A soliton completely separated from the other solitons is called a solitary wave. In the past, it has been assumed that solitary waves can be used to model tsunami waves in the nearshore area (Goring, 1978). These solitary waves move water and they all lay above mean sea level. Solitary waves have the advantage that the wave can be described with only two parameters, the water-depth (d) and the wave height (H) (Goring, 1978).

Figure 2.6 shows two ways to model tsunami generation and propagation. The red line is computed with the SWE and forms an asymmetric wavefront which can lead to bore formation later on. The blue line is computed with the solitary theory, which forms a soliton wave retaining the identity with an oscillatory tail staying behind.

$$\frac{\partial u}{\partial t} + \frac{\partial^3 u}{\partial x^3} - 6u\frac{\partial u}{\partial x} = 0 \tag{2.5}$$

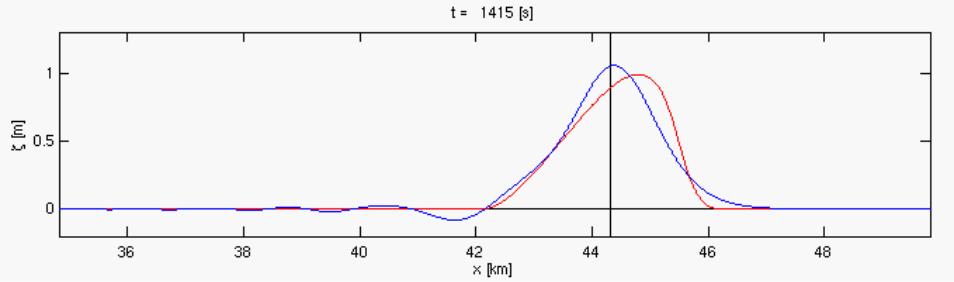

Figure 2.6: Blue line: solitary wave theory with frequency dispersion; Red line: SWE without frequency dispersion (Wikipedia, 2018)

Once the KdV threshold is exceeded, the tsunami wavefront will start to develop as a nonlinear undular bore and eventually, the leading wave may turn into a separate solitary wave. However, the justification of this solitary wave forming is rather weak because the link to geophysical tsunamis has never been established (Madsen et al., 2008). Madsen et al. (2008) concluded that tsunamis, in general, do not generate solitons in the ocean or on the continental shelf because of these geophysical constraints. Therefore, undular bore formation is covered in this research but solitary wave formation is not.

$$\eta(x,t) = H sech^2(K_s(x-ct)); \qquad K_s = \frac{1}{h}\sqrt{\frac{3}{4}\frac{H}{d}}, \qquad c = \sqrt{g(d+H)} \tag{2.6}$$

Undular bore formation

During tsunami events (Thailand 2004, Japan 2011), observed tsunami waves are sometimes described as

breaking waves in front of the coastline. However, most likely is that these breaking waves are the short waves riding on top of the main wave which we call an undular bore. In the nearshore area, the front of a tsunami wave can evolve into a large range of bore types, from an undular non-breaking bore to purely breaking bore (Tissier et al., 2011). Tsunami waves in the open ocean are non-dispersive long waves. When they propagate to the nearshore area, dispersive effects can become significant (Dalrymple et al., 2015). Madsen et al. (2008) investigated the phenomenon of the disintegration of long waves into shorter waves, typically of the order 10s-15s. As mentioned, the further transition of these undular bores into leading solitons rarely happens due to geophysical constraints. Therefore, solitary wave forming is not part of this research.

Grue et al. (2008) studied numerically how undular bore formation can occur from the initial tsunami wave when propagating over a shallow slope. Breaking was not taken into account in these studies. Tissier et al. (2011) researched the transition from undular to purely breaking bores when propagating over an initial step over a flat bottom. The Froude numbers varied from 1.10 to 1.90 and some results are shown in figure 2.7. The Froude number is a dimensionless number for the ratio of flow speed to the characteristic speed of a shallow water wave, see equation 2.7 where u is the averaged flow speed over a cross-section and d is the depth. For Fr<1.40, the initial step evolves into an undular jump. For Fr=1.40, the front of the wave is broken. For higher Froude numbers (Fr>1.40), purely breaking bores were obtained. Experiment results from Chanson (2009) shows that the maximum amplitude of the wave train is in the range of Fr=1.27 and Fr=1.7 and that the undulated wave train is disappearing for Fr=1.5 to 3. This is in good agreement with the results of Tissier et al. (2011).

$$Fr = \frac{u}{\sqrt{(gd)}} \tag{2.7}$$

Shimozono et al. (2014) investigated the variety of waveforms along the northern Pacific coast of Japan during the 2011 Tohoku Earthquake Tsunami. The short wavelength components, localized in the leading wave, was found to play a key role in tremendous amplification in small bays or inlets (Shimozono et al., 2014). Short wavelength components, in undular bores, can thus be really important in tsunami wave amplification at the Sanriku coast. Besides the impact on amplification, the transformation of bores in the nearshore area is important for the impact on coastal structures, since the Froude number and the momentum flux will change and therefore the velocity and forces in front of the structure will change (Chock, 2016).

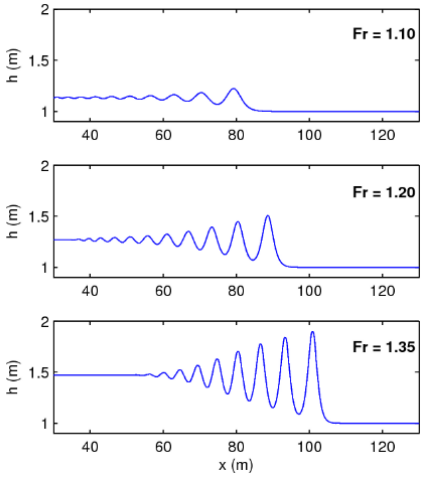

(a) Froude number: 1.10 to 1.35

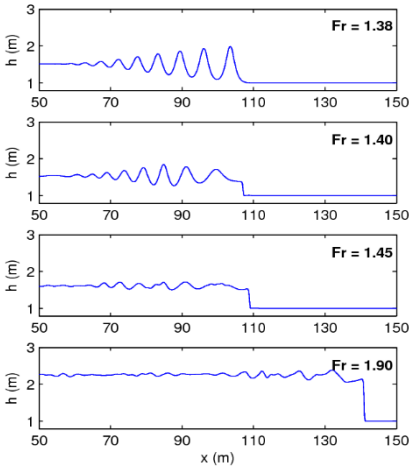

(b) Froude number: 1.38 to 1.90

Figure 2.7: Bore shapes for varying Froude numbers (Tissier et al., 2011)

3

Previous studies and Standards

Where in chapter 2 the fundamental theory is explained about hydrodynamics and tsunami behaviour, this chapter gives an overview of the studies carried out so far in this field of research. The main goal of the literature study is to investigate the knowledge about tsunami wave transformation approaching a ria type of coast, like Sanriku in the northern part of Japan.

Several standards have been proposed for tsunami loads on structures. The standards of the American Society of Civil Engineers (ASCE) and the Federal Emergency Management Agency (FEMA) are discussed in section 3.1 and 3.2 respectively. Since this research is a follow-up study of Glasbergen (2018), some results and study approaches of this previous study are given in section 3.3, 3.4 and 3.5. The type of a tsunami wave depends on the bathymetry and the type of coastline. Therefore, a classification of the Japanese coast is made in section 3.6. The 2011 Tohoku Earthquake Tsunami was a huge tragedy, but many lessons can be learned from this event which is discussed in section 3.8. An overview of the current defence structures and their design guide lines are outlined in section 3.9. Finally, in section 3.10 a summary and discussion is given in which the importance of the literature review emerges for this research.

3.1. ASCE 7-16: Design for Tsunami Loads and Effects

Velocity is an important parameter to see what the impact will be on a coastal structure like a seawall. ASCE (2016) gives the energy grade line analysis to determine the inundation depth and associated flow velocity across the inland profile. The velocity is calibrated to the Froude number at the coastline.

When a tsunami travels over a mild sloping continental shelf, short-period waves can be generated on the front of the main wave, which is called undular bore formation and can become soliton fission if it travels for a long time (ASCE, 2016; Grue et al., 2008; Madsen et al., 2008; Tissier et al., 2011). Bore forming can occur in the nearshore area, where the short-period waves break. The existence of bore formation on the front of a tsunami wave is important for the wave speed and thus for the impulsive impact on the seawall. ASCE (2016) assumes that the Froude number coefficient at the coastline is 1.0 for situations without bore formation and 1.3 for situations with bore formation. They consider bore formation for prevailing nearshore bathymetric slopes of 1/100 and milder, when historically documented, described by recognized literature or determined by a site-specific inundation analysis.

To calculate run-up a surf similarity parameter is proposed, given by equation 3.1. However, this surf similarity parameter is not valid where there is an expectation of wave focussing such as in V-shaped bays.

$$\xi_{100} = \frac{T_{TSU}}{cot\Phi}\sqrt{\frac{g}{2\pi H_T}} \tag{3.1}$$

3.2. FEMA - Loads on vertical structures

FEMA published a guideline for designing structures for vertical evacuation from tsunamis. The most important wave forces on a seawall or dyke are the hydrostatic (F_h), the hydrodynamic forces (F_d) and impulsive

forces (F_s).

Hydrostatic forces may be relevant for long structures such as seawalls and dykes, where the water level differs between the two sides of the structure. For surging waves, where standing or slowly moving water encounters the vertical structure, hydrostatic forces become significant. Hydrodynamic forces occur due to high velocity of water flowing around a structure. For seawalls, these forces become significant after fully overflow.

The combination hu^2 represents the momentum flux per unit mass per unit width. This parameter $(hu^2)_{max}$ is important for the hydrodynamic forces on the structure. The maximum momentum flux can be obtained by numerical modelling such as SWASH and needs a fine grid near the structure to ensure adequate accuracy in the prediction of hu^2 (FEMA, 2012).

$$F_h = \rho_c A_w = \frac{1}{2}\rho_s g b h_{max}^2 \tag{3.2}$$

$$F_d = \frac{1}{2}\rho_s C_d B (hu^2)_{max} \tag{3.3}$$

Impulsive forces are really important for the design of a seawall or sea dyke since the force during initial impact can about 50% higher than the resistance force during the bore passing (Árnason, 2005). The impulsive forces are caused by the leading edge of a surge of water (FEMA, 2012). Experiments performed by Ramsden (1993) concluded that the impulsive forces are not significant for dry-bed surges, but an "overshoot" of this force was seen for bores propagating when the site was inundated. Since the impact momentum increases with the steepness of the bore front (Yeh, 2006), the relatively mild slope for the wavefront of dry-bed surges is the cause of the minimum impulsive impact.

$$F_s = 1.5 F_d \tag{3.4}$$

3.3. Sensitivity of offshore tsunami parameters

Glasbergen (2018) investigated the sensitivity of tsunami wave and bathymetry parameters. The methodology is comparable to this research, where a 1D SWASH model was used to see the tsunami propagation from the origin to the coastline near Sendai.

The wave used for the SWASH tests was a sine-wave that looks like the 2011 Tohoku Earthquake Tsunami wave with a crest of 8 m and a proceeding trough of 2 m. The length is 100 km for the crest and 50 km for the trough, which gives a total wavelength of 150 km.

Continental slope α_1
Simulations were done for continental slopes α_1 ranging from vertical to 1:50. The difference between the smallest and highest wave elevation is 11.2% maximum. The most common continental slopes are between 1:10 and 1:20. The difference between these slopes is only 4% in wave elevation and 1.2% in wavelength, so the continental slope will be kept constant in this research.

Offshore depth d_o
For the offshore depth, simulations are done for depths ranging from 3000 to 6000 m. The elevation height differences between the highest and smallest wave is a 14% difference. Besides, the wavelength of the simulations is 30% larger for the simulation with a depth of 3000m compared to the 6000m simulation. This could be important for the breaking of the tsunami wave. However, this research is applied to the Japanese coast where the offshore depth is constantly 6000m. The offshore depth d_0 will therefore be kept constant.

Initial wavelength L_0
Simulations were done for three different offshore wavelengths; 100, 150 and 200 km. The shortest wavelength has the highest water elevation, but the difference is only 1.3%. However, the offshore wavelength is an important parameter for the steepness of the front of the wave and is therefore important for wave breaking. Since tsunamis can have wavelengths ranging from 10 to 500 km (Bryant, 2014), more research needs to be done about the sensitivity of L_0 on the tsunami characteristics near the coastline.

3.4. Bore simulations

Since it is hard to define the height of the wavefront of a tsunami and the corresponding velocity, Glasbergen (2018) gave some simple definitions for these characteristic parameters. For simulations where bore formation occurs, there is a maximum velocity at the bore front. This location, just behind the bore front, is where the maximum local depth-averaged velocity (u_{bore}) and the bore front height (h_{bore}) are defined. In the simulations, the wavefront shows a sloped front with a change in slope at the location of the wavefront height.

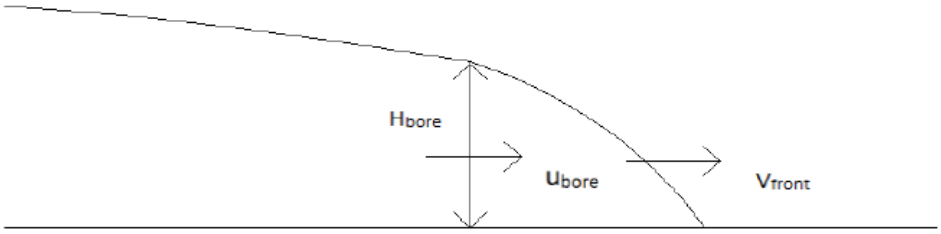

Figure 3.1: Sketch of a bore with their characteristics (Glasbergen, 2018)

Glasbergen (2018) used a dimensionless parameter, the local Froude number (Fr_{bore}), to analyse different bores. u_{bore} is the maximum velocity when the wavefront reaches the coastline and h_{bore} is the height of the bore at the location of this maximum velocity. This parameter is only used for simulations where a bore is formed before the coast or on the coast.

$$Fr_{bore} = \frac{u_{bore}}{\sqrt{g * h_{bore}}} \tag{3.5}$$

In this thesis, it is important to distinguish whether a wave breaks or not. Not every broken tsunami front is immediately a bore. This is the reason that in this thesis 'bore' is replaced by 'front'.

3.5. Tsunami breaker parameter

As described by ASCE (2016), it is important to know if bores are formed in front of a tsunami wave since the impact on the structure can be different for these situations. Glasbergen (2018) combined the Iribarren number, equation 2.2, with tsunami parameters and proposed a breaker parameter for tsunami waves ($\xi_{tsunami}$).

$$\xi_{tsunami} = \frac{tan(\alpha_2)}{\sqrt{\frac{H_\xi}{L_\xi}}} \tag{3.6}$$

where α_2 is the slope of the continental shelf, H_ξ is the wave amplitude at the location where the depth is 100 m and L_ξ is taken as the length from the wave peak to the wavefront, see figure 3.2. The tail of the wave is left out because Glasbergen (2018) showed that the length of the tail does not influence the breaking of the wave.

The tsunami parameter describes the tsunami wave as a plunging or a surging wave. The plunging wave is described as all the waves where the maximum local depth-averaged bore front velocity (u_{bore}) is located no further than 30m inland. A surging wave is a wave where this maximum velocity is further than 30 m inland.

$$\begin{aligned} Plunging: &\quad \xi_{tsunami} < 0.35 \\ Surging: &\quad \xi_{tsunami} > 0.35 \end{aligned} \tag{3.7}$$

Figure 3.3 shows the relation between the breaker parameter and the Froude number. (Glasbergen, 2018) recommended improving the breaker parameter by investigating the exact location of breaking. Another

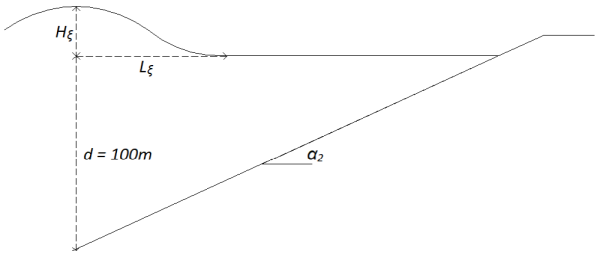

Figure 3.2: Sketch of parameters for Tsunami breaker parameter (Glasbergen, 2018)

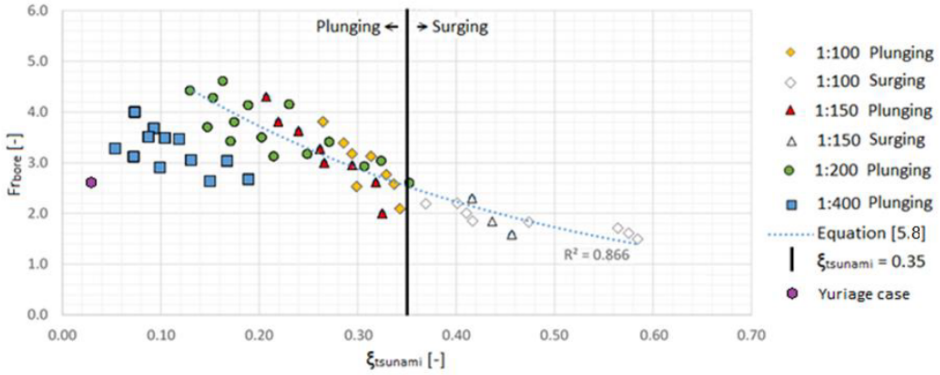

Figure 3.3: Froude number at maxiumum velocity vs breaking parameter. Relation between the Froude number and the breaker parameter for slopes steeper than 1:200 (dotted line). Breaker relation equation 3.7 (black line). Empty markers are surging breakers. (Glasbergen, 2018)

shortcoming is that equation 3.7 only gives a distinction between plunging and surging waves. More numerical simulation need to be performed to find the transition from plunging to spilling breakers, which is called 'bore front breaking' and 'undular breaking' in this report.

3.6. Classification of the Tohoku coastline

To predict the tsunami behaviour at the coastline, it is important to consider the morphology along the Tohoku coastline. This coastal zone can be classified into two categories: 1) the ria coast in the northern half of Tohoku, and 2) the coastal plain in the southern half. Rias are fyord-like shaped coastal inlets formed by the submergence of former river valleys (Tsimopoulou, 2012). The research mainly focuses on ria type of coasts as in the north of Japan. These results will be compared with the results of Glasbergen (2018), where the main focus was a gently sloping beach at the Sendai Plain.

3.6.1. Type of tsunami wave

Figure 1.5 shows that for different topographies of the coast, different types of run-up will occur. The southern part of Tohoku, from Sendai city until Fukushima, is characterized by mild sloping sandy beaches. The intrusion of tsunami waves is not obstructed by high grounds. Therefore, the tsunami wave can break at the shore and propagate inland and inundate large areas with 'low' inundation heights. The northern part of Tohoku is characterized by rias coasts, where due to the focusing effect of the bathymetry the tsunami height can increase enormously. At these coasts, the intrusion of tsunamis is obstructed by the cliffs around the bays. Together with the increase of tsunami height, this resulted in large inundation and run-up heights.

3.6.2. Bathymetry

A clear difference in bathymetry between the Sendai Plain and the Sanriku ria coast is shown in Figure 3.4. The continental shelf is considered to be limited within the areas up to 200 meters depth, according to the Convention on the Continental Shelf (Sato and Oshima, 1988), which can also be seen in figure 3.4. The slope of the continental shelf is much smaller for the Sendai Plain compared to the Otsuchi and Kuji Bay. Kim and Son (2018) described the energy, mass, and momentum of travelling nearshore tsunamis to analyse the

tsunami damping mechanism at typical geophysical scales. The results of the research were consistent with field observations; continental shelves with long and mild slopes can effectively diminish tsunami impacts. According to Kim and Son (2018), the potential energy becomes significant due to the energy transformation process on steeply sloped bathymetries like the east coast (rias) of Japan. This can be explained by a simple mechanical model of energy distribution. When a tsunami travels over a gently sloping shelf, energy is dissipated mainly by friction. For steep slopes, this dissipation is much less which results in a larger transformation from kinetic to potential energy at the coast(Ogami and Sugai, 2018). All these conclusions give strength to the fact that the tsunami impact along the ria coast of Japan was much higher than for the mild slope coastal plains. However, for the impact on coastal structures, the loads can be higher for tsunami waves with bore formation. This seems contradictory, but it depends on if you look to the impact on the structure or if you look at the run-up and inundation heights without a structure.

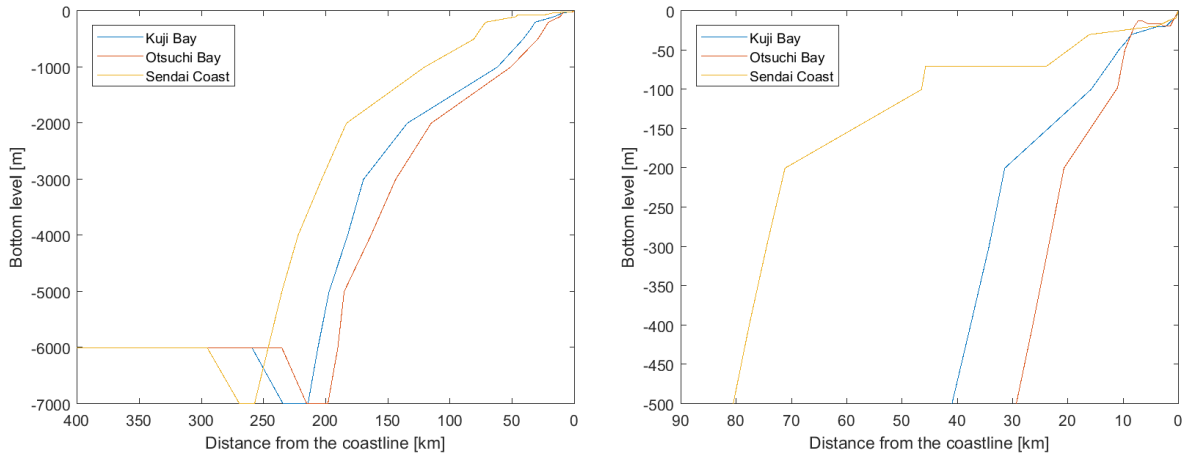

(a) Cross-section bathymetry Otsuchi

(b) Cross-section bathymetry Otsuchi (zoom in)

Figure 3.4: Bathymetry perpendicular to the coast; data obtained from 'Navionics'

3.6.3. Sanriku Ria coast

As been explained, the Sanriku coast is characterised by a ria type of coast which is an intended coastline. The different geometries of the intended coastline are seen in figure 3.5. The bays can be classified into three different shapes: the U-shaped, V-shaped and intermediate shaped bays (Shimozono et al., 2012). Apart from this classification, the bays differ in bay slope (α_3), bay length (L_b), bay mouth depth (d_b), bay mouth width (W_b) and bayhead width (W_h).

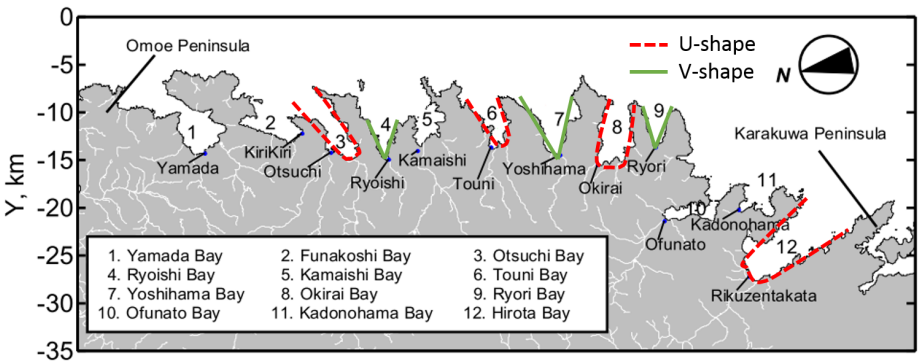

Figure 3.5: Classification Ria coast (Shimozono et al., 2012)

3.7. Converging estuaries

Bonneton et al. (2015) investigated the formation and dynamics of tidal bores in funnel-shaped estuaries. This is interesting since tidal wave transformations are similar to other long wave phenomena, such as tsunami waves. The influence of a converging estuary is also one of the important aspects of this research.

Bonneton et al. (2015) considers that a tidal bore is well formed when the bathymetry slope, α_2 in this research, is larger than 1/100. The intensity of the primary wave (mean jump/bore) is characterized by the Froude number:

$$Fr = \frac{u_1 - c_b}{\sqrt{gD_1}} \tag{3.8}$$

where, c_b is the bore celerity, u_1 is the averaged velocity over the cross-section and d_1 is the water depth ahead of the bore.

They showed that tidal bore formation is mainly governed by a dissipative parameter $\mathfrak{D}$, which characterizes the amount of nonlinearity. $\mathfrak{D}$ depends on the bottom friction C_{f0}, the wave characteristics (tidal amplitude at the mouth A_0) and the estuary geometry (convergence length L_{b0} and water depth D_0). The $\mathfrak{D}$ parameter is enhanced by the increase of the tidal range, friction coefficient, converging length and bathymetry slope. When $\mathfrak{D}$ is large, the dissipative character of the estuaries is large and the conditions are favourable for bore formation.

$$\mathfrak{D}_i = C_{f0}\frac{A_0 L_{b0}}{D_0^2} \tag{3.9}$$

Comparing the results of Bonneton et al. (2015) and (Treske, 1994) shows that tidal whelps, small amplitude waves due to undular bore formation, in a funnel-shaped estuary differ significantly from those in rectangular channels. The dimensionless wavelength and the wave steepness respectively decrease and increase with increasing Fr (Bonneton et al., 2015). This transformation of the undular bores can be explained because tidal bores strongly interact with the gently sloping river banks.

3.8. The 2011 Tohoku Earthquake Tsunami

Inversion analyses of available tsunami data, done by Shimozono et al. (2012), have clarified that the wave profiles near the Sanriku coast consist of two major components, caused by a combination of deep interplate slip and the large displacement near the trench. The first event is characterized by a long wavelength and the second event represents an impulsive wave with a narrow width. The superposition of these two components give different wave waveforms along the Sanriku coast, figure 3.6.

3.8.1. Numerical simulations

Shimozono et al. (2012) studied the tsunami wave behaviour along the central Sanriku coast to clarify responses of different bays to the incoming tsunami. Figure G.1 shows the study area including 12 bays with the corresponding bathymetry, topographic slope, run-up and inundation heights. Some results and conclusions are discussed in this section.

Topographic slope

The relation between the tsunami height, topographic slope and local coastline orientation is given in figure 3.7. There is an overall tendency that the tsunami height increases with the topographic slope (Shimozono et al., 2012). The tendency is more evident for bays with their opening towards the tsunami source area, which highlights the importance of the direction parameter when looking at tsunami intrusion in these bays. Another important observation is that the tsunami heights tend to be larger around the heads of peninsulas, due to the positive relation between topographic slopes and tsunami heights. The type of the nearshore tsunami wave differs for different locations, depending on land and seabed slopes. The waves that propagate in progressive modes accompanying wave breaking over gentle slopes while they have features of standing waves over steep coasts (Shimozono et al., 2012).

Geometry of the bay

As described in figure 3.5, the bays can be classified in V-shaped and U-shaped bays. The temporal vari-

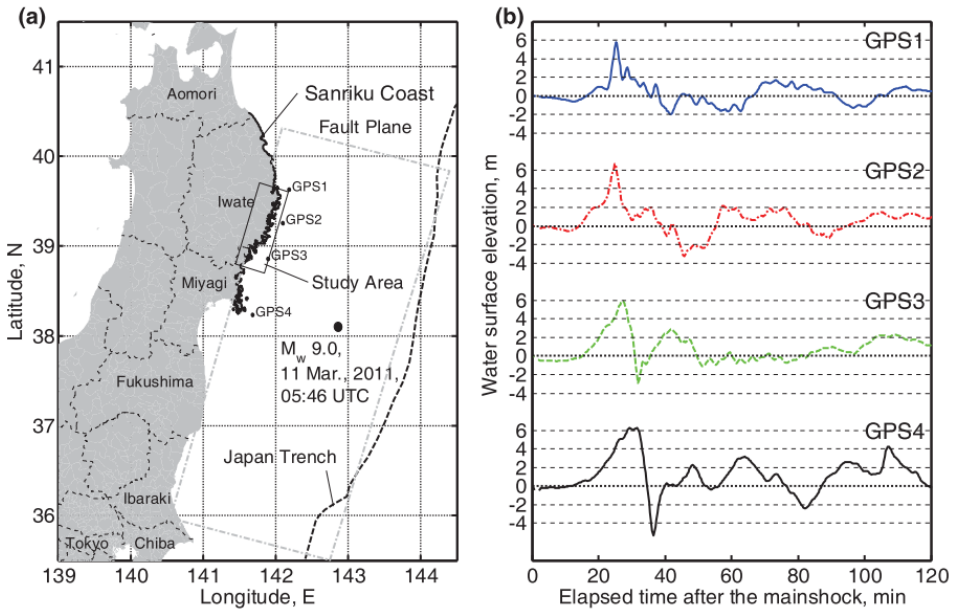

Figure 3.6: Location of the Sanriku coast and the offshore tsunami recordings (Shimozono et al., 2012)

ations of water surface elevations and the depth-integrated mass and momentum fluxes are shown in 3.8. The tsunami wave is significantly amplified due to the funnel effect in the V-shaped bays (Ryoishi and Ryori) and due to local resonance. The waves have a feature of standing waves where the fluxes are large but narrow-peak over time, which ensures that the flooding occurs in a short time. For U-shaped bays, long-lasting flooding with high horizontal velocities has been found since the wave have features of a progressing wave. The maximum velocities at Ryori and Ryoishi (V-shape) were calculated at 2-3 m/s and 5-6 m/s at Rikuzentakata (U-shape).

3.8.2. Real-life observations

Table 3.1 shows the behaviour of the tsunami wave during the 2011 Tohoku Earthquake. The information in the table is gathered from an online article ExtremePlanet (2014). Most of the observed tsunami types follow the explained theory above, but the interesting places are Kuji Bay, Noda Bay and Ishinomaki City due to their deviant behaviour. In Youtube videos of Kuji and Noda Bay (figure 1.4a) several tsunami bores are observed instead of an expected rapid rising water. On the other hand, near Ishinomaki City, which is a flat coastal plain, a rising water level was characterizing the tsunami wave instead of the expected bores. The goal of this research is to explain these different observed wave types.

Location	Coast Type	Wave Type	Bay Length [km]	Bay mouth Width [km]	Bay Area [km2]	Depth bay mouth [m]	Deaths	Notes
Kuji Bay	Ria coast	Bores	3.0	4.3	11.5	20	4	bore height: 6.1 m
Noda Bay	Ria coast	Bores	3.9	9.5	28	21	38	
Miyako Bay	Ria coast	Rising water	10.7	3.9	20	20	423	
Otsuchi Bay	Ria coast	Rising water	8	3.5	17.5	19	1378	
Kamaishi Bay	Ria coast	Rising water	2.5	2.3	8.7	29.5	1082	
Ofunato Bay	Ria coast	Rising water	8.1	2.6	10.8	5	446	L-shaped bay
Hirota Bay (Rikuzentakata)	Ria coast	Rising water	8.8	5	34.7	20	2000	1st wave (rising water) 2nd wave (surging)
Kesennuma Bay	Ria coast	Rising water	8.9	1.7	12.5	12	1404	Two inlets
Shizugawa Bay (Minamisanriku)	Ria coast	Rising water	7.9	6.3	45.5	20	907	
Onagawa Bay	Ria coast	Rising water	5.7	4.0	24.8	1.5	914	
Ishinomaki City	Flat plain	Rising water					3890	Giant tide (wrapped around peninsula, 15 minutes delayed
Sendai/Natori	Flat plain	Series of bores					1711	Bores started >3.2 km offshore

Table 3.1: Coastal Classification (ExtremePlanet, 2014)

3.9. Design of defence systems

Japan, with a rich history of sea defence, is known as the best prepared countries in the world against tsunamis. Before the distaster in 2011 massive detached breakwaters were constructed in bays to protect low laying settlements like Kamaishi. However, the most frequently built 'hard' structures along the Sanriku coast are sea-

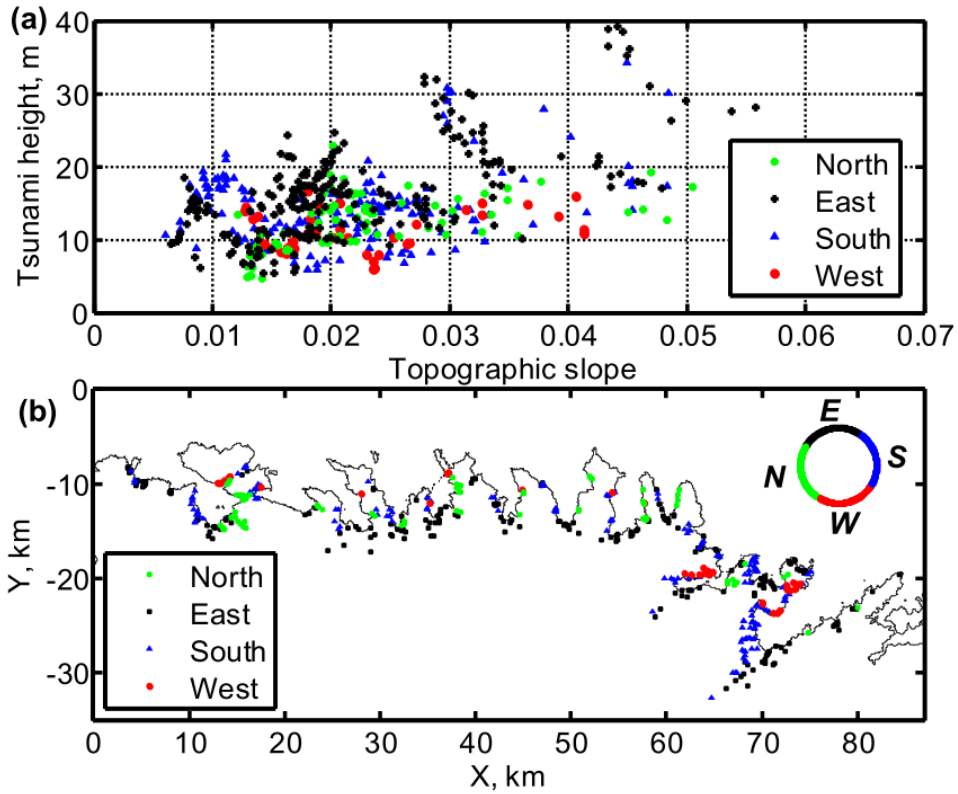

Figure 3.7: Tsunami height, topographic slope and local coastline orientation of the study area (rectangle in figure 3.6) (a) Relationship between the tsunami heights and topographic slopes. (b) Classification of the data points by the local coastline orientation. (Shimozono et al., 2012)

walls and sea dykes. The design rules for sea dykes and seawalls, before and after the 2011 Great East Japan Eartquake, are outlined. Besides that, the most effective 'soft' measure against tsunami impact is shortly described.

3.9.1. Seawalls and sea dykes

Even with the constructed seawalls and sea dykes up to 10 m or more, the 2011 tsunami led to many deaths and damage. In Japan, this event results in a rethinking of the design rules for the tsunami defence structures. One of the key problems was the design height of the defence structure that was too low to protect against the magnitude experienced in 2011. Design water levels were based upon tsunamis from fairly recent history e.g. the Meiji Sanriku tsunami of 1896, which caused a significant number of casualties but had smaller record run-up than the 2011 tsunami (Raby et al., 2015). After the disaster, a two-level description of tsunami hazard, purely according to their return period at a specific location, was proposed and accepted. Level 1 tsunamis correspond to a return period of several decades to 100+ years, with inundation heights of 7-10 m. Level 2 events have return periods of a few hundred to a few thousand years and would result in much higher inundation heights, over 10 m (Esteban et al., 2017). Currently built structures are designed to protect inundation against a Level 1 event tsunami. However, while they are not designed against the inundation of a Level 2 event they should resist structural failure during larger events. For Level 2 events, tsunami warning systems and evacuation plans become important.

There is a relation between tsunami velocity and the optimal location of the sea dyke. For offshore breaking tsunamis, the velocity is high at the coastline and decreases inland, which makes a sea dyke more efficient when it is placed a few hundred meters inland. In ria coast areas, a tsunami wave mostly come ashore as a surging wave where the velocity increases from the coastline to inland. In that case, it is better to place the sea dyke near the coastline, i.e. in Otsuchi Town in figure 1.3.

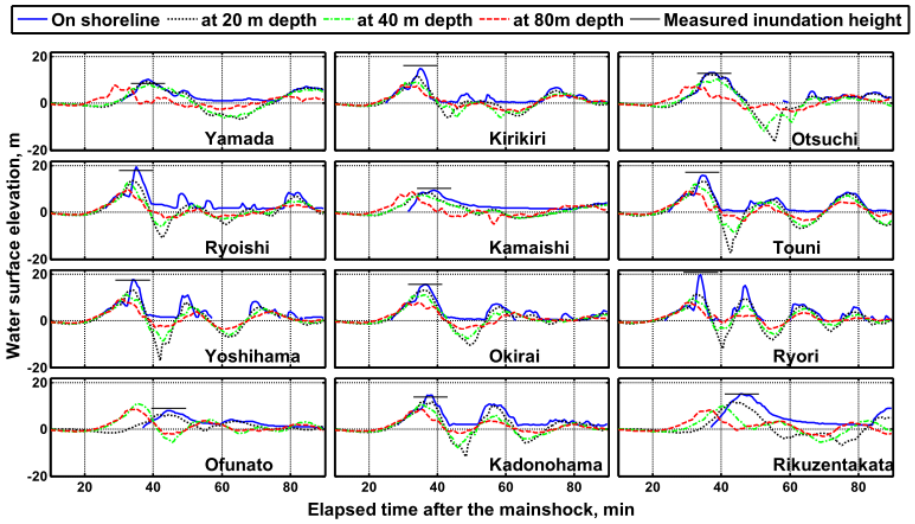

(a) Calculated temporal variations of water surface elevations in different bays by using a numerical model. (Shimozono et al., 2012)

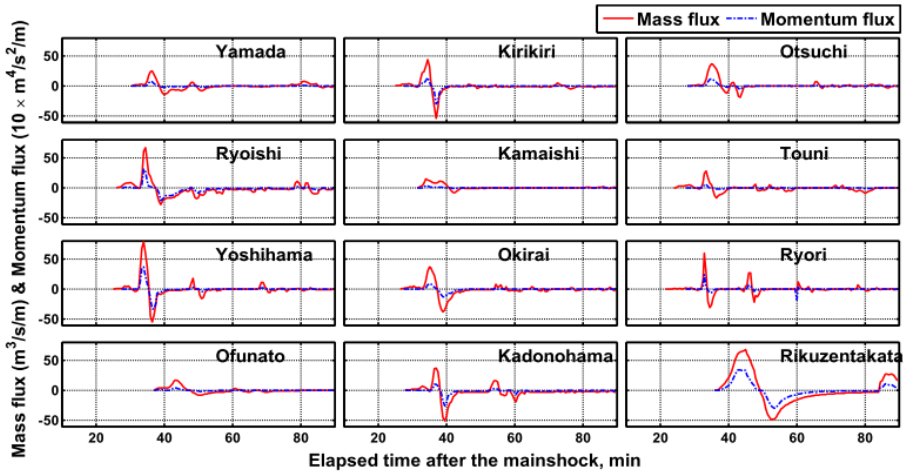

(b) Calculated temporal variations of the depth-integrated mass and momentum fluxes (divided by the fluid density) in the cross-shore direction at 12 different bays. The values are taken positive onshoreward. (Shimozono et al., 2012)

Figure 3.8: Results of the numerical simulations of Shimozono et al. (2012)

3.9.2. Warning system and evacuation plan

A reliably warning system, which can predict the arrival time as well as the inundation area correctly, will save many lives if the people exactly know what to do in case of emergency. An emergency evacuation plan is needed, which must be activated when an earthquake is felt. Such an evacuation plan requires a detailed predicted inundation map for several tsunami cases. Numerical modelling can be of great importance in the development of these inundation maps.

3.10. Summary and discussion

(Yeh, 2006) concluded that the impact momentum increases with the steepness of the bore front. Since the Froude number is related to the steepness of the wavefront, this is a good dimensionless parameter to compare different tsunami wave impact on coastal structures. To analyse different kind of tsunami types near the Tohoku coastline, a local Froude number (Fr_{coast}) can be used, based on the Froude number proposed by Glasbergen (2018). Since the definition of a bore is not that clear for tsunami waves, the name 'bore' is replaced by 'front' in this research. As described by ASCE (2016), it is important to know if the front of a tsunami wave breaks since the impact on the coastal structures can be different. ASCE (2016) considers bore formation for prevailing nearshore bathymetric slopes of 1/100 and milder or when historically documented, described by recognized literature or determined by a site-specific inundation analysis. To give a better clas-

sification in tsunami waves approaching the shore, the breaker parameter of Glasbergen (2018) is improved by doing more 1D simulations with a steeper shelf slope (α_2 is 1:50 and 1:75) and a more gentle slope (1:500). Besides that, Glasbergen (2018) recommended doing research about the exact location of breaking.

Tsunami transformation is a bay along the Sanriku coast can be compared with the investigations of Bonneton et al. (2015) about the formation and dynamics of tidal bores in funnel-shaped estuaries. They showed that tidal bore formation is mainly governed by a dissipative parameter $\mathfrak{D}$, which characterizes the amount of nonlinearity. $\mathfrak{D}$ depends on the bottom friction, the wave characteristics and the estuary geometry. The $\mathfrak{D}$ parameter is enhanced by the increase of the tidal range, friction coefficient, converging length and bathymetry slope. When $\mathfrak{D}$ is large, the dissipative character of the estuaries is large and the conditions are favourable for bore formation. In this research, the influence of bottom friction on the tsunami wave transformation will be investigated during the calibration of the model. However, the main focus will be the influence of the wave characteristics and the geometry of the bay.

Many lessons are learned from the 2011 Tohoku Earthquake Tsunami. Shimozono et al. (2012) studied the tsunami wave behaviour of this event along the central Sanriku coast. There is an overall tendency that tsunami wave height increases with the topographic slope. Another observation is that the tsunami wave was different for the locations. The waves propagate in progressive modes accompanying wave breaking over gentle slopes while they have features of standing waves over steep coasts (Shimozono et al., 2012). Figure 3.5 gives a classification of the Sanriku coast in V- and U-shaped bays. For U-shaped bays, long-lasting flooding with high horizontal velocities has been found since the wave have features of a progressing wave. The maximum velocities at Ryori and Ryoishi (V-shape) were calculated at 2-3 m/s and 5-6 m/s at Rikuzentakata (U-shape). To better quantify this distinction in wave types, 2DH SWASH simulations will be performed during this research.

4

Offshore modelling

In this chapter, the model used to simulate tsunami propagation from the origin of the earthquake to the nearshore area is explained. First, an approach is given to solve problems with this model. After that, the input of the model is shown and the calibration and validation of the model are discussed by simulating different input commands and giving relevant reference studies. Finally, the results and conclusions from the model are outlined.

4.1. Approach

A tsunami wave will be modelled in the program SWASH, which is explained in section 1.3 in more detail. The goal of this chapter is to see if a numerical simulation like SWASH can be approximated by an analytical solution. Making a numerical model is time-consuming, where an analytical calculation can be easily done to obtain a first impression of the output. The first step is to make a 1D SWASH model from the origin of the 2011 Tohoku Earthquake Tsunami to the nearshore area. In the second step, the results of the model will be validated by comparing them with observed buoy data (GB802) along the Japanese coast during the tsunami in 2011. Finally, an analytical calculation is made with the Green's law approximation to see if the analytically obtained tsunami height, in the nearshore area, matches the numerically simulated tsunami height.

4.2. Validation

4.2.1. Input

The command file for the SWASH program is given in appendix B.1. The computational grid is regular and is built out of 600 grid cells with a length of 500 m. The total dimensions are 300,000 m in x-direction and 0 m in y-direction (1D-model). The model improves its frequency dispersion by simply increasing the number of vertical layers (TeamSWASH, 2010). Since dispersion effects are limited for long waves in the open ocean (d/L«1), 1 vertical layer is used in this model, see table 5.1 in the SWASH Manual (TeamSWASH, 2010) and the calculations in appendix B.1. The dimensions of the bottom and water level grid are equal to the computational grid, only the resolution of the grid is increased to grid cells with a length of 1m. A hydrostatic pressure assumption can be made since long waves are modelled. Descriptions of the input commands are outlined in the SWASH User Manual (TeamSWASH, 2010) and the substantiating of the choices can be found in appendix B.1.

Tsunami source water elevation

During the 2011 Tohoku earthquake, a large slip occurred at a depth of 20 km. Another large slip took place at a very shallow location near the trench, which caused a tsunami wave. Saito et al. (2011) estimated the initial water level elevation by the inversion analysis based on the dispersive tsunami simulations, which is shown in Figure 4.1a.

The simplified initial water elevation from Figure 4.1b is used as an initial condition for the 1D SWASH model, to simulate the tsunami wave propagation from the origin of the earthquake to the nearshore area. Two cross-sections of the water elevation and two corresponding bathymetries are considered, one perpendicular to the

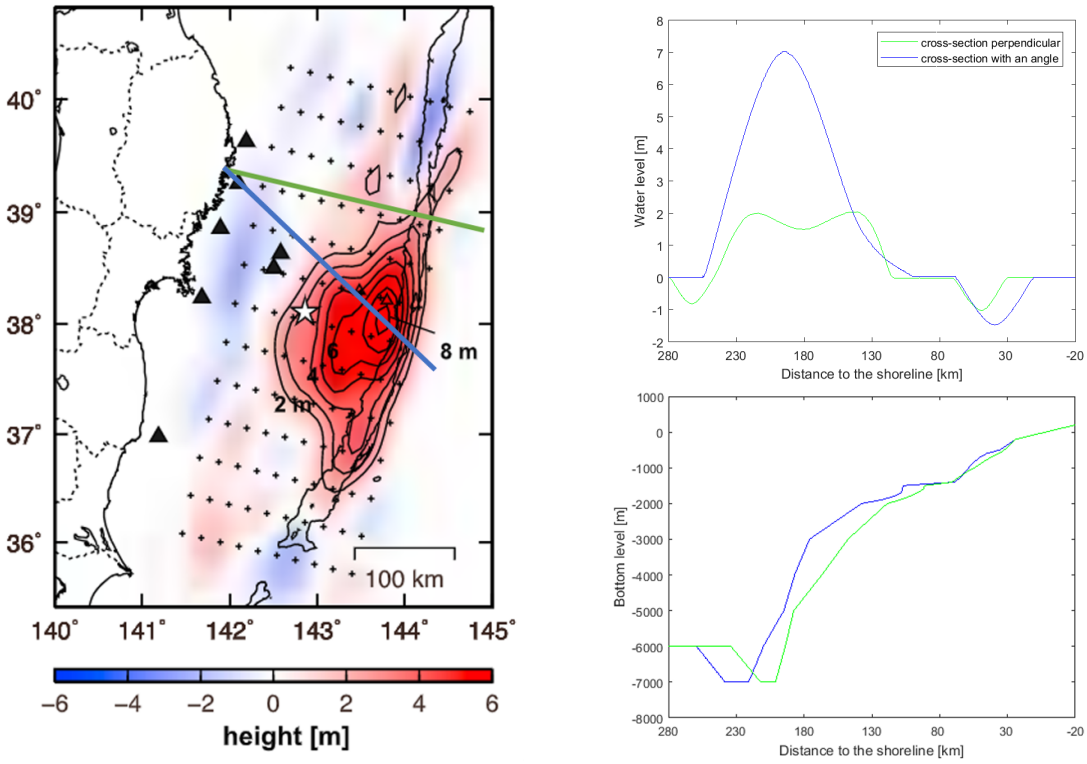

(a) The initial height distribution estimated from the tsunami waveform inversion analysis (Saito et al., 2011)

(b) Input SWASH: interpolated initial height distribution and bathymetry along the 1D cross-section

Figure 4.1: 2011 Tohoku Earthquake Tsunami water elevation

fault line and one with an angle.

Bathymetry

Two cross-sections of the bottom level, obtained from Navionics (Navionics, 2018), are considered as input for the bathymetry, one perpendicular to the fault line and one with an angle. Parts of the maximum water elevation can reach Otsuchi by a refracted propagation line, which is simplified as a straight (blue) line in this model. A clear trench is observed between 220-260 km from the shoreline, which is the location of the moving tectonic plates. In the next section, the best approximation is analysed.

4.2.2. Output

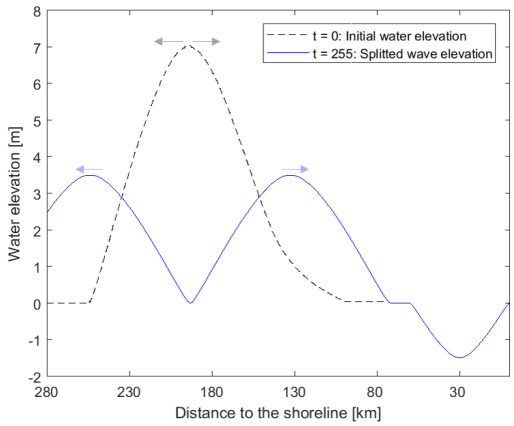

Figure 4.2: Splitting of a tsunami wave

Tsunami propagation and transformation
Since the initial water elevation during the 2011 Tohoku Earthquake Tsunami is used as an initial condition, the elevated water is forced into two opposite directions (1D model) due to gravity. The elevated water level splits up in two tsunami waves, one propagating into the sea and one to the coastline, see figure 4.2.

After the initial water elevation has split up in two directions, the wave will undergo shoaling when approaching the shore. Due to this shoaling effect, the wave height increases and the wavelength shortens. Snapshots from the 1D animation are given in figure 4.3.

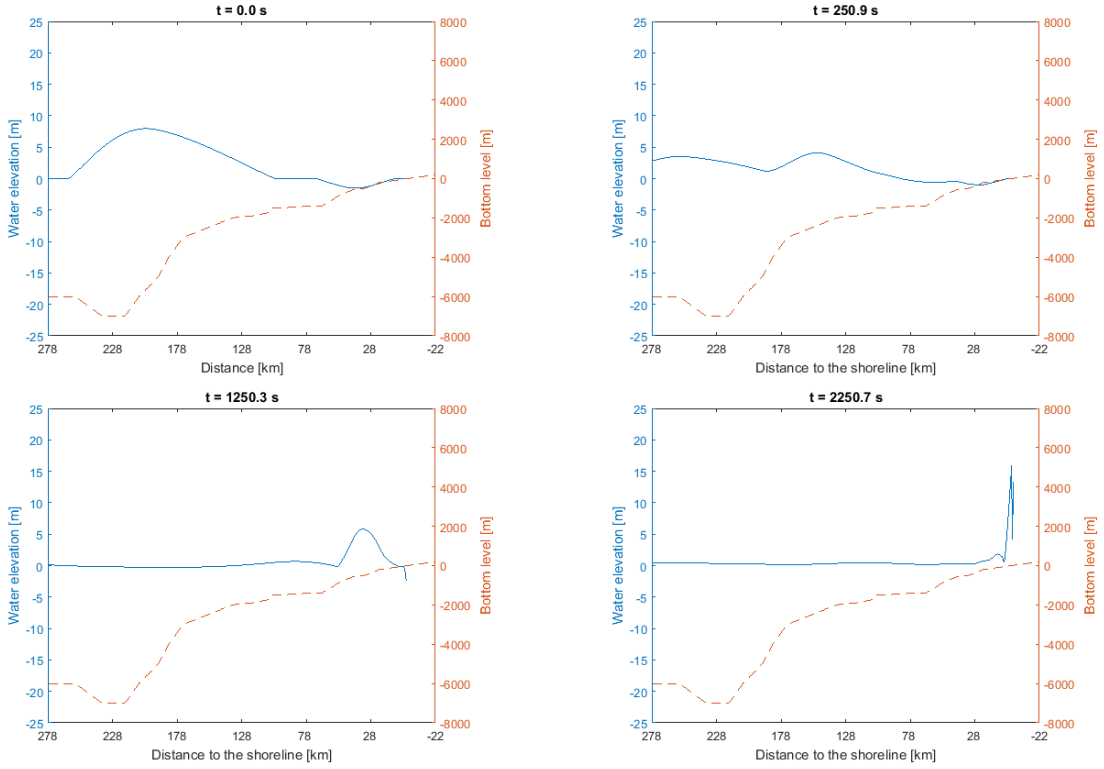

Figure 4.3: Tsunami propagation and transformation from the origin of the tsunami to the nearshore area

Otsuchi case
The result of this model is compared to the measured wave data of a GPS buoy 'GB802' during the 2011 Tohoku Earthquake Tsunami. The GPS buoy is moored by a steel chain at a spot of 204 m in water depth and 10-20 km from the coastline of Kamaishi (Kawai et al., 2011), which is shown with a triangle in Figure 4.1a. This buoy has been chosen for its nearest location to Otsuchi, which is the case study of this research.

Since the input of the SWASH model is the initial water level during the tsunami, the start of the model will be at 2.46pm, the 11th of March. The observed wave heights are plotted against the SWASH results in Figure 4.4.

The maximum water elevation at the 11th of March is 6.67m, measured by the GPS wave buoy. The maximum water elevation calculated by SWASH is 1.99m for the situation perpendicular to the coast and 6.78m for the situation with an angle. From now on, the second situation, Figure 4.4b, will be analysed since these results better match the actual water elevation measurements.

Apparently the highest initial elevation level travels in multiple directions and will refract to the coast. Because the real propagation path is more curved than the straight line in this simulation, there can be some mismatches in the results. The other reasons can be the simplified initial water elevation and the simplified bathymetry which are used in the simulations.

The GPS buoy data show multiple secondary small amplitude tsunami waves which are not well simulated by the 1D SWASH model. Small amplitude secondary tsunamis are well correlated with possible waves generated by the aftershocks of the earthquake, which created the original large magnitude tsunami (Royer and

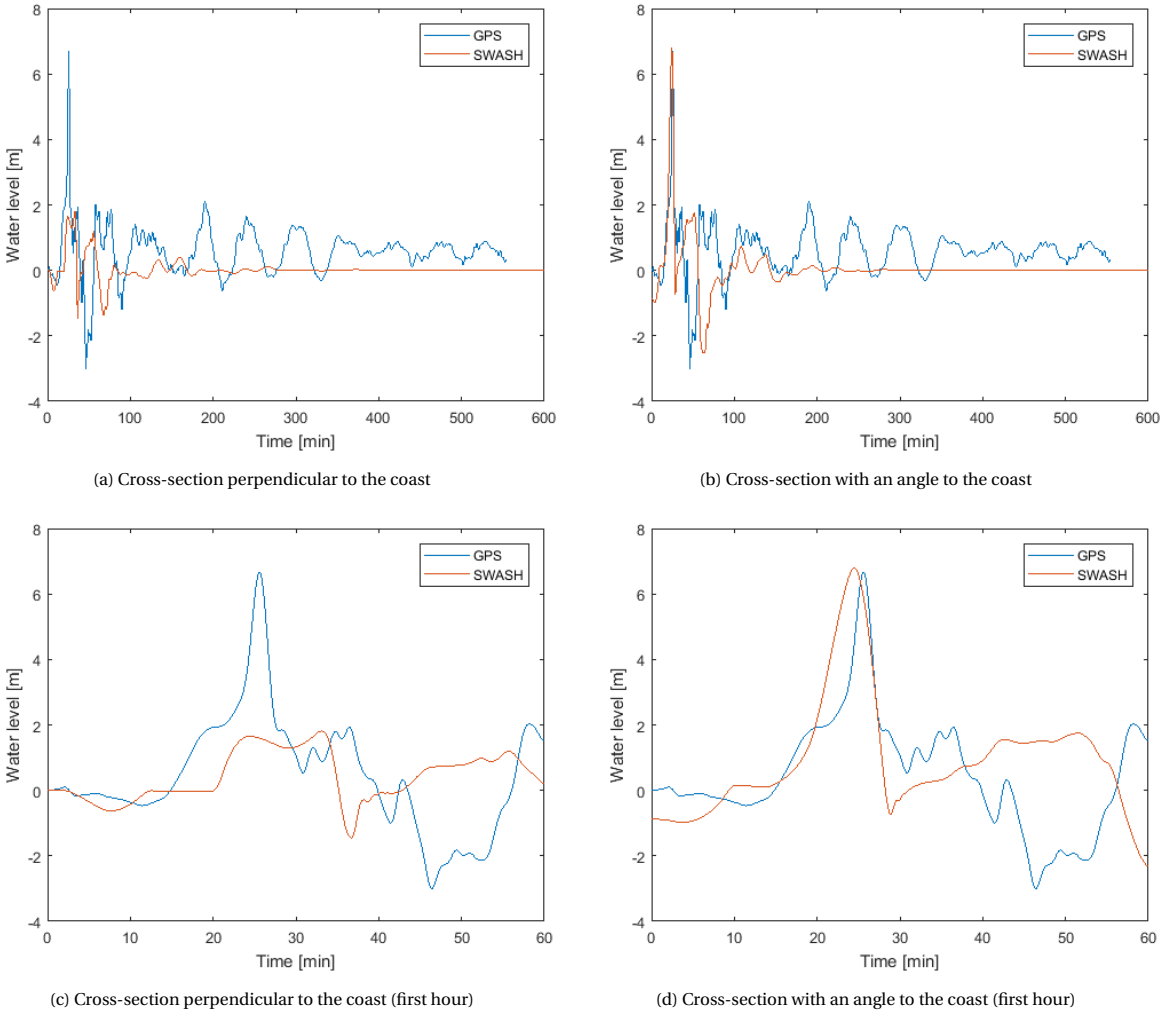

(a) Cross-section perpendicular to the coast

(b) Cross-section with an angle to the coast

(c) Cross-section perpendicular to the coast (first hour)

(d) Cross-section with an angle to the coast (first hour)

Figure 4.4: SWASH results vs. GPS buoy GB802 on March 11, 2011

Reid, 1971). The initial water elevation of the main shock is used as input for the SWASH model, which explains the absence of the secondary tsunami waves due to missing aftershocks in the SWASH results. Another explanation could be the absence of 3D wave effects like edge waves in the 1D SWASH model. Edge waves are waves running along the shore, formed by the reflection of waves off the beach and their refraction and entrapment within the surf zone (McLachlan and Brown, 2006).

4.2.3. Calibration

To increase the accuracy of the SWASH model different test simulations are performed to calibrate the model.

Grid size

To see the impact of the grid size of the SWASH model, simulations with different resolutions are performed. The first wave shape is exactly similar for the grid sizes 1 m, 100 m and 500 m. After increasing the grid size to 2000 m the wave shape is changing and becomes less steep. A grid size of 500 m appears to be a valid option.

Hydrostatic vs. non-hydrostatic

A decrease in wave height can be observed in figure 4.5b when applying the non-hydrostatic pressure in the NLSW equations. The reason for that is the dispersive effects of the non-hydrostatic model, which moves the energy of the main wave to the offshore side due to frequency dispersion. Because of the slightly overestimated wave height in figure 4.4d, a non-hydrostatic assumption will give a more accurate solution.

Manning's friction coefficient

Figure 4.5c shows that the effect of friction on the shape of the first wave is not significant. However, the bottom friction gains more importance when simulating nearshore propagation and have to be taken into account in the next chapter.

Vertical layers
The model improves its frequency dispersion by simply increasing the number of vertical layers. To check the influence of this increase over the vertical, a non-hydrostatic assumption is needed to include frequency dispersion. Figure 4.5d shows the result of the simulations with different amount of vertical layers. A slightly higher wave height, in the order of 0.5%, is observed when running simulations with 1 vertical layer. Therefore, it is assumed that simulations with 1 vertical layer are sufficient to simulate the shape of the first tsunami wave.

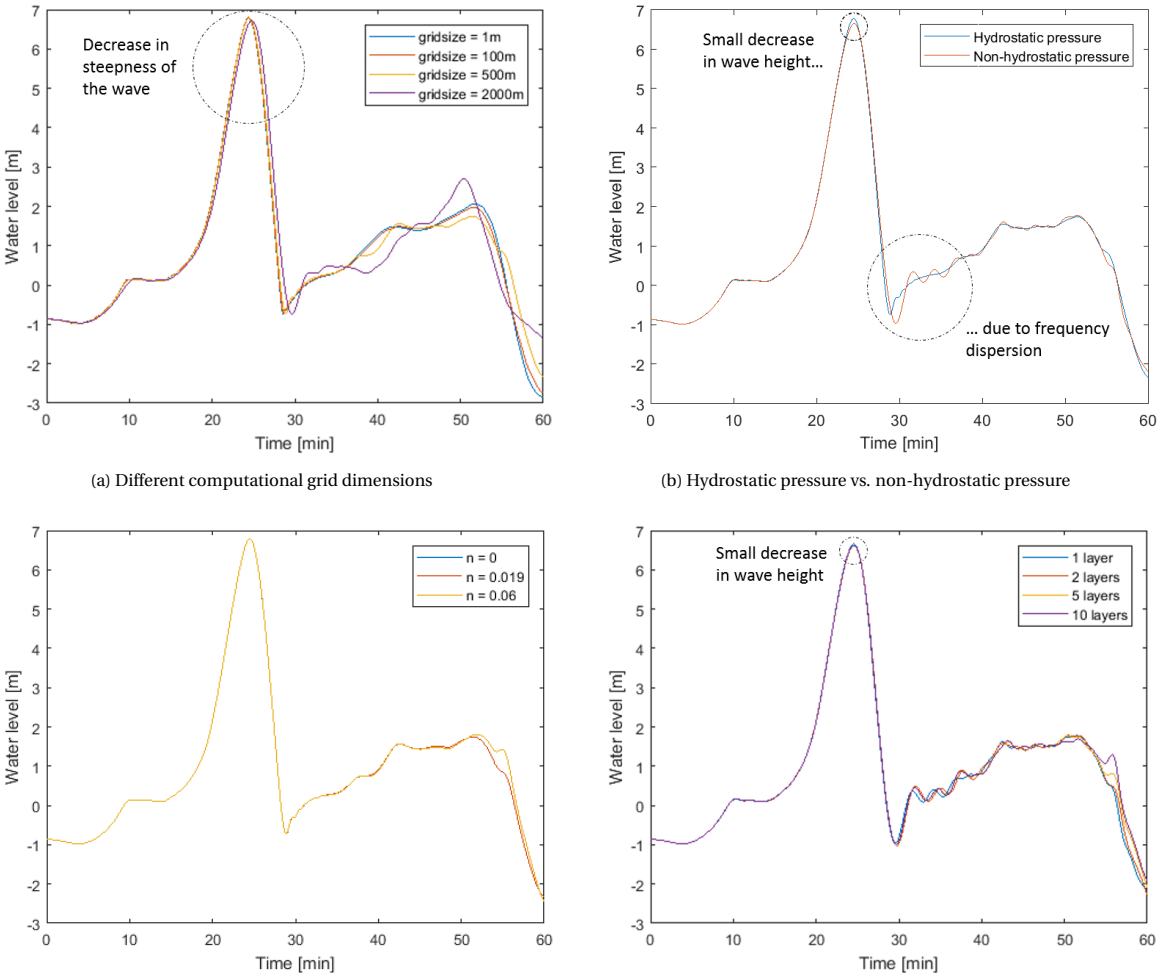

(a) Different computational grid dimensions

(b) Hydrostatic pressure vs. non-hydrostatic pressure

(c) Friction vs. no friction (Manning)

(d) Different amount of vertical layers

Figure 4.5: Tests 1D model

4.3. Green's law

In different models, the linear SWE can be used as a first approximation to calculate changes in tsunami wave height as the wave moves across an ocean (Bryant, 2014). Therefore, the propagation of a tsunami wave is independent of the wavelength L and only depends on the local depth d on the sloping bathymetry. According to this assumption, tsunami waves are seen to evolve far from the shoreline like what is referred to as Green's law (equation 2.1) (Tadepalli and Synolakis, 1996) (Eze et al., 2009). Here, the Green's law approximation is compared with the modelled SWASH results, based on the NLSW equations, and the observed wave data during the 2011 Tohoku Earthquake Tsunami.

As described in Section 2.1, the raised initial water level after an earthquake causes a tsunami wave. In this 1D model, the initial water level causes a tsunami wave which travels in two opposite directions, with approximately a wave height half of the initial raised water level (figure 4.2). At the same time, the tsunami wave starts to shoal toward the coastline, where the water depth becomes less. The comparison between the Green's law approximation, the wave buoy GB802 and the SWASH model for the maximum tsunami wave height H_{max} is given in figure 4.6a. The SWASH results give a decay in water elevation in the beginning, since the initial water elevation splits up into two waves which is more dominant than the water level increase due to shoaling. After splitting up, the water level will increase due to shoaling.

To see if the analytical solution, Green's law, can be used as a good approximation of the tsunami height and shape near the coastline of Kamaishi, a timeseries is plotted at the location of the GPS buoy GB802 (depth of 204m) in figure 4.6b.

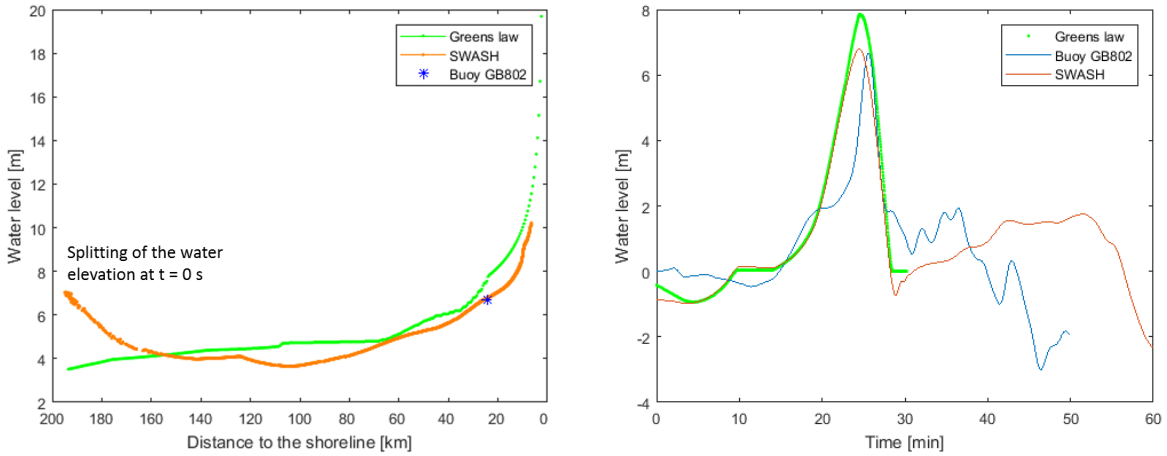

(a) H_{max} over distance approximated by Green's law. Splitting of the water elevation at t = 0 s is explained in figure 4.2

(b) Timeseries of H at the location of the buoy GB802

Figure 4.6: Green's Law approximation for Kamaishi

The maximum wave height is overestimated, but the arrival time and the shape of the tsunami wave can be perfectly approximated with the analytical solution Green's law.

4.4. Behaviour along Tohoku coastline

Buoy observations during the 2011 Tohoku Earthquake Tsunami are analysed to compare the SWASH simulations with reality. GB801, GB802 and GB807 are the buoys located near the Sendai coast (d=144 m), Kamaishi Bay (d=204m) and Kuji Bay (d=125 m) respectively. These buoy locations are indicated with a triangle in figure 4.8.

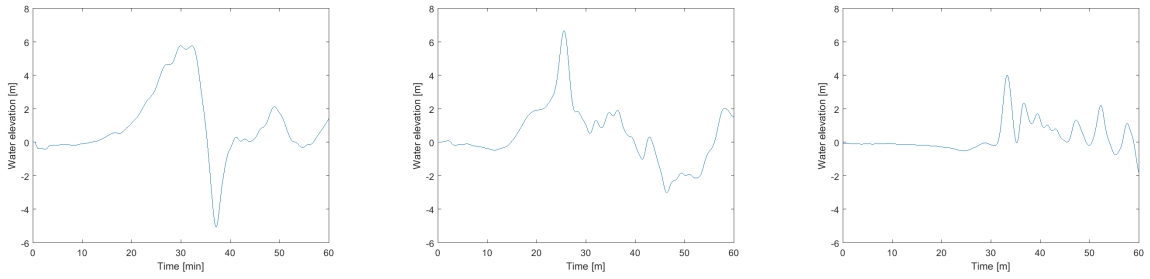

(a) Buoy GB801: Sendai

(b) Buoy GB802: Kamaishi

(c) Buoy GB807: Kuji

Figure 4.7: Wave buoy observations along the Tohoku coastline

The disadvantage of a simplified 1D SWASH model is that some 2D effects like bottom refraction and reflected edge waves are not taken into account correctly. In this chapter, the wave propagation is simulated with a 1D

model, from the origin of the earthquake up to the buoy of Kamaishi. Figure 4.4b gives a good match between the buoy observations and the SWASH simulations. Glasbergen (2018) conducted a similar 1D simulation to compare the wave buoy results near Sendai with the results of the model, and a good match was found too. However, the water level observations near Kuji Bay were smaller than near the Kamaishi bay, see figure 4.7c. This implies that a 1D model can not be used any more to model accurate water levels near the Kuji Bay. Based on these findings and the angles given in figure 4.8, the Green's Law approximation seems to be valid for locations with an angle of 0-33° relative to the perpendicular propagation path of the 2011 Tohoku Earthquake Tsunami.

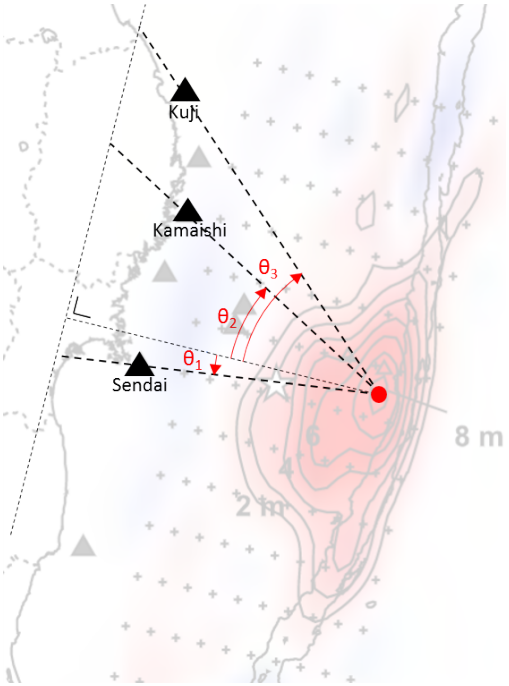

Figure 4.8: Locations buoy observations relative to the highest initial water elevation. θ gives the angle relative to the perpendicular propagation path of the tsunami wave. θ_1 is 7.7°, θ_2 is 32.7°and θ_3 is 46.9°.

5

Nearshore modelling

First, a short introduction and the research approach are given in section 5.1 and 5.2 respectively. After that, section 5.3 explains the input and output of the SWASH models. Section 5.4 gives the results of the nearshore 1D simulations, performed by SWASH. The results of the 2DH SWASH model, where the influence of the bay geometry is included, is outlined in section 5.5. Finally, a short discussion and the conclusions are given for this chapter.

5.1. Introduction

Since the nearshore area of the Tohoku coastline can be classified as different kind of coastlines, the goal of this chapter is to give more insight into the differences of tsunami wave behaviour. The main focus is the tsunami wave transformation near a ria, which is characterised by an indented coastline. The results will be compared with the simulations of tsunami wave transformation over a gently sloping beach without bays near the Sendai Plain, performed by Glasbergen (2018).

Table 5.1 gives an overview of the geometries of the bays along the Tohoku coastline. Navionics (2018) is a good tool to find out the dimensions of the bay, but the bathymetry along the Sanriku coast was found to be incorrect at some places. Therefore, the bathymetry is obtained from survey results of Shimozono et al. (2012) after the 2011 Tohoku Earthquake Tsunami.

Table 5.1: Classification of the Sanriku coastal bays (Navionics, 2018; Shimozono et al., 2012)

	Name	**Bay type**	α_2	d_b	W_b	W_h
North Sanriku	Kuji Bay	U-shape	1/160	40-60	5.5	2.5
	Noda Bay	U-shape	1/150	40-60	9.6	5.6
	Miyako Bay	U-shape	1/145	60	3.5	1.4
Central Sanriku	Yamada Bay	U-shape	1/90	80	3	3
	Otsuchi Bay	U-shape	1/110	60	3.5	1.5
	Ryoshi Bay	V-shape	1/70	60	2.7	0.5
	Kamaishi Bay	U-shape	1/70	60	2.3	4
	Toni Bay	U-shape	1/66	80	3.3	1.8
	Yoshima Bay	V-shape	1/75	80	7.3	1.2
	Ryori Bay	V-shape	1/70	60	3	1
South Sanriku	Hirota Bay	U-shape	1/160	60	8.7	2.2
	Shizukawa Bay	U-shape	1/135	60	7.3	4 5
	Oppa Bay	U-shape	1/107	60	6.5	6.5
	Onagawa Bay	U-shape	1/120	60	5	5
Sendai Plain	Yuriage	x	1/590	x	x	x

A clear difference can be seen in the slope of the continental shelf between the Sendai Plain and the Sanriku

coastline. Where the Sendai Plain is characterized by a wide and gentle sloped continental shelf, $\alpha_2 = 1/590$, the Sanriku coastline has a narrow and steep sloped continental shelf where α_2 varies roughly between 1/60 and 1/160. The width of the bay along the Sanriku coastline W_b varies between 2.3 and the 9.6, the width of the bay head W_h between 1 and 6.5 and the length of the bay L between 3 and 11.6.

5.2. Approach

In this chapter, the influence of the wave characteristics and the bathymetry parameters on tsunami wave transformation is investigated by performing 1D and 2DH simulations. The 1D model is a simplified model where the goal is to clarify the influence of the wave height, wavelength and the slope of the continental shelf. A numerically depth-integrated 2DH-model, including non-hydrostatic calculations, is used to reproduce the complex tsunami behaviour along the Sanriku coast. These detailed calculations are based on the schematized model, explained in subsection 1.3.2, to find the influence of bay geometry parameters on the transformation of a tsunami wave. Wave breaking is very important to classify tsunami wave types for these simulations. Wave breaking in SWASH depends on the maximum wave steepness given by equation 1.1, where an α_s 0.6 is advised based on experimental data (Smit et al., 2013). The offshore boundary conditions used for these simulations are adjustable sinus wave timeseries (figure 5.1), which have similar characteristics as the observed timeseries along the d=100m depth contour line during past tsunami events. The added value of this approach is that the results can be used for different magnitude tsunamis and not only for the 2011 Tohoku Earthquake Tsunami. Since the influence of the geometry of the bay along the Sanriku coast is not clear, several simulations have been performed for different geometries of a schematic bay.

The observed wave signals during the 2011 Tohoku Earthquake Tsunami in figure 3.6 are an indication of the range in wave signal parameters during this research, where the wave height fluctuates around 6 m and the wave period between 10 and 20 min. For the range in bay parameters, the dimensions along the Sanriku coast in table 5.1 are used. The following parameters are used in this thesis to simulate different tsunami wave behaviour along the Sanriku coast, where the bay geometry parameters are given in the schematized model of subsection 1.3.2:

- Wave height at d=100m (H_ξ): 4 and 6 m;
- Wavefront period at d=100m (T_ξ): 300 and 600 s;
- Continental shelf slope (α_2): 1/50 and 1/100;
- Bay mouth width (W_b): 1 - 6 km;
- Bay head width (W_h): 0.5 - 3 km.

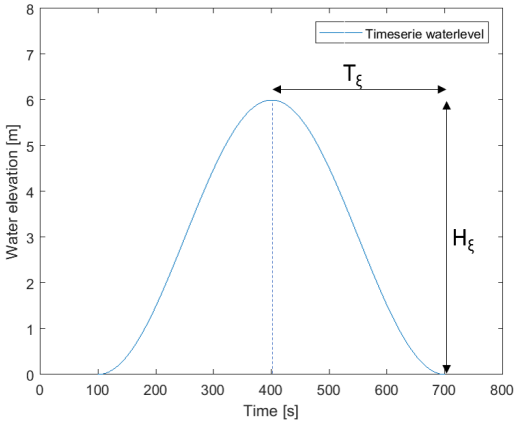

Figure 5.1: Boundary condition: timeseries of the water level coming in to the bay

To compare the different simulations, the tsunami breaker parameter (Glasbergen, 2018) is used in the 1D simulations. A new tsunami breaker paramater for 2DH simulations is proposed later in this chapter. To classify different tsunami wave types along the coastline, the Froude number Fr_{coast}, defined in subsection 1.3.3, and the maximum momentum flux $(hu^2)_{max}$ are used as an indication.

5.3. Input

The command files for the SWASH program is given in appendix B.2. The computational grid is regular for the 1D nearshore model with a grid size of 1 m. The computational grid for the 2DH model is curvilinear, with a grid size of 1 m for the first 1000 meter in front of the coastline and 50 m for the rest of the grid. This is done

to accurately simulate wave breaking in the nearshore area and to obtain accurate results for the momentum flux at the coastline. The 2D computational grid is built out of customizable dimensions, to compare the influence of different bay shape parameters. Concerning the wave transformation, the number of vertical layers is determined by frequency dispersion. The dimensionless depth, kd with k the wave number, decides the number of layers (TeamSWASH, 2010). For L = 20,000 m and d = 100 m, kd = 0.0314. This is in the range $kd < 0.5$ for which 1 vertical layer is sufficient to approximate dispersion according to Table 5.1 in the SWASH Manual. The bottom grid has the same dimensions as the computational grid. Momentum conservation is used in this model to ensure that the wave properties under breaking waves are modelled correctly. The SWASH User Manual (TeamSWASH, 2010) describes all the commands in more detail.

5.4. Simulations: 1D model

The transformation of tsunami waves can be influenced by wave characteristics, bathymetry and topography. The wave characteristics are the wave height H and the wavelength L. The slope of the continental shelf is the only parameter for the bathymetry that changes in these 1D simulations. The part of interest in this research is the transformation of a tsunami wave before it reaches the coastline, therefore the influence of topography is left out of the scope. For all simulations, the slope of the topography α_4 is similar to the slope of the continental shelf α_2.

5.4.1. Wave characteristics

The wave height and the wave period near the continental shelf differ per location due to the shoaling effect. Glasbergen (2018) performed simulations to compare a changing wavelength L with a changing wavefront L_{front}. He concluded that the breaking of the wavefront depends on L_{front} only, independent of L_tail. Therefore, simulations are performed for two different wavefront lengths (600 and 1200 seconds). Linear theory is assumed to be valid to calculate the boundary conditions for this nearshore model. Therefore, the wavelength can be calculated with the formula $L = cT$, where c is the wave celerity given by equation 2.4. To see the impact of the different wave characteristics on the transformation of the tsunami wave, simulations are performed with H_{100}=4 m, H_{100}=6 m and H_{100}=8m.

Figure 5.2 and 5.3 give a clear relation between wave height and the Froude number or momentum flux. for an increasing wave height, the Froude number and the maximum momentum flux at the coastline increases. For the wavelength, the opposite relation applies. When the wavelength increases, the Froude number and the maximum momentum flux at the coastline decreases. An interesting result is that the maximum Froude number and the maximum momentum flux depends on the slope and the wave period. For simulations with T = 600 s, the maximum Froude number and maximum momentum flux are reached for a slope of 1/300. When T is increased to 1200 s, the maximum occurs for slopes of 1/500. This can be explained by the fact that shorter waves break earlier for a given slope than longer waves.

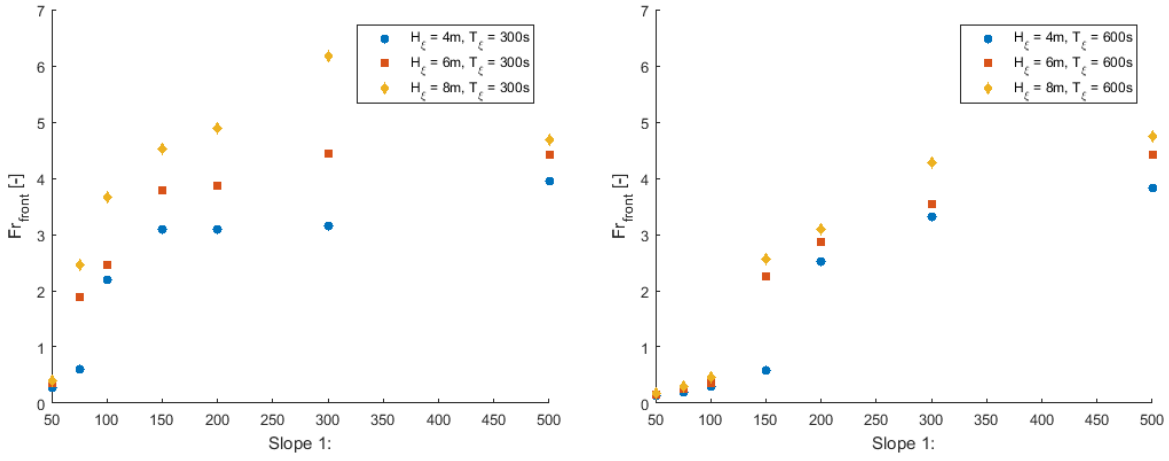

(a) T_ξ = 300s (b) T_ξ = 600s

Figure 5.2: The slope of the continental shelf (α_2) vs the Froude number of the wavefront (Fr_{coast}) at the coastline for 3 different wave heights (H_ξ) and 2 different wavefront periods (T_ξ) at a depth of 100 m.

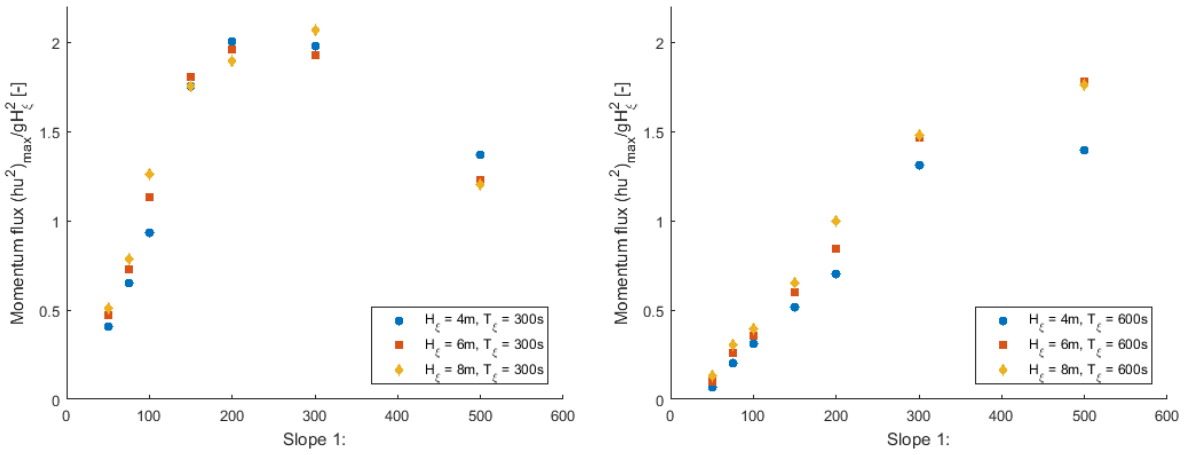

(a) T_ξ = 300s (b) T_ξ = 600s

Figure 5.3: The slope of the continental shelf (α_2) vs the maximum momentum flux at the coastline $(hu^2)_{max}$ divided by (gH_ξ^2) for 3 different wave heights (H_ξ) and 2 different wavefront periods (T_ξ) at a depth of 100 m.

5.4.2. Continental shelf slope (α_2)

To show the influence of the continental shelf slope a few 1D simulations are made with slopes of 1/50, 1/100, 1/150 and 1/500, where the first three slopes are representative for the Sanriku coast and the last slope is similar to the slope of the Sendai Plain. The boundary condition is given by a sinusoidal wave with a wave height H of 6m and a period T of 600s.

A few interesting observations can be made from these 1D simulations, shown in figure 5.4. The steepest slope ensures that the tsunami wavefront does not break before it reaches the coast. The wave will run-up the coast like a rapidly rising tide, which is called a surging wave. For the intermediate slopes, the wavefront steepens and will eventually break into a bore-like shape. Since the continental slope along the Sanriku coast varies between 1/50 and 1/150, the different observed wave types at different locations during the 2011 Tohoku Earthquake Tsunami are consistent with the results of these simple simulations.

For the simulations with the most gentle slope, undular bore formation can be observed. Because the continental shelf is really wide and shallow, nonlinearities, dispersive effects and energy dissipation can play an important role in the transformation of the wavefront and undular bore formation can occur. This formation of short waves means that there will be a transfer of energy from the long tsunami wave to the short waves. The train of short waves extends behind the steep front since they travel with the group velocity $\partial\omega/\partial k$ which is smaller than the shallow water speed $\sqrt{gh}$ at the steep front (Grue et al., 2008). A more detailed description of undular bore formation is given in section 2.4.2.

5.4.3. Breaker parameter for 1D approximations

Glasbergen (2018) did research about tsunami wave transformation over different continental shelf slopes, which results are outlined in section 3.3 and 3.5.

To obtain a more accurate classification of tsunami wave types, similar but more extensive simulations are conducted. The purpose of these simulations is to distinguish different breaking wavefronts. For normal waves breaking waves are classified in plunging and spilling waves, see section 2.3.3. This classification is somewhat different for tsunami wave. In this research, it is suggested to classify tsunami wavefronts into four different types. The non-broken wavefront (surging), broken wavefront, undular bore formation and broken undular bore front. See figure 5.5 for four different simulations with four different wavefront types.

The tsunami breaker parameter $\xi_{tsunami}$ proposed by Glasbergen (2018) is given in equation 5.1. This parameter is plotted against the proposed Froude number at the coastline Fr_{coast} in figure 5.6a and the maximum momentum flux at the coastline in figure 5.6b.

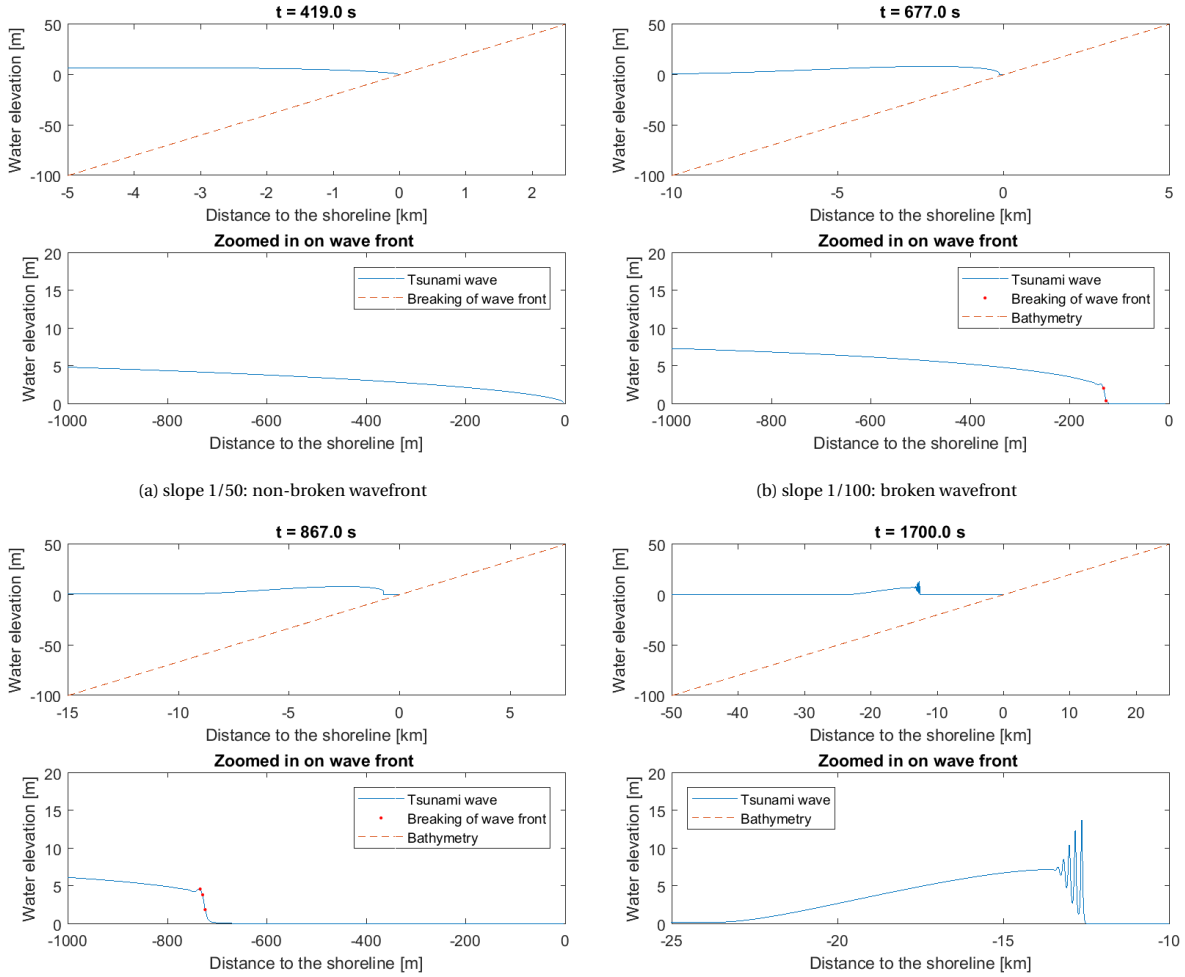

(a) slope 1/50: non-broken wavefront

(b) slope 1/100: broken wavefront

(c) slope 1/150: broken wavefront

(d) slope 1/500: undular bore formation

Figure 5.4: 1D simulations of tsunami transformation for different slopes. BC: sinusoidal wave H = 6m and T = 600s

$$\xi_{tsunami} = \frac{tan(\alpha_2)}{\sqrt{\frac{H_\xi}{L_\xi}}} \tag{5.1}$$

For all performed simulations, undular bore formation eventually turns into undular bore breaking. This is the reason why the final wave type distinction, which is described by the parameter $\xi_{tsunami}$, is made in for three kind of wavefronts; undular breaking, breaking front and non-breaking front (surging). Undular bore formation and undular bore breaking occurs for small values of $\xi_{tsunami}$, where the wavefront has features of a surging wave for large values of $\xi_{tsunami}$. Interesting is that the momentum flux at the coastline is much higher for undular bore tsunamis than for broken wavefront tsunamis.

- $\xi_{tsunami} < 0.27$ Undular breaking
- $0.27 < \xi_{tsunami} < 0.54$ Breaking front
- $\xi_{tsunami} > 0.54$ Surging front

5.4.4. Empirical formulas for 1D tsunami wave breaking

Figure 5.7 shows the results of the simulations and the trend lines for the location of undular bore formation, undular bore breaking and wavefront breaking (without undular bore formation). The Coefficient of Determination R^2 is a statistical measure that tells you how close the data fits the trend line. The closer R^2 to 1.00,

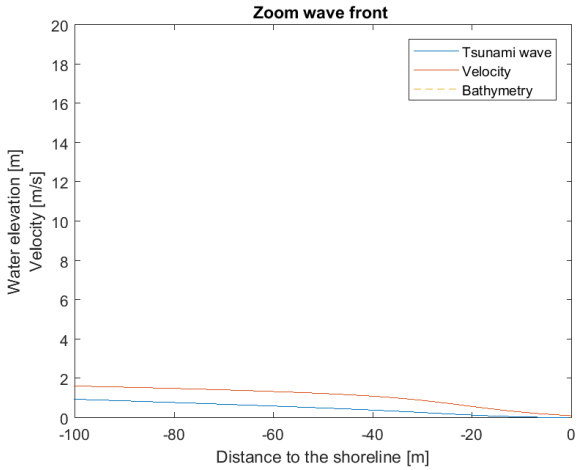

(a) slope 1/50: non-breaking wavefront

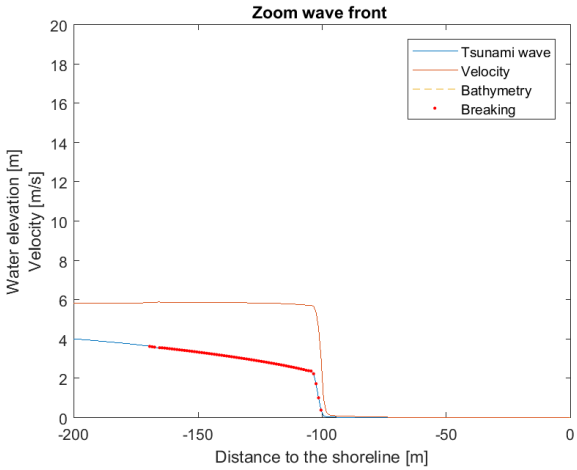

(b) slope 1/100: breaking wavefront

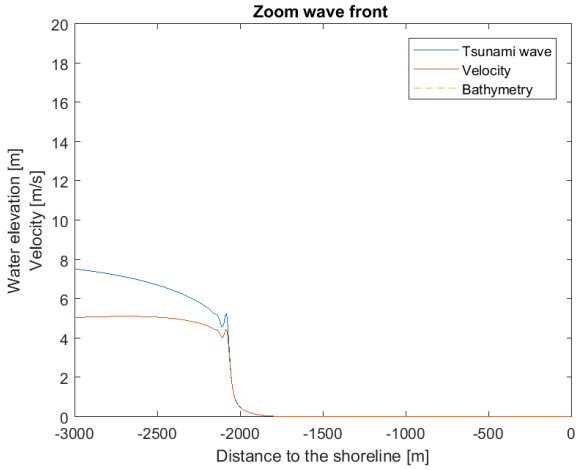

(c) slope 1/200: undular bore formation

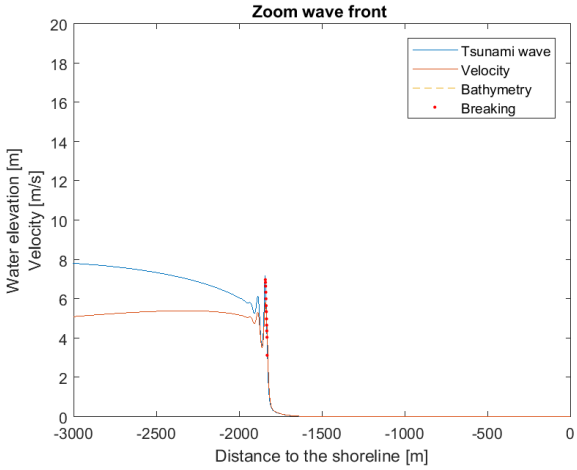

(d) slope 1/200: breaking undular bore front

Figure 5.5: 4 simulations with 4 different wavefront types. BC: sinusoidal wave H = 6m and T = 600s

the better the fit. Equation 5.2, 5.3 and 5.4 are the empirical equations that describes the trend line for the different tsunami types. The fit of the trend lines for undular bore formation and undular bore breaking is quite good in contrast to the trend line for the wavefront breaking.

$$Undular\ bore\ formation: \quad x = 34.7 * \xi_{tsunami}^{-2.46} \quad [m] \tag{5.2}$$

$$Undular\ bore\ breaking: \quad x = 60.7 * \xi_{tsunami}^{-2.03} \quad [m] \tag{5.3}$$

$$Wave\ front\ breaking: \quad x = 1.97 * \xi_{tsunami}^{-4.13} \quad [m] \tag{5.4}$$

5.5. Simulations: 2DH model

The indented coastline along the Sanriku coast ensures that 2D effects become important in the nearshore area. 2DH simulations are performed to provide more insight into the influence of different bay geometries on the transformation of a tsunami wavefront. Figure 5.8 gives an example of a simulation with α_2 = 1/100 W_b = 3000 m, W_h = 1500 m and a boundary condition wave with H = 6 m and T = 600 s. In figure 5.9 small irregularities can be seen near the boundaries of the bay. However, these can be neglected in the middle of the bay. Therefore, the obtained results in the following simulations are based on the output values in the middle

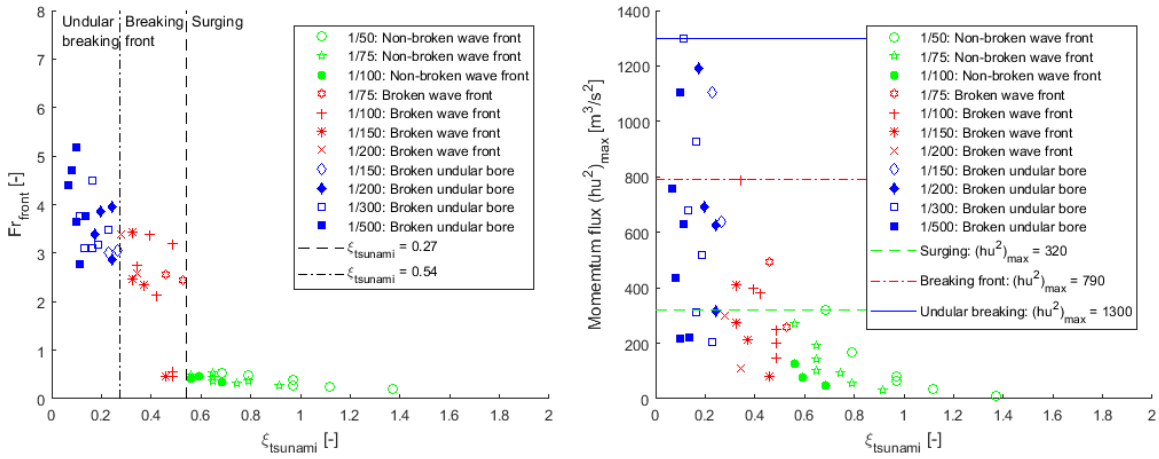

(a) Breaker parameter ($\xi_{tsunami}$) vs. Froude number (Fr_{coast})

(b) Breaker parameter ($\xi_{tsunami}$) vs. Momentum flux (hu^2)

Figure 5.6: Breaker parameter ($\xi_{tsunami}$) vs Froude number (Fr_{coast}) and Momentum flux (hu^2).

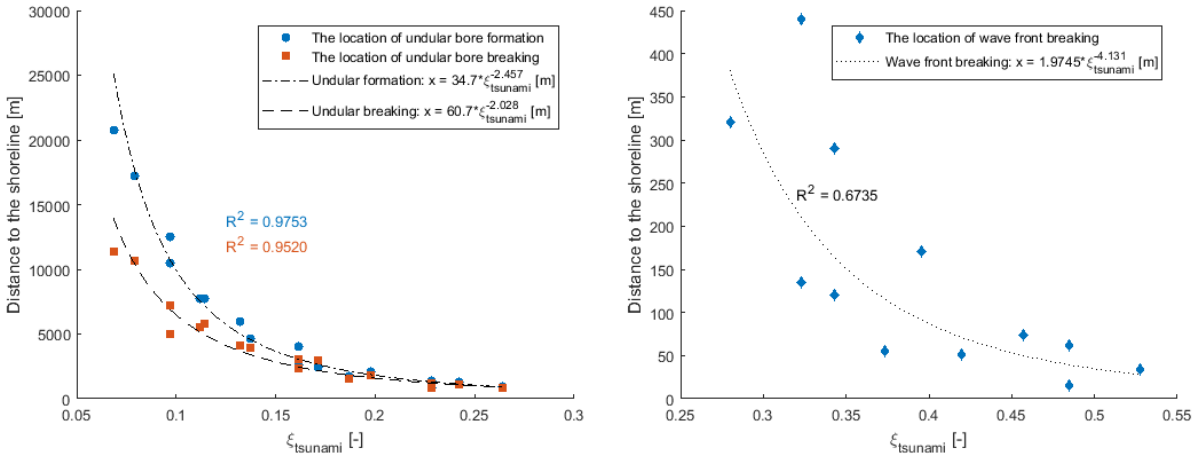

(a) Undular bore formation and breaking

(b) wavefront breaking

Figure 5.7: Empirical fitting to obtain formulas to predict the location of undular bore formation, undular bore breaking and purely wavefront breaking. R^2 is the coefficient of Determination.

of the bay, given by the red line in figure 5.8a. All the results of the simulations can be found in appendix E.

5.5.1. Bay geometry

The Sanriku coastline is an indented coastline consisting of several bays. Since the narrowing of the bay influences the amplification of the wave, and therefore the breaking, the following hypothesis is established:

The amount of narrowing of the bay, averaged over the length of the bay, is the most important 2D parameter in the transformation of a tsunami wave in a bay.

Besides the slope of the continental shelf (α_2) and the wave characteristics (H_{100} and T_{front}), this bay geometry is an important parameter in this research since the change in geometry of the bay is assumed to affect the wave transformation of the tsunami wave near the Sanriku coastline due to the shoaling effect of Green's Law. To include the effect of bay geometry a bay factor β is proposed. This factor describes the ratio of narrowing over the length of the bay. Assumed is that the bay mouth is located at a depth of 100 m, therefore the bay factor β is given by equation 5.5. In the following subsections, the results of the 2DH simulations are discussed to strengthen the hypothesis.

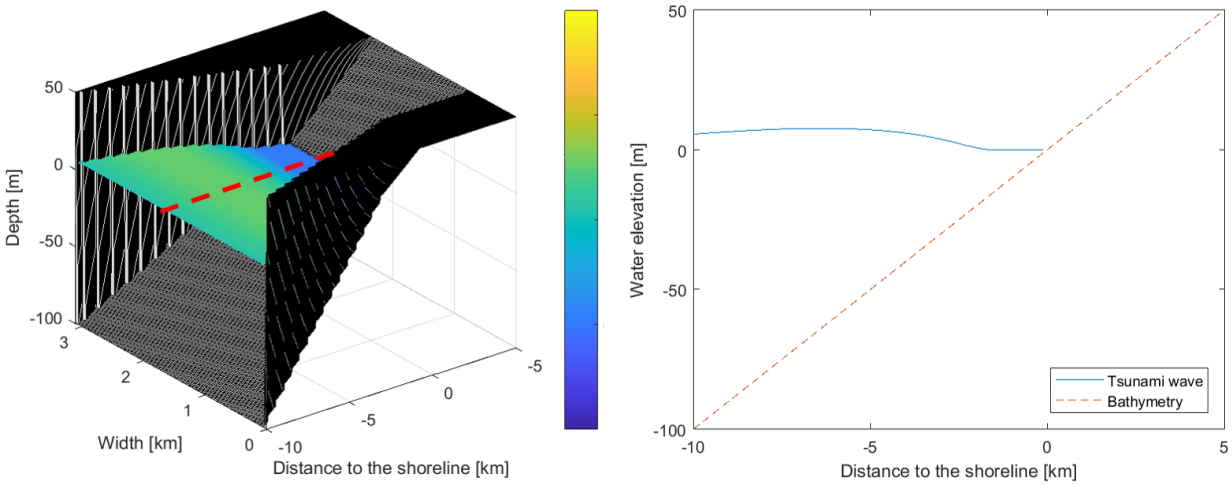

(a) 3D animation, red dashed line indicates the section of the 1D plot

(b) Plot of the section indicated in figure 5.8a

Figure 5.8: Example of a 2DH SWASH simulation

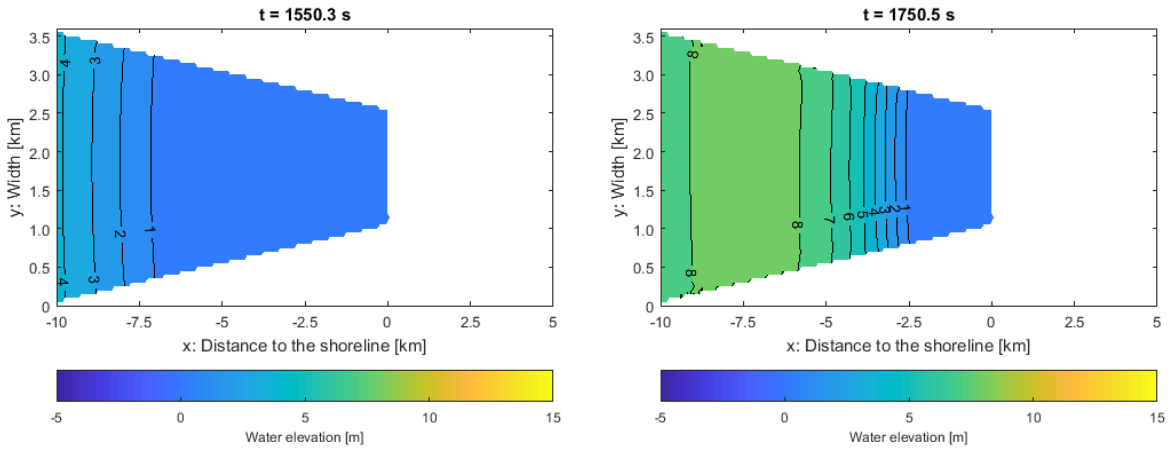

(a) t = 1550.3 s

(b) t = 1750.5 s

Figure 5.9: Top view simulation with 2D effects

$$\beta = \frac{W_b}{W_h} \tag{5.5}$$

As a reference bay, a schematic bay of Otsuchi is taken with the following dimensions:

- Width of the bay mouth (W_b) = 3500m;
- Width of the bay head (W_h) = 1500m;
- Length of the bay (L_b) = 10000m;
- Slope of the bay (α_2) = 100m/10000m = 1/100.

First, the influence of each geometry parameter is explained separately. After that, the final results of the 2DH simulations are outlined.

Length of the bay (L_b)
Since the bay mouth is assumed to be located at a depth of 100 m, the length of the bay is related one to one to the slope of the bathymetry α_2. The influence of a changing slope of the bay was given in section 5.4 for the 1D case.

Bay mouth (W_b)

For a changing W_b, the bay factor (β) will change. The results of the simulations, with the only changing parameter W_b, are shown in table 5.2. The funnelled shaped geometry of the bay will amplify the tsunami wave and therefore the steepness of the wave increases. The larger the bay mouth opening, the larger this amplification factor becomes. This ensures that the wavefront breaks earlier when the bay mouth increases. Besides that, the wave height at the coastline, the velocity at the coastline and the momentum flux at the coastline increase when W_b increases.

- The wave breaks earlier, more offshore, when W_b increases;
- The wave height at the coastline H_{coast} increases when W_b increases;
- The velocity at the coastline u_{coast} increases when W_b increases;
- The momentum flux hu^2 increases when W_b increases.
- Fr_{coast} is larger for 1D simulations compared to 2DH simulations.

Table 5.2: 2DH simulations: Influence of a changing bay mouth width W_b. *1D simulations, without influence of bay geometry.

Test	α_2	L_{front} **[m]**	H_ξ **[m]**	W_b **[m]**	W_h **[m]**	β **[-]**	**Wave type**	**Breakpoint [m]**	Fr_{coast} **[-]**	$(hu^2)_{max}$ $[m^3/s^2]$
8*	1/75	9396.276	6	x	x	1.00	Breaking front	34	2.43268	257.15
10	1/75	9396.276	6	2000	1500	1.33	Breaking front	58	1.186456	332.05
11	1/75	9396.276	6	3000	1500	2.00	Breaking front	85	1.356257	490.87
12	1/75	9396.276	6	4000	1500	2.67	Breaking front	88	1.226679	654.05

Head of the bay (W_h)
The influence of this changing width is quite similar to the change in bay mouth width since it is changing the bay factor in an opposite but equal way. The results, with the only changing parameter W_h, are shown in table 5.3. When W_h increases, the amplification of the wave decreases and therefore the steepness decreases. The tsunami wave will break in a later stage. The wave height, velocity and momentum flux at the coastline decreases when W_h increases.

- The wave breaks later, more nearshore, when W_h increases;
- The wave height at the coastline H_{coast} decreases when W_h increases;
- The velocity at the coastline u_{coast} decreases when W_h increases;
- The momentum flux hu^2 decreases when W_h increases.

Table 5.3: 2DH simulations: Influence of a changing bay headwidth W_h. *1D simulations, without influence of bay geometry.

Test	α_2	L_{front} **[m]**	H_ξ **[m]**	W_b **[m]**	W_h **[m]**	β **[-]**	**Wave type**	**Breakpoint [m]**	Fr_{coast} **[-]**	$(hu^2)_{max}$ $[m^3/s^2]$
8*	1/75	9396.276	6	x	x	1.00	Breaking front	34	2.43268	257.15
9	1/75	9396.276	6	3000	2000	1.50	Breaking front	61	1.362107	387.1
11	1/75	9396.276	6	3000	1500	2.00	Breaking front	85	1.356257	490.87
13	1/75	9396.276	6	3000	1000	3.00	Breaking front	105	1.400238	675.55
14	1/75	9396.276	6	3000	500	6.00	Breaking front	125	1.3713	678.19

Bay shape factor (β)
The bay shape factor β is an important parameter for the amplification of a tsunami wave. When the factor is equal to 2, it means that all the incoming water volume has to be 'squeezed' trough half of the bay mouth width. This squeezing effect will amplify the wave and it therefore affects the breaking of the wave. Simulations 11, 15 and 16 have the same β, shown in table 5.4. The point of breaking, the Froude number and the momentum flux is approximately equal for these simulations. This corroborates the hypothesis that the bay factor β is one of the most important parameters of the bay geometry.

An interesting conclusion can be made when comparing simulations 6 and 7, where the only changing parameter is β. Simulation 6 is a 1D simulation (β = 1) and simulation 7 is 2DH simulation where bay geometry is included (β = 2). The wave type at the coastline is different for the simulations, a surging wave for a simulation without the influence of bay geometry and a breaking wave for a simulation including bay geometry. Since the tsunami parameter $\xi_{tsunami}$ (Glasbergen, 2018) gives the same value for both simulations, the bay geometry influence have to be included in the tsunami parameter.

- The wave breaks earlier, more offshore, when β increases;
- The wave height at the coastline H_{coast} increases when β increases;

- The velocity at the coastline u_{coast} increases when β increases;
- The momentum flux hu^2 increases when β increases.

Table 5.4: 2DH simulations: Influence of the bay geometry (β). *1D simulations, without influence of bay geometry.

α_2	**Test**	L_{front} **[m]**	H_ξ **[m]**	β [-]	**Wave type**	**Breakpoint [m]**	Fr_{coast} [-]	$(hu^2)_{max}$ $[m^3/s^2]$	$\xi_{tsunami}$ [-]
1/75	6*	9396.276	4	1.00	Surging	x	0.5411	102.61	0.64627
	7	9396.276	4	2.00	Breaking front	60	1.28118	142.12	0.64627
	8*	9396.276	6	1.00	Breaking front	34	2.43268	257.15	0.527675
	10	9396.276	6	1.33	Breaking front	58	1.186456	332.05	0.527675254
	9	9396.276	6	1.50	Breaking front	61	1.362107	387.1	0.527675254
	11	9396.276	6	**2.00**	Breaking front	**85**	**1.356257**	**490.87**	0.527675254
	12	9396.276	6	2.67	Breaking front	88	1.226679	654.05	0.527675254
	13	9396.276	6	3.00	Breaking front	105	1.400238	675.55	0.527675254
	14	9396.276	6	6.00	Breaking front	125	1.3713	678.19	0.527675254
	15	9396.276	6	**2.00**	Breaking front	**75**	**1.382527**	**488.05**	0.527675254
	16	9396.276	6	**2.00**	Breaking front	**80**	**1.208836**	**501.32**	0.527675254

5.5.2. Breaker parameter for 2DH approximations

As explained in the last subsection, the bay geometry needs to be included in the tsunami breaker parameter. Therefore, a new tsunami parameter $\xi_{tsunami,2DH}$, including 2D effects, is proposed by including the bay factor β in the tsunami breaker parameter $\xi_{tsunami}$. To include the influence of a converging geometry of the bay, it is assumed that the wave height in the bay will increase by the refraction factor K_r from the Green's Law formula (equation 2.1). Green's Law describes the increase in wave height due to a varying width by a factor $\sqrt{b_o/b_i}$. When applying this factor to a varying bay width, the refraction factor becomes $\sqrt{W_b/W_h} = \sqrt{\beta}$. Therefore, β is put in the denominator in front of the wave height, given by equation 5.6.

$$\xi_{tsunami,2DH} = \frac{tan(\alpha_2)}{\sqrt{\frac{\beta H_\xi}{L_\xi}}} = \xi_{tsunami} * \beta^{-1/2} \tag{5.6}$$

The proposed parameter $\xi_{tsunami,2DH}$ is plotted against the Froude number and the maximum momentum flux at the coastline in figure 5.10. A clear distinction between a surging wave and a breaking wavefront is obtained. One simulation, for a slope of 1/75, does not meet this boundary for an unknown reason. Therefore, the boundary of breaking for $\xi_{tsunami,2DH}$ = 0.46 is a good approximation but not 100% reliable.

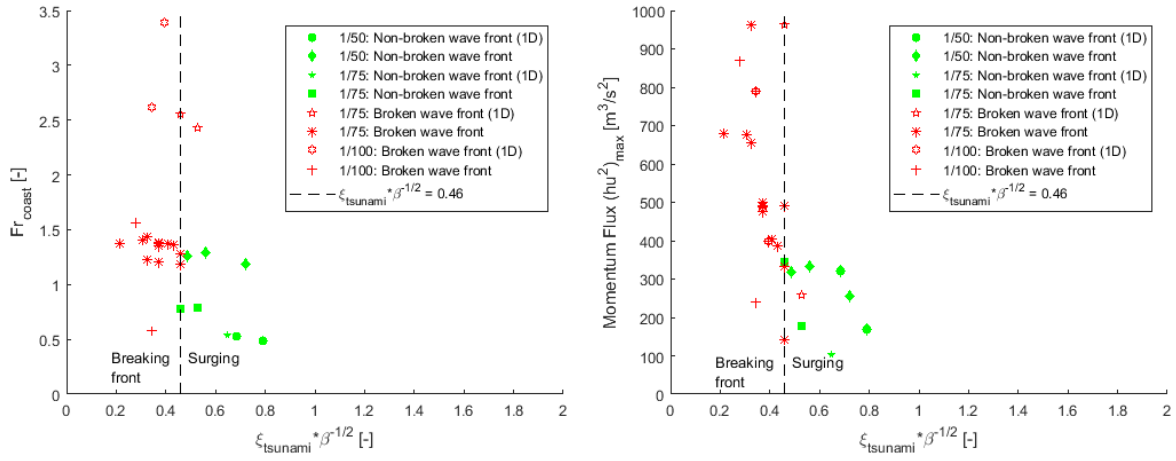

(a) Froude number (Fr_{coast})

(b) Momentum flux ($(hu^2)_{max}$)

Figure 5.10: $\xi_{tsunami}{}^*\beta^{-1/2}$ vs Froude number (Fr_{coast}) and Momentum flux ($(hu^2)_{max}$).

The wave characteristics in the proposed tsunami breaker parameter $\xi_{tsunami}$, H_ξ and L_ξ, are the wave height and wavelength at a depth of 100 meter. Since the transformation of tsunami waves can be approximated by Green's Law, these wave characteristics can be converted to parameters without a fixed depth. By substituting

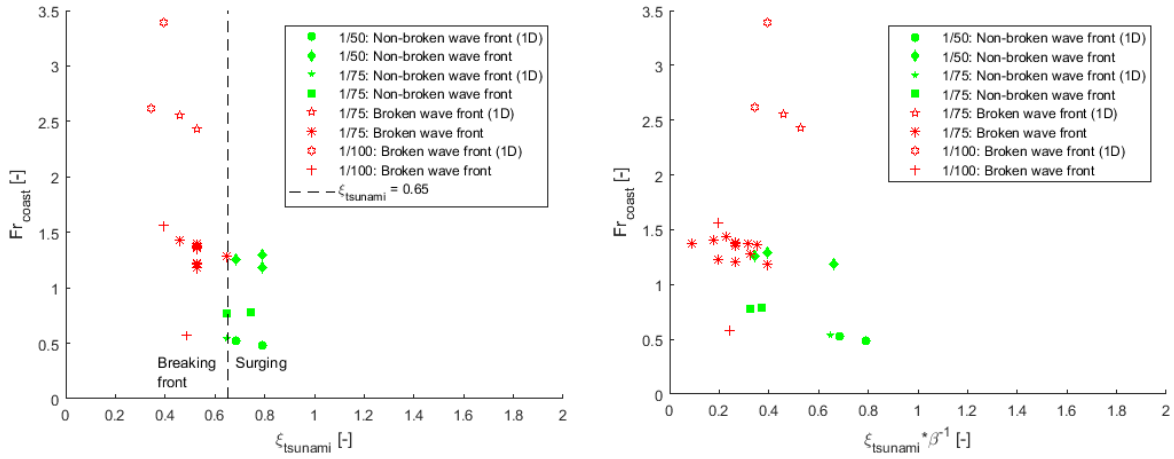

(a) $\xi_{tsunami}$ (b) $\xi_{tsunami}{}^{*}\beta^{-1}$

Figure 5.11: Comparison tsunami parameters vs Froude number (Fr_{coast}).

offshore parameters in equation 2.1 and applying $L/\sqrt{gd} = constant$ (Green's Law), the tsunami parameters can be described by equation 7.2 and 7.3. The input parameters for the breaker parameter, H_ξ and L_ξ, can be obtained by any offshore depth d_o, offshore wave height H_o and offshore wavelength L_o. Investigation of the accuracy of this approach can be part of a further study.

$$H_\xi = \sqrt[4]{\frac{d_o}{100}} H_o \tag{5.7}$$

$$L_\xi = \frac{1}{2} L_o \frac{\sqrt{g * 100}}{\sqrt{g * d_o}} = L_o \frac{5}{\sqrt{d_o}} \tag{5.8}$$

5.6. Application of the results

To see if the proposed method can be used for predicting tsunami wave types along the Tohoku coastline, a small case study is done with the observations during the tsunami in 2011. 12 different locations where the observed wave type is known, shown in figure 5.12, are used to see if the wave type along the coastline can be predicted with the tsunami parameter $\xi_{tsunami}$ (Glasbergen, 2018) or by the new proposed 2DH tsunami parameter $\xi_{2DH,tsunami}$. The results can be seen in table 5.5.

For the 1D prediction ($\xi_{tsunami}$), four locations are predicted incorrectly. An interesting observation is that only 2 predictions were incorrect when using the new proposed parameter $\xi_{2DH,tsunami}$. This can be due to the bay geometry that is taken into account, which influences the steepness of the wave and therefore the wave breaking. The wrong prediction in the Miyako Bay can probably be explained by the fact that the direction of the incoming tsunami wave is very different for this case. Figure 5.12 shows that the opening of the Miyako Bay is directed to the north-east, where the tsunami wave is coming from the south-east. The wrong prediction for the Hirota Bay cannot be explained immediately. Since the bay slope is gentle and the narrowing effect of the bay is small a breaking wavefront is expected, in contrast to the observations during the 2011 Tohoku Earthquake Tsunami.

Table 5.5: Case study 2011 Tohoku Earthquake Tsunami

		Name	α_2	W_b	W_h	β	H_ξ	T_ξ	L_ξ	$\xi_{tsunami}$	**Prediction 1D**	$\xi_{tsunami} * \sqrt{\beta}$	**Prediction 2DH**	**Observed wave type**
North Sanriku	1	Kuji Bay	1/160	5.5	2.5	2.2	4.20	300	9396.276	0.30	Breaking front	0.20	Breaking front	Breaking
	2	Noda Bay	1/150	9.6	4.5	2.13	4.20	300	9396.276	0.32	Breaking front	0.22	Breaking front	Breaking
	3	Miyako Bay	1/145	3.5	1.4	2.5	4.20	300	9396.276	0.33	Breaking front	0.21	Breaking front	Surging
Central Sanriku	4	Yamada Bay	1/90	3	3	1	6.80	900	28188.83	0.72	Surging	0.72	Surging	Surging
	5	Otsuchi Bay	1/110	3	2.5	1.2	6.80	900	28188.83	0.59	Surging	0.53	Surging	Surging
	6	Toni Bay	1/66	3.3	1.8	1.833333	6.80	900	28188.83	0.98	Surging	0.72	Surging	Surging
	7	Yoshima Bay	1/75	7.3	1.2	6.083333	6.80	900	28188.83	0.86	Surging	0.35	Breaking front	Breaking
	8	Ryori Bay	1/88	3	1	3	6.80	900	28188.83	0.73	Surging	0.42	Breaking front	Breaking
South Sanriku	9	Hirota Bay	1/140	5.7	2.6	2.19	6.40	900	28188.83	0.32	Breaking front	0.24	Breaking front	Surging
	10	Oppa Bay	1/104	6.5	6.5	1	6.40	900	28188.83	0.62	Surging	0.62	Surging	Surging
	11	Onagawa Bay	1/120	5	5	1	6.40	900	28188.83	0.55	Surging	0.55	Surging	Surging
Sendai Plain	12	Yuriage	1/590	x	x	x	6.00	900	28188.83	0.12	Undular breaking			Breaking

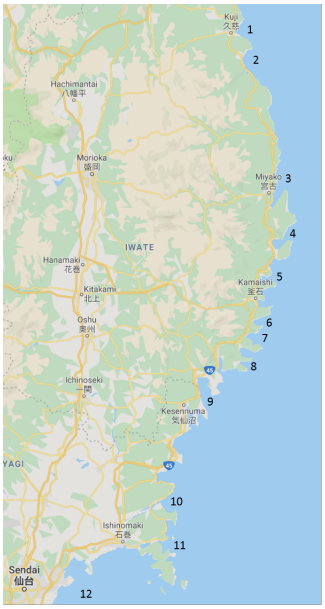

Figure 5.12: Sanriku coast with numbered bays which are used for the case study.

6

Discussion

The objective of this study is to gain more insight into the characteristics of a tsunami wavefront near the Japanese Tohoku coastline. This chapter provides a discussion about the relevance of this research, the made assumptions and the results obtained by the simulations.

6.1. Offshore modelling

For the most tsunami events, both the frequency dispersion and the nonlinearity effects are small and could be neglected for offshore propagation (Liu, 2009). Therefore, the linear theory can be used as a first approximation to calculate changes in tsunami wave height as the wave moves across an ocean (Bryant, 2014). A classic linear theory for shoaling is called Green's Law and applies for cases where the depth varies slowly (Lipa et al., 2016). Glasbergen (2018) compared wave buoy measurements near Sendai, during the 2011 Tohoku Earthquake Tsunami, with the results of a 1D SWASH model and with a Green's Law approximation. Before the point of breaking, Green's Law and the SWASH model gave a rather good match with the buoy observations.

However, when the fault plane is elongated like the one of the 2011 Tohoku Earthquake, the initial free surface profile is almost uniform over the fault line and the tsunami propagates mainly in perpendicular direction of the fault line. It therefore seems unlikely that Green's Law, which is a 1D analytical solution, is valid for all locations along the Tohoku coast. Sendai is located with a small angle relative to the perpendicular propagation path, figure 4.8, which can be the reason that Green's Law gives a good approximation of the observations. To establish that Green's Law can predict the shoaling water level up to the point of breaking over more locations along the Tohoku coast, simulations have been performed for the Kamaishi (central Sanriku) location. Again, Green's Law turned out to be a good approximation of the water level near the Kamaishi Bay, after comparing this analytical solution with the buoy observations and the SWASH simulations in figure 4.6b. Another location with recorded buoy observations is the Kuji Bay, located more northwards of the tsunami source area. The buoy observations near Kuji show that the first tsunami wave height is smaller than near Sendai and near the Kamaishi Bay. Since the depth of the buoy near Kuji is located at a smaller depth than the buoy near Sendai and Kamaishi, Green's Law will give a highly overestimated value of the water level. This implies that 1D simulations and 1D analytical solutions are not valid any more. Based on these findings and the angles given in figure 4.8, the Green's Law approximation seems to be valid for locations with an angle of 0-33° relative to the perpendicular propagation path of the 2011 Tohoku Earthquake Tsunami. Given the fact that these conclusions are made based on only three locations, this boundary of 33° is not very strict. However, it can be said that the wider the angle θ, the worse the Green's Law approximation becomes.

A two-dimensional bathymetry, which influences the effects of refraction, diffraction and reflection, is needed for proper simulation of a tsunami wave propagation. However, making a 3D-model of the offshore to the nearshore area is highly time-consuming, problematic and is not the main goal of this study. The goal is to document the transformation of the leading tsunami wave up to the shallow continental shelf with an initial wave shape at time is zero. The most important parameters for this initial wave shape are a realistic leading depression, wave height and front part of subsequent wave crest. Reflection due to bottom topography is

assumed to be small since the change in bathymetry changes smoothly.

Finally, the validation of the 1D model is a point of attention. The initial height distribution, estimated from the tsunami waveform inversion analysis of Saito et al. (2011), is used as an initial condition of the SWASH simulations. After that, the model is validated based on the tsunami waveforms obtained along the Tohoku coastline. This is a wrong approach for validation since the initial condition and the validation is based on the same data. However, it shows that SWASH correctly simulates the shoaling effect of long tsunami waves, which is important for this research.

6.2. 1D nearshore model

Several Design Standards have been proposed that deal with tsunami loads on coastal structures, like the American Society of Civil Engineers (ASCE) and the Federal Emergency Management Agency (FEMA), discussed in chapter 3. ASCE (2016) distinguishes two different tsunami loads on the structure, one for tsunami waves with bore formation and one for tsunami waves without bore formation. They assume bore formation for prevailing nearshore bathymetric slopes of 1/100 and milder or when historically documented, described by recognized literature or determined by a site-specific inundation analysis. FEMA (2012) came up with a classification of coastal inundation in figure 1.5. This classification shows that tsunami waves will attack the shoreline differently, but it is not quantitative in the sense that it is not linked to real values. Therefore, a more quantitative understanding of the transformation due to breaking is needed to predict tsunami attack on defence systems like a seawall or seadyke built near the coastlines of Tohoku.

Yeh (2006) concluded that the impact momentum increases with the steepness of the bore front. Since the Froude number is related to the steepness of the wavefront, this is a good dimensionless parameter to compare different tsunami wave impacts on coastal structures. To analyse different kind of tsunami types, a local Froude number at the coastline (Fr_{bore}) was performed by Glasbergen (2018). A tsunami breaker parameter ($\xi_{tsunami}$) was proposed to describe the tsunami wave at a depth of 100 m. A tsunami that breaks and develops into a bore before it reaches the coastline is defined as a plunging breaker, and a non-broken wave that develops a bore inland is defined as a surging breaker. For cases where ($\xi_{tsunami}$) is smaller than 0.35, the wave is plunging and when ($\xi_{tsunami}$) is larger than 0.35 the wave is surging. Glasbergen (2018) recommended to improve the breaker parameter by performing simulations for a steeper slope, to do more research about the exact location of breaking and to classify the breaking wave in 'spilling' and 'plunging'.

$$\xi_{tsunami} = \frac{tan(\alpha_2)}{\sqrt{\frac{H_\xi}{L_\xi}}} \tag{6.1}$$

For tsunami waves, the classification of breaking or not breaking is not that clear since there are two types of breaking. Wave dissipation due to undular bore formation (section 2.4.2) can occur when propagating over a gentle slope, where the small amplitude waves can break eventually. Wavefront breaking without undular bore formation can happen for steeper slopes because of the limited propagation length and therefore the absence of wave dispersion. Since the definition of a bore is not that clear for tsunami waves, the name 'bore' is replaced by 'front' in this research. To give a better classification in tsunami waves approaching shore the breaker parameter of Glasbergen (2018) is improved by doing more 1D simulations with a steeper shelf slope (α_2 is 1:50 and 1:75) and a more gentle slope (1:500). Tsunami waves approaching the shore are now classified in three different types: non-broken wavefront (surging), broken wavefront and broken undular bore. An overview of the results is shown in figure 5.6a. The value found for the transition from a surging to a breaking front is different from the one found by Glasbergen (2018). $\xi_{tsunami}$ is shifted from a value of 0.35 to 0.54. This can be explained by the fact that the definition of breaking is different. In this research, a surging wave is defined when the wavefront is not broken when it reaches the coastline, based on the SWASH threshold of breaking given by equation 1.1. Glasbergen (2018) defined a surging wave as waves where the maximum local depth-averaged bore front velocity u_{front} is further than 30 m inland, not based on the SWASH threshold of breaking. Due to this more accurate way of describing breaking waves, some simulates waves can be classified as 'broken' in this research, where it was 'surging' according to Glasbergen (2018).

Research has been done about more detailed empirical equations, based on the results of the 1D SWASH simulations. The coefficient of determination R^2 confirms that equation 6.2 is a good fit to describe the location

of undular breaking formation and undular breaking. An equation for the location of wavefront breaking is not found because the data points of the simulations cannot be described with an accurate fit.

$$\begin{aligned} Undular\ bore\ formation: &\quad x = 34.7 * \xi_{tsunami}^{-2.457} \quad [m] \\ Undular\ bore\ breaking: &\quad x = 60.7 * \xi_{tsunami}^{-2.028} \quad [m] \end{aligned} \tag{6.2}$$

Lastly it must be said that the obtained Froude numbers Fr_{coast} differ from the Froude numbers given in other literature Chanson (2009) (Tissier et al., 2011) (ASCE, 2016), where values <1.4 were found for undular bores and >1.4 for purely breaking bores. This is because of the definition of the Froude number, which is different in this research.

6.3. 2DH nearshore model

Tsunami transformation is a bay along the Sanriku coast can be compared with the investigations of Bonneton et al. (2015) about the formation and dynamics of tidal bores in funnel-shaped estuaries. They showed that tidal bore formation is mainly governed by a dissipative parameter $\mathfrak{D}$ given in equation 3.9, which characterizes the amount of nonlinearity. $\mathfrak{D}$ depends on the bottom friction, the wave characteristics and the estuary geometry. The $\mathfrak{D}$ parameter is enhanced by the increase of the tidal range, friction coefficient, converging length and bathymetry slope. When $\mathfrak{D}$ is large, the dissipative character of the estuaries is large and the conditions are favourable for bore formation. These findings can be used as a hypothesis for tsunami behaviour in the bays along the Sanriku coast. In this research, the influence of bottom friction on the tsunami wave transformation before the coastline turned out to be not important. The influence of wave characteristics and bay geometry throughout this thesis is therefore in line with the approach of Bonneton et al. (2015).

To investigate this influence of bay geometry, a schematic model (figure 1.8) is used to perform several 2DH SWASH simulations. After setting out the influences of the parameters separately, the W_b/W_h-ratio turned out to be the most important. For simulations with the same W_b/W_h-ratio but different bay dimensions, the transformation of the waves were approximately similar. This implies that the bay shape factor β is an important parameter in the transformation of tsunami waves along the Sanriku coast.

An important process in these simulations is wave breaking. However, SWASH is a non-hydrostatic model which cannot be directly applied to details of breaking waves, since essential processes such as overturning, air-entrainment and wave generated turbulence, are absent. But, if only the macro scale is important, the conservation of mass and momentum can be used to treat discontinuities in flow variables (free surface, velocities) in a proper way, to determine energy dissipation of waves (Smit et al., 2013). SWASH uses a hydrostatic front approximation, which is an effective and efficient method to approximate wave-breaking phenomenons in the non-hydrostatic phase resolving model. The hydrostatic pressure is assumed at the front of the wave when it exceeds a certain threshold of the steepness of the wave, equation 1.1. The range of maximum steepness (α_s) varies in literature, from α_s = 0.3 (Schäffer et al., 1993) to α_s = 0.6 (Lynett, 2006). The threshold used in SWASH is based on simulations of flume experiments and a α_s of 0.6 is advised, which correspond to a local front slope of 25° (Smit et al., 2013). There is no need to calibrate this value since it seems to work well for all test cases carried out by the authors of SWASH.

The proposed tsunami breaker parameter for 2DH situations $\xi_{tsunami,2DH}$ gives another distinction between surging waves and breaking wavefronts, given in figure 5.10. The quantitative classification of tsunami waves in bays is a good improvement of the surf similarity parameter given by (ASCE, 2016) in equation 3.1, which is not valid where there is an expectation of wave focussing in bays. Unfortunately, the 2DH simulations are only conducted for a slope of 1/50, 1/75 and 1/100. Since the slope of the Sanriku coast near Kuji Bay is around 1/150, these simulations have to be included. Due to problems with the SWASH model, this is not done yet.

To reduce the simulation time, curvilinear grids are used in the model with a finer resolution of 1 m in front of the shore and 50 m more offshore. During the simulations, small discontinuities can be observed at the boundary between the coarse and the fine grid size. The influence of these discontinuities on the transformation of the wavefront is assumed to be negligible.

The schematized model used for the simulations is a simplified representation of reality. Since the bathymetry and geometry in reality is much more complicated, the observations may differ from the results of the model.

The advantage of the simplified model is that it is easy to see what the influence is of each parameter individually and to give a general overview of the processes, which is the aim of this thesis.

A small is case study is conducted to see if the wave type along the Tohoku coastline can be predicted with the new proposed method. It turned out that $\xi_{2DH,tsunami}$ gives a more accurate prediction in wave type since the bay geometry is included. Still some locations cannot be predicted in a good way since the incoming wave direction is different. Therefore, it would be a good option to include the incoming wave angle in the tsunami breaker parameter too.

7

Conclusions and recommendations

In section 7.1 the final conclusions of this study are presented and in section 7.2 the recommendations for further research are proposed.

7.1. Conclusions

This research aimed to **predict the characteristics of a tsunami wave along the Tohoku coastline** in the northern part of Japan. Based on literature, Youtube videos, numerical modelling and analytical reasoning it can be concluded that both the continental shelf slope (α_2) and the bay geometry (β) have a significant influence on the transformation of a tsunami wave near the coastline. The sub-questions, stated in section 1.2, are used to describe the conclusions of this research.

How can the Tohoku coastline in Japan schematically be classified?

This research focusses on the Tohoku coastline, which mainly consists of the Sendai Plain and the Sanriku coastline. Where the Sendai Plain features a fluvial lowland and a flat coastal plain, the Sanriku coast is known as a "ria-coast" and is a rugged coastline that consists of numerous small bays of variable geometry that stretches over 300 km (figure 1.2).

The observations of the tsunami wave type during the 2011 Tohoku Earthquake Tsunami differed along the Tohoku coastline, where the bathymetry is one of the main reasons for this. An important parameter to classify a coastline is the slope of the continental shelf, in this research assumed as the averaged slope from a depth of 100 m up to the coastline (α_2). The continental shelf slope near Sendai is 1/500 and the slope along the Sanriku coast varies between 1/50 and 1/150 (Navionics, 2018; Shimozono et al., 2012).

A further classification is needed along the Sanriku coast since 2D effects become important due to the presence of an indented coastline consisting of converging bays/estuaries. The shape of the bays are defined in two types: a U-shape bay and a V-shape bay, figure 3.5 (Shimozono et al., 2012). A schematization is used to describe the geometry of the bays along the Sanriku coast, given in subsection 1.3.2. The Tohoku coastline in Japan can be described schematically by the following parameters:

- Continental shelf slope α_2;
- Bay slope α_3;
- bay mouth depth d_b;
- Bay length L_b;
- Bay mouth width W_b;
- Bay head width W_h.

The slope of the bay is assumed to be equal to the continental shelf slope and the bay mouth depth is kept constant at a depth of 100 m.

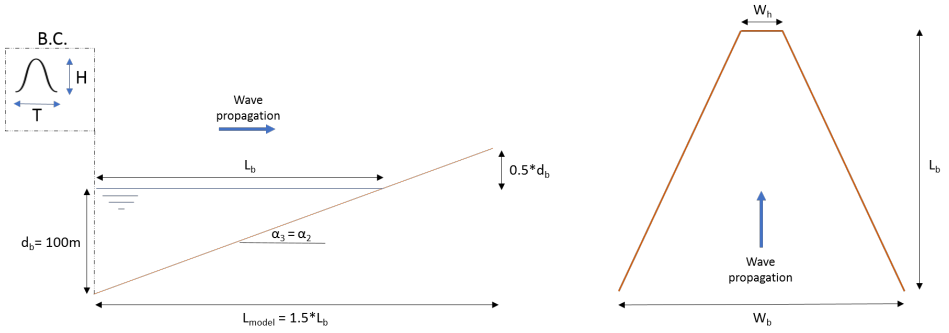

Figure 7.1: Schematic ria bay at the Sanriku coast

What are the most important parameters to model tsunami waves propagating towards the coast?

It has been shown that nonlinear effects can be neglected for long wave propagation in the deep ocean (d/L«1). Since nonlinear effect can be neglected during the offshore propagation of tsunami waves, the most important offshore parameters are the ones that influence the linear transformation of the wave; the offshore wave height H_o, the offshore wavelength L_o, the offshore depth d_o and the depth of the continental shelf d_c.

A 1D numerical model like SWASH is a good tool to obtain the order of magnitude of the first tsunami wave. The main propagation path of a tsunami wave is perpendicular to the fault lane. Since this fault plane is parallel to the coastline in the northern part of Japan, the waves will travel mainly from the source of the tsunami perpendicular to the coast. Green's Law, an analytical solution, appears to give a good approximation of the water level near the coastline for locations with an angle of 0 to roughly 33°relative to the perpendicular propagation path.

A 1D model to describe tsunami wave propagation is very limited since 2D effects like refraction are not taken into account. Therefore, Green's Law can only be used for tsunami wave propagation perpendicular to the coast.

Which parameters influence the type of tsunami at the coastline?

The nearshore transformation of tsunami waves is affected by two sets of parameters: wave characteristics and geophysical properties. The wave characteristic parameters, wave height H and wavelength L, are important because the wave steepness H/L is the ultimate cause of breaking. The change in H and L is influenced by geophysical properties like the continental shelf α_2 and bay geometries (W_b, W_h, d_b and L_b).

Figure 5.2 shows that an increase in offshore wave height H is related to an increase in the Froude number $Fr_{coast} = u_{coast,max}/\sqrt{gh_{coast}}$ at the coastline for every kind of tsunami wave. Besides that, an increase in wavelength L is related to a decrease in Fr_{coast}. Therefore, a larger steepness of the wave causes a higher Fr_{coast} and a higher momentum flux at the coastline.

The continental shelf slope α_2 turned out to be one of the most important nearshore parameters. Table D.1 gives all the results of the 1D simulations. Undular bores develop over continental shelf slopes of 1/150 up to 1/500, depending on the initial wave characteristics. Wavefront breaking, without undular bore formation, occurs for slopes between 1/75 and 1/200. For continental slopes varying between 1/50 and 1/150, which is exactly the range of slopes along the Sanriku coast, the waves have features of a non-breaking surging wave.

A bay shape factor β is introduced to describe the amount of narrowing over the length of the bay, given by the W_b/W_h-ratio. The following conclusions can be made after simulating the influence of the bay geometry on the transformation of a tsunami wave:

- The wave breaks earlier, more offshore, when β increases;
- The Froude number Fr_{coast} increases when β increases;
- The wave height at the coastline H_{coast} increases when β increases;
- The velocity at the coastline u_{coast} increases when β increases;
- The momentum flux hu^2 increases when β increases.

In front of the coastline or after inundation of the coastline the tsunami wave is propagating in extremely shallow water or over a dry-bed. For these situations, bottom friction becomes important. (Esteban et al., 2019) concluded that an increase of the bottom roughness causes a lower Froude numbers and steeper fronts for tsunami bores. The lower Froude number ensures that the impact on the coastal structure decreases for an increasing bottom roughness.

How to find a breaking parameter for a tsunami wave in a bay?

A breaker parameter for tsunamis $\xi_{tsunami}$, based on the work of Glasbergen (2018), can be used to obtain more insight in tsunami wave transformation. This parameter, given by equation 7.1, is obtained by conducting 1D and 2DH SWASH simulations for typical continental slopes along the Tohoku coastline and bay geometries along the Sanriku coast. The tsunami breaker parameter shows a distinction in three different tsunami wave types; undular bore breaking, a breaking wavefront and a non-breaking (surging) wavefront. These wave types occur for a gentle, an intermediate and a steep continental shelf respectively. The first classification is based on 1D simulations where there is no bay forming along the coast ($\beta = 1$), with a continental slope (α_s) in the range of 1/50 to 1/500. The second classification is based on 2DH simulations where bay geometry plays a role along the coastline ($1< \beta <6$), with a continental slope in the range of 1/50 to 1/100.

$$\xi_{tsunami} = \frac{tan(\alpha_2)}{\sqrt{\frac{\beta H_\xi}{L_\xi}}} \qquad where \begin{cases} \beta = 1, & \text{for straight lines} \\ \beta > 1, & \text{for indented coastlines} \end{cases} \tag{7.1}$$

$$\begin{aligned} &\xi_{tsunami} < 0.27: && Undular\ bore\ breaking \\ (1D:\beta=1) \qquad &0.27 < \xi_{tsunami} < 0.54: && Breaking\ wavefront \\ &\xi_{tsunami} > 0.54: && Non-breaking\ wavefront\ (surging) \end{aligned}$$

$$\begin{aligned} (2DH: 1<\beta<6) \qquad &\xi_{tsunami} \leq 0.46: && Breaking\ wavefront \\ &\xi_{tsunami} > 0.46: && Non-breaking\ wavefront\ (surging) \end{aligned}$$

The wave characteristics in the proposed tsunami breaker parameter $\xi_{tsunami}$, H_ξ and L_ξ, are the wave height and wavelength at a depth of 100 meter. Since the transformation of tsunami waves can be approximated by Green's Law, these wave characteristics can be converted to parameters without a fixed depth. By substituting offshore parameters in equation 2.1 and applying $L/\sqrt{gd} = constant$ (Green's Law), the tsunami parameters can be described by equation 7.2 and 7.3. The input parameters for the breaker parameter, H_ξ and L_ξ, can be obtained by any offshore depth d_o, offshore wave height H_o and offshore wavelength L_o.

$$H_\xi = \sqrt[4]{\frac{d_o}{100}} H_o \tag{7.2}$$

$$L_\xi = \frac{1}{2} L_o \frac{\sqrt{g*100}}{\sqrt{g*d_o}} = L_o \frac{5}{\sqrt{d_o}} \tag{7.3}$$

Based on several 1D numerical simulations, empirical equations are proposed for the location of undular bore formation, undular bore breaking, and wavefront breaking, given by equation 7.4. The momentum flux increases for wave front breaking and undular bore formation.

$$\begin{aligned} Undular\ bore\ formation: &\quad x = 34.7 * \xi_{tsunami}^{-2.46} \quad [m] \\ Undular\ bore\ breaking: &\quad x = 60.7 * \xi_{tsunami}^{-2.03} \quad [m] \\ Wavefront\ breaking: &\quad x = 1.97 * \xi_{tsunami}^{-4.13} \quad [m] \end{aligned} \tag{7.4}$$

7.2. Recommendations

7.2.1. Simulations

The offshore propagation of tsunami waves can be modelled more accurately with a 2DH model. Since the bathymetry varies over the long-shore direction of the coast, 2D effects like refraction and diffraction become important and this will influence the propagation path to the coast. The secondary small amplitude waves, observed in the buoy data during the 2011 Tohoku Earthquake Tsunami, were not visible in the 1D SWASH simulations. The occurrence of these waves can be explained by edge wave propagation, which can be included with a 2DH model.

To increase the accuracy of the results of the nearshore 2DH model, a fine grid of 1 m has to be used for the entire computational grid. This will increase the computational time significantly, but it will solve the problem of the discontinuities in water level near the coarse to fine grid transition.

Similar 2DH simulations have to be conducted for a slope of 1/150 to include potential undular bore formation along the north part of the Sanriku coast. Besides, more simulations with different wave characteristics have to be conducted to increase the accuracy of transition between surging and wavefront breaking.

7.2.2. Green's Law approximation

The Green's Law approximation seems to be valid for places located with an angle of 0-33°relative to the perpendicular propagation path of the 2011 Tohoku Earthquake Tsunami. Given the fact that these conclusions are made based on 3 locations (Sendai, Kamaishi and Kuji), this boundary of 33°is not very strict. To increase the accuracy of this boundary, Green's Law approximations need to be done for more locations along the Sanriku coast.

7.2.3. Tsunami breaker parameter

The used shematized model is a major simplification of reality. In this research, the bay mouth depth is kept constant at a depth of 100 m. To include the influence of a varying bay depth and a varying bay length more simulations have to be performed including these varying parameters.

Another shortcoming is that the incoming wave angle is not included in tsunami breaker parameter. Section 5.6 describes that the tsunami wave type in the Miyako Bay cannot be predicted in a correct way since the bay mouth opening is directed to the north-east, where the tsunami wave is coming from the south-east. Probably, the wave type in this bay can be predicted in a more accurate way if this incoming wave angle is included.

During this thesis, the input wave parameters (H_ξ and L_ξ) are used at a depth of 100 meter. Equations 7.2 and 7.3 are proposed to use the tsunami parameter $\xi_{tsunami}$ for wave characteristics at variable depths. To obtain the accuracy of this approach, more simulations have to be performed for wave characteristics at different depths.

Bibliography

Allsop, W., Chandler, I., and Zaccaria, M. (2014). Improvements in the physical modelling of tsunamis and their effects. In *Coastlab2014*, pages 1–22.

Árnason, H. (2005). *Interactions between an Incident Bore and a Free-Standin Coastal Structure*. PhD thesis, University of Washington.

ASCE (2016). Tsunami loads and effects for the ASCE 7-16. In *Minimum Design Loads and Associated Criteria for Buildings and Other Structures*, pages 25–50.

Atwater, B. F., Cisternas, M., Bourgeois, J., Dudley, W. C., Hendley II, J. W., and Stauffer, P. H. (1999). Surviving a Tsunami — Lessons from Chile , Hawaii , and Japan. *U.S. Geological Survey*, pages 1–17.

Battjes, J. A. (1974). *Surf Similarity*. Civil Engineering Department Delft University of Technology, Delft.

Bonneton, P., Bonneton, N., Parisot, J.-P., and Castelle, B. (2015). Tidal bore dynamics in funnel-shaped estuaries. *Journal of Geophysical Research: Oceans*, 120(2):923–940.

Bryant, E. (2014). *Tsunami*. Springer International, Chichester, 3 edition.

Chanson, H. (2009). Current knowledge in hydraulic jumps and related phenomena. A survey of experimental results. *European Journal of Mechanics, B/Fluids*, 28:191–210.

Chock, G. Y. K. (2016). Design for Tsunami Loads and Effects in the ASCE 7-16 Standard. *Journal of Structural Engineering*, 142(11).

Clancy688 (2012). Youtube: Tsunami at Kuji port, Iwate Prefecture.

CNN (2011). CNN Breaking News: Japan's Earthquake and Tsunami.

Constantin, A. and Henry, D. (2009). Solitons and Tsunamis. *School of Mathematics*, pages 65–68.

Dalrymple, R. A., Grilli, S. T., and Kirby, J. T. (2015). Tsunamis and Challanges for Accurate Modeling. *Oceanography*, 19(1):142–151.

Esteban, M., Glasbergen, T., Takabatake, T., Hofland, B., Nishizaki, S., Nishida, Y., Stolle, J., Nistor, I., Bricker, J., Takagi, H., and Shibayama, T. (2017). Overtopping of Coastal Structures by Tsunami Waves. *Geosciences*, 7(4):121.

Esteban, M., Roubos, J., Salet, J., Ishii, H., Hamano, G., Iimura, K., Takabatake, T., Hofland, B., Bricker, J., Takagi, H., Nistor, I., Stolle, J., and Shibayama, T. (2019). Role of surface roughness on tsunami bore overtopping of coastal dykes. *To be submitted*.

ExtremePlanet (2014). Detailed Analysis of the 2011 Japan Tsunami – Video Footage , Wave Heights and Damage Imagery.

Eze, C., Uko, D., Gobo, A., Sigalo, F., and Israel-Cookey, C. (2009). Mathematical Modelling of Tsunami Propagation. *Journal of Applied Sciences and Environmental Management*, 13(3):9–12.

FEMA (2012). Guidelines for Design of Structure for Vertical Evacuation from Tsunamis. Technical Report April.

Glasbergen, T. (2018). *Characterization of incoming tsunamis for the design of coastal structures A numerical study using the SWASH model*. PhD thesis, TU Delft.

Goring, D. G. (1978). *Tsunamis - the propagation of long waves onto a shelf*. Phd, California Institute of Technology.

Grilli, S. T., Svendsen, I. A., and Subramanya, R. (2002). Breaking criterion and characteristics for solitary waves on slopes. *Journal of Waterway Port Coastal and Ocean Engineering*.

Grue, J., Pelinovsky, E. N., Fructus, D., Talipova, T., and Kharif, C. (2008). Formation of undular bores and solitary waves in the Strait of Malacca caused by the 26 December 2004 Indian Ocean tsunami. *Journal of Geophysical Research: Oceans*, 113(5):1–14.

Hansen, W. (1949). *Die halbtagigen Gezeiten im Nordatlantsipen Ozean*.

Irwanto, D. (2015). Earthquakes and Tsunamis.

James, S. (2016). Wave Characteristics.

Kaiser, G., Scheele, L., Kortenhaus, A., Løvholt, F., Römer, H., and Leschka, S. (2011). The influence of land cover roughness on the results of high resolution tsunami inundation modeling. *Natural Hazards and Earth System Science*, 11(9):2521–2540.

Kato, Y., Suzuki, Z., Nakamura, K., Takagi, A., Emura, K., Ito, M., and Ishida, H. (1961). The Chile Tsunami of 1960 Observed along the Sanriku Coast of Japan. *Tour*.

Kawai, H., Satoh, M., Kawaguchi, K., and Seki, K. (2011). Recent tsunamis observed by GPS buoys off the pacific coast of Japan. 33:1–15.

Kim, D.-h. and Son, S. (2018). Lagrangian-like Volume Tracking Paradigm for Mass , Momentum and Energy of Nearshore Tsunamis and Damping Mechanism. *Scientific Reports*, 8(1):1–11.

Lipa, B., Barrick, D., and Isaacson, J. (2016). Coastal Tsunami Warning with Deployed HF Radar Systems. In *Tsunami*, pages 73–111.

Liu, P. L. F. (2009). Tsunami. *Earth Systems and Evironmental Sciences*, pages 127–140.

Lynett, P. (2006). Nearshore Wave Modelling with High-Order Boussinesq-Type Equations. *Journal of Waterway Port Coastal and Ocean Engineering*, 132(5):348–357.

Madsen, P. A., Fuhrman, D. R., and Scha, H. A. (2008). On the solitary wave paradigm for tsunamis. 113(October).

Matuo, S. (2013). Youtube.

McLachlan, A. and Brown, A. (2006). *The Physical Environment*. Academic Press, 2 edition.

Mori, N. and Takahashi, T. (2012). Nationwide Post Event Survey and Analysis of the 2011 Tohoku Earthquake Tsunami. *Coastal Engineering Journal*, 54(01):1250001.

Navionics (2018). Navionics ChartViewer.

Ogami, T. and Sugai, T. (2018). Effects of longitudinal valley slopes on runup of the 2011 Tohoku tsunami on the Sanriku coast, northeastern Japan. *Quaternary International*, 471:253–266.

Pignatelli, C., Sansò, P., and Mastronuzzi, G. (2009). Evaluation of tsunami fl ooding using geomorphologic evidence. *Marine Geology*, 260(1-4):6–18.

Proudman, J. (1953). *Dynamical Oceanography*.

Raby, A., Macabuag, J., Pomonis, A., Wilkinson, S., and Rossetto, T. (2015). Implications of the 2011 Great East Japan Tsunami on sea defence design. *International Journal of Disaster Risk Reduction*, pages 332–346.

Ramsden, J. D. (1993). *Tsunamis : forces on a vertical wall caused by long waves, bores, and surges on a dry bed*. Ph.d. dissertation, California Institute of Technology.

Royer, T. C. and Reid, R. O. (1971). The detection of secondary tsunamis. *Taylor ad Francis Group LLC*, pages 136–142.

Sainte-Marie, J. and Bristeau, M.-O. (2008). Derivation of a non-hydrostatic shallow water model; Comparison with Saint-Venant and Boussinesq systems. *INRIA*, pages 3–28.

Saito, T., Ito, Y., Inazu, D., and Hino, R. (2011). Tsunami source of the 2011 Tohoku - Oki earthquake , Japan : Inversion analysis based on dispersive tsunami simulations. *Geophysical Research Letters*, 38:1–5.

Sato, T. and Oshima, S. (1988). Continental shelf survey project of Japan. *International Hydrographic Review*, pages 41–63.

Schäffer, H., Madsen, P. A., and Deigaard, R. (1993). A Boussinesq model for waves breaking in shallow water. *Coastal Engineering*, 20(3-4):185–202.

Shimozono, T., Cui, H., Pietrzak, J. D., Fritz, H. M., Okayasu, A., and Hooper, A. J. (2014). Short Wave Amplification and Extreme Runup by the 2011 Tohoku Tsunami. *Pure and Applied Geophysics*, 117:3217–3228.

Shimozono, T., Sato, S., Okayasu, A., Tajima, Y., Fritz, H. M., Liu, H., and Takagawa, T. (2012). Propagation and Inundation Characteristics of the 2011 Tohoku Tsunami on the Central Sanriku Coast. *Coastal Engineering Journal*, 54(1):1250004.

Smit, P., Zijlema, M., and Stelling, G. (2013). Depth-induced wave breaking in a non-hydrostatic, near-shore wave model. *Coastal Engineering*, 76:1–16.

Stelling, G. S. and Zijlema, M. (2009). Numerical modeling of wave propagation, breaking and run-up on a beach. In *Advanced Computational Methods in Science and Engineering. Lecture Notes in Computational Science and Engineering*, volume 71, pages 373–401.

Synolakis, C. (1987). *Fluid Mechanics*.

Tadepalli, S. and Synolakis, C. E. (1994). The Run-Up of N-Waves on Sloping Beaches. *Proceedings of the Royal Society A*, 445:99–112.

Tadepalli, S. and Synolakis, C. E. (1996). Model for the Leading Waves of Tsunamis. *Physical Review Letters*, 77:2141–2144.

Tang, L., Titov, V. V., Bernard, E. N., Wei, Y., Chamberlin, C. D., Newman, J. C., Mofjeld, H. O., Arcas, D., Eble, M. C., Moore, C., Uslu, B., Pells, C., Spillane, M., Wright, L., and Gica, E. (2012). Direct energy estimation of the 2011 Japan tsunami using deep-ocean pressure measurements. *Journal of geophysical Research*, 117:1–28.

TeamSWASH (2010). SWASH User Manual. Technical report.

Tissier, M., Bonneton, P., Marche, F., Chazel, F., Lannes, D., Montpellier, D., and Eugène, P. (2011). Nearshore Dynamics of Tsunami-like Undular Bores using a Fully Nonlinear Boussinesq Model. *Journal of Coastal Research*, (64):603–607.

Treske, A. (1994). Undular bore (Favre-waves) in open channels - Experimental studies. *Journal of Hydraulic Research*, 32(3):355–370.

Tsimopoulou, V. (2012). *The Great Eastern Japan Earthquake and Tsunami Facts and implications for flood risk management*.

Wei, Y., Chamberlin, C., Titov, V. V., Tang, L., and Bernard, E. N. (2012). Modeling of the 2011 Japan Tsunami: Lessons for Near-Field Forecast. *Pure an*.

Wikimedia (2016). Breaking wave types.

Wikipedia (2018). Shallow Water Equations.

Yeh, H. (2006). Maximum Fluid Forces in the Tsunami Runup Zone. *Journal of Waterway, Port, Coastal, and Ocean Engineering*, 132(6).

Youtube (2011). Youtube: Miyako Tsunami footage.

Zijlema, M., Stelling, G., and Smit, P. (2011). SWASH : an operational public domain code for simulating wave fields and rapidly varied flows in coastal waters.

A

Physical modelling

A.1. Introduction

Esteban et al. (2017) has set out overtopping flow patterns that result from a variety of different bore-type tsunami conditions performed trough a dam-break flume. These laboratory experiments were followed by detailed numerical SWASH simulations by Glasbergen (2018), using a slope in bathymetry similar to the beach profiles along the Sendai Plain.

The laboratory experiments of Esteban et al. (2017) were conducted on a smooth bed, which is limited in the fact that the impact of roughness coefficients were not taken into account. Glasbergen (2018) concluded that for the laboratory experiments, depending on scaling, either the bore height is too small or the bore front velocity is too large compared to the simulations. The 'inland' Froude numbers obtained during the experiments are equal to the Froude numbers near the coastline obtained by numerical modelling. Therefore, a new set op experiments is conducted on a rough bed, which can be compared to the original results in Esteban et al. (2017). The goal is to find wavefront characteristics in the wave flume that matches the tsunami wavefront in reality.

A.2. Wave flume set-up

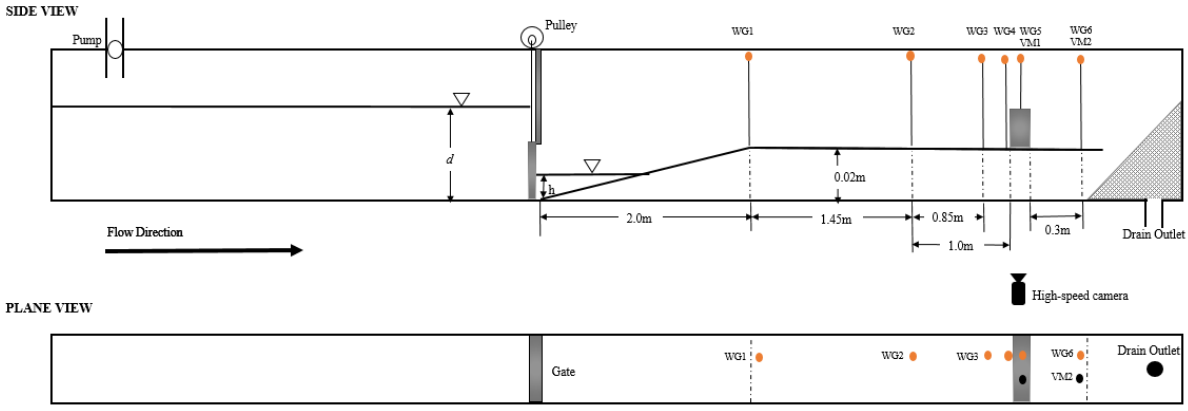

Figure A.1: Setup wave flume

A schematic representation of the wave tank used for the experiments is given in figure A.1. The experiments were performed in a wave flume (dimensions 14 m x 0.41 m x 0.6 m) at the Waseda University, Tokyo, Japan. The left part of the tank becomes a reservoir by closing it with a gate. The opening of the gate is 15 cm and can be opened instantaneously, which is necessary to perform dam-break tests.

4 sets of 12 experiments were carried out, 1 set with no structure, 1 set with a infinite vertical wall, 1 with a 15cm high vertical wall and 1 with a 9.5cm high seadyke. For each set, experiments were performed for a

water level in the reservoir d = 30, 40, 50 and 60 cm, and a water level in front of the gate h = 0, 10 and 20 cm.

A sloping bathymetry of 1:10 is installed 2 cm behind the reservoir gate, to an elevated horizontal bed of 20 cm above flume bed. On the sloping bathymetry and the horizontal bed, small diameter stones (3-5 mm, corresponding to a Manning n = 0.016) were being glued over the entire surface. 6 Wave Gauges (WG) were used to measure the water level during the experiments. The velocity meters (VM) were not able to record the accurate velocities in the flume due to air bubbles entrained within the turbulent wavefront.

A.3. Results

The results of the experiments with a rough bed are compared with the experiments of a smooth bed (Esteban et al., 2017) in Table A.1. The most important result for this research is given in this chapter, about the differences in Froude numbers for an increase in bottom friction. More detailed results, including the effect of bottom roughness on the energy in a tsunami bore and the impact on seawall overtopping, are outlined in the paper of (Esteban et al., 2019).

Table A.1: Results of the experiments with a rough bed compared to the experiments with a smooth bed (Esteban et al., 2017). Including the Froude numbers of the wavefront.

Rough bed	Fr_{coast}	Structure type:		No structure		High vertical wall	Low vertical wall			Dyke		
		d *[cm]*	*h* *[cm]*	*Hi* *[cm]*	*Vi* *[m/s]*	*Hf0* *[cm]*	*Hf* *[cm]*	*Ho* *[cm]*	*Hb* *[cm]*	*Hf* *[cm]*	*Ho* *[cm]*	*Hb* *[cm]*
				WG5	*WG2-4*	*WG3*	*WG3*	*WG5*	*WG6*	*WG3*	*WG5*	*WG6*
No	2.14	30	0	3.42	1.24	8.24	8.57	0	0	8.06	0.41	1.43
	1.92		10	3.67	1.15	7.79	7.15	0	0.02	8.57	0	0.61
	1.45		20	3.73	0.88	8.2	7.49	0	0.02	8.7	0.04	0.12
	2.29	40	0	5.49	1.68	16.15	15.21	0.9	1.48	13.73	5.55	4
	1.84		10	5.64	1.37	14.59	14.46	0.21	1.41	13.39	4.41	2.4
	2.41		20	5.64	1.79	15.41	14.85	0.57	1.62	13.58	3.89	2.58
	2.31	50	0	8.59	2.12	24.3	21.04	10.76	5.31	17.61	11.35	7.56
	2.20		10	7.79	1.92	22.38	19.28	4.92	3.26	17.11	9.22	6.88
	1.84		20	8.32	1.66	21.41	20.16	5.31	4.3	17.97	10.45	7.38
	2.37	60	0	12.17	2.59	33.69	27.55	16.33	9.45	20.32	16	9.92
	2.37		10	10.74	2.43	28.61	24.35	11.11	6.95	20.36	13.16	8.95
	2.69		20	10.27	2.7	28.63	24.17	12.38	6.88	20.89	13.48	10.12
Yes	1.72	30	0	3.38	0.99	8.59	8.81	0.03	0.04	7.62	0	0
	1.56		10	3.11	0.86	7.44	6.89	0	0	7.48	0	0
	1.37		20	3.28	0.78	8.32	7.38	0.03	0.04	8.01	0	0
	1.83	40	0	5.63	1.36	18.13	16.07	0.32	0.62	15.27	5.19	2.61
	1.79		10	5.23	1.28	16.46	14.18	0.28	0.03	13.87	2.99	2.02
	1.70		20	5.86	1.29	17.66	16.13	0.72	1.99	13.85	3.22	2.21
	2.06	50	0	7.95	1.82	25.98	21.59	6.518	3.784	19.138	9.234	4.844
	1.74		10	7.5	1.49	24.08	22.54	4.1	3.69	18.09	7.22	4.2
	1.43		20	8.01	1.27	26.35	21.88	7.63	2.61	18.4	11.06	3.37
	1.93	60	0	10.55	1.96	33.55	28.38	12.29	7.15	24.34	13.67	8.13
	1.67		10	9.96	1.65	32.95	35.55	10.27	6.24	21.21	12.08	7.6
	1.38		20	10.76	1.42	32.38	31.45	11.65	4.66	21.43	12.38	6.09

The Froude number used in the results are not the steady flow Froude number which is usually used, given that this is a bore front propagation over a dry bed and that the front velocity and (maximum) flow depth is measured at different times. Figure A.2 shows the difference in Froude numbers for the smooth and rough bed. The figure indicates that the bore front slows down and steepens up do to the roughness. These lower Froude numbers of the rough bed are more realistic to describe tsunami bores than those of the smooth bed (Glasbergen, 2018).

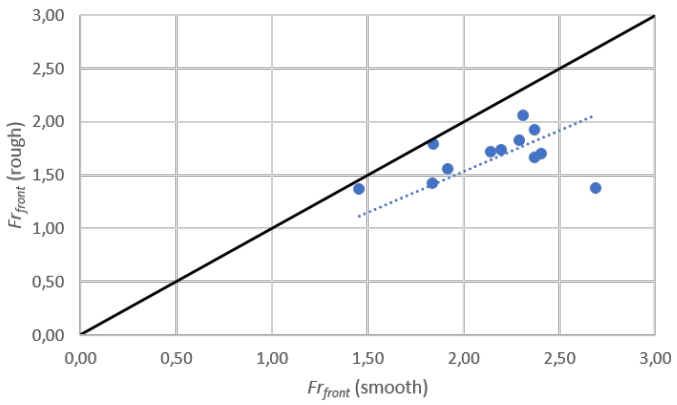

Figure A.2: Comparison of the Froude numbers of a rough and a smooth bed for the range of experiments provided in table A.1

B

Command files SWASH

B.1. 1D model: offshore - nearshore

```
$*************HEADING************************************
$
PROJect  'Test'  'offshore'
$
$ Tsuanmi propagation from origin earthquake to the continental shelf
$
$*********MODEL INPUT*************************
SET depmin = 0.001 !Default: depmin=0.00005
MODE  DYNamic ONEDimensional
CGRID REGular 0. 0. 0. 300000. 0. 600 0 !300000. = lenght, 600 = number of meshes in comp. grid (grid size:0.5km)
VERTical 1
$
INPgrid BOTTOM 0. 0. 0. 300000 0 1. 0. !300000 = nr of meshes 1. = mesh size in x-direction in meters
READinp BOTTOM 1. 'bottomfile.bot' 1 0 FREE
$
INPgrid WLEVel 0. 0. 0. 300000 0 1. 0.
READinp WLEVel 1. 'waterlevel.wlev' 1 0 FREE
$
$*********CONDITIONS****************************
$
BOUndcond SIDE W CCW BTYPe SOMMerfeld
$
FRICtion MANNing 0.019
$
BREaking
$
$NONHYDrostatic STAndard
$
TIMEI METH EXPLicit !An automatic time step control is implemented by the Courant number.
$
$*********OUTPUT REQUESTS************************
$
GROUP 'data1'  1 600 1 1
POINts 'data2' 256000. 0.
QUANTity HRUN depth=-200 !the total depth where inundation takes place.
TABLE 'data1' NOHEAD 'Table_group.tbl' TSEC DIST BOTLEV WATL HRUN OUTPUT 000000.000 1 SEC
TABLE 'data2' HEAD 'Table_point.tbl' TSEC DIST BOTLEV WATL HRUN OUTPUT 000000.000 1 SEC
$
COMPute 000000.000 0.01 SEC 010000.000
STOP
```

Figure B.1: Input file 1D model SWASH

The SWASH Manual (TeamSWASH, 2010) can be used as a reference for all input commands. Some important commands are outlined here to give a quick overview of the choices.

Computational grid
The dimensions of the computational domain in the horizontal plane is defined. A sufficient number of grid poits per wavelength is taken associated with the peak wave energy. For low waves, i.e. $H/d \ll 1$, it is sufficient to take 50 grid cells per peak wavelength. For relatively high waves, it is better to take at least 100 grid cells per peak wavelength. Since tsunami waves are low waves, 50 grid cells per wavelength is sufficient. However, since the waves become shorter near the coastline (shoaling) a much finer grid is chosen.

The domain of the 1D model is 300 km cross-shore of which the deepest part is 7 km. The wavelength is around 200 km near the west boundary (origin earthquake) of the model, which decreases when propagating to the shoreline. A grid size of 500 m is used and seems to be a good resolution to obtain the shape of the first tsunami wave.

A depth averaged model, 1 layer in the vertical, is used to describe the tsunami wave propagation. The number of layers is determined by the linear frequency dispersion. The dimensionless depth, kd with k the wave number, decides the number of layers (TeamSWASH, 2010). For L = 200,000 m and d = 7000 m, kd = 0.22. This is in the range $kd < 0.5$ for which 1 vertical layer is sufficient according to Table 5.1 in the SWASH Manual.

Input grids and data
The bathymetry obtained for the model is based on 'Navionics' (Navionics, 2018), which gives electronic navigation charts of coastal areas. This bathymetry is assumed to be a good representation of the reality for such a coarse resolution model. However, the accuracy is too low to perform a perfect validation.

Initial and boundary conditions
The initial condition is a raised water level at t=0 s, right after the earthquake took place. This initial tsunami height on the plate boundary is estimated from the tsunami waveform inversion analyses (Saito et al., 2011). Since the input water level in SWASH is a simplified form of the one given by Saito et al. (2011), the simulated results can deviate from the observed buoy results. However, the shape of the main wave is important and this can be approximated in a proper way.

A Sommerfeld's radiation condition is employed at the west boundary of the model, where the waves are coming in. This condition allows the long waves to cross the outflow boundary without reflections. At the east boundary no condition is given since this B.C. is given by the moving coastline.

Numerical parameters
An explicit time integration is applied, for which the time step is controlled by the Courant number, since this is a more accurate way to describe propagation of waves. Usually, Cr_{min} is set to 0.2, while the maximum Courant number Cr_{max} is specified in the range of 0.5 to 0.8. It is advised not to choose a value higher than 0.8 since nonlinear processes, e.g. wave breaking and wave-wave interactions, can affect the stability condition. For high, nonlinear waves, or wave interaction with structures with steep slopes, a Courant number of 0.5 is advised (TeamSWASH, 2010). Cr_{max} is taken as 0.8 is this offshore model, where nonlinear terms are not of most importance.

The non-hydrostatic pressure can be included in the SWE. For the offshore model this command is not used, and therefore a hydrostatic pressure is assumed in the SWASH model. In this offshore 1D model, a hydrostatic pressure can be assumed since the tsunami wave is classified as a long wave (TeamSWASH, 2010).

Physical parameters
Neither Boussinesq-type wave models nor non-hydrostatic wave-flow models can be directly applied to details of breaking waves, since in both models essential processes such as overturning, air-entrainment and wave generated turbulence, are absent. In this model, only the macro-scale effects of wave breaking are of interest and therefore the details of wave breaking can be ignored. A coarse resolution (1 layer in this model) will result in an underestimation of the horizontal velocities near the wave crest, and thus an underestimation of the amplitude dispersion. This will result in a postponed onset of dissipation and breaking of the wave. By giving the command input BREAK, the model assumes a hydrostatic pressure distribution at the front of a wave and the wave then rapidly transits into the characteristic saw-tooth shape and dissipation is captured by ensuring momentum conservation over the resulting discontinuity. (Zijlema et al., 2011)

When the waves are traveling over a long distance, the influence of bottom friction becomes more important. For wave simulations, a Manning coefficient of 0.019 is recommended (TeamSWASH, 2010).

Output
The GROUP command gives an output over the whole computational grid, which can be used for the animation of the water level over the whole model. The POINTS command is used to extract date at a certain point, x = 256000 in this case where the depth is around 200m, to make timeseries of the water level.

B.2. 1D and 2DH model: nearshore

Most of the input commands are similar to the 1D offshore model. Therefore, only the important changed input commands for the nearshore models are discussed here. The command file for the nearshore 1D model and 2DH is given in figure B.2 and B.3 respectively.

Computational grid
The wavelength of the input wave signals are in the range 20-40 km. Since the waves propagate in the nearshore shallow area the waves can not be classified by low waves any more. For the nearshore 1D model, a grid size of 1 m in used. For the 2DH model a curvilinear grid is used with a much higher resolution of 50 m for part of the computational grid to reduce the computational time. The computational grid 1000 meter in front of the coastline, has a much smaller grid size of 1 m. This is done to simulate the breaking of the waves and the momentum flux at the coastline in an accurate way.

The dimensionless depth, kd with k the wave number, decides the number of layers (TeamSWASH, 2010). For L = 20,000 m and d = 100 m, kd = 0.0314. This is in the range $kd < 0.5$ for which 1 vertical layer is sufficient according to Table 5.1 in the SWASH Manual.

Input grids
An exception value for -50 is given, to introduce permanently dry points for the computational grid. These grid point are not taken into consideration during the computations.

For the onshore topography a different Manning's factor, n = 0.06, is applied. This Manning's n is classified as a middle density urban area (Kaiser et al., 2011) and is calibrated by (Glasbergen, 2018) for tsunami run-up.

Initial and boundary conditions
A weakly reflective condition is given as a B.C. to simulate entering waves without some reflections at the west boundary of the model. This condition requires a timeseriesof the wave input.

Numerical parameters
A non-hydrostatic assumption is made for the nearshore simulations sice the hydrostatic assumption does not hold in case of propgation of flows over a steep bottom, which is the case for some of the 2DH simulations.

For simulation of breaking waves, hydraulic jumps and bores, momentum must be conserved (TeamSWASH, 2010). Conservation properties become crucial for rapidly varied flows. These properties are often sufficient to get solutions that are acceptable in terms of local energy losses, location of incipient wave breaking, propagation speed of a bore, etc. The u- and v-momentum equations are approximated such that they are consistent with momentum conservation (Zijlema et al., 2011).

Output
The output files are created over a depth contour in the middle of the bay, see figure 5.8a.

```
$*************HEADING***********************************
$
PROJect  '1D_1_50'  '1'
$
$ Breaking nearshore Sendai
$
$*********MODEL INPUT*************************
SET depmin = 0.001
MODE  DYNamic ONEDimensional
CGRID REGular 0. 0. 0. 7500. 0. 7500 0
VERTical 1
$
INPgrid BOTTOM 0. 0. 0. 7500 0 1. 0.
READinp BOTTOM 1. 'bottomfile_1_50_gr1.txt' 1 0 FREE                                                                    !1
$
INPgrid FRICtion 0. 0. 0. 7500 0 1. 0.
READinp FRICtion 1. 'roughness_1_50_gr1.txt' 1 0 FREE
$
$*********CONDITIONS****************************
$
INITial ZERO !Both the initial water level and velocity components are set to zero.
$
BOUndcond SIDE W BTYPe WEAKrefl CONstant SERIes 'timeserie_bc_H8_T1200.txt'
$
FRICtion MANNing 0.019
$
BREaking 0.6 0.3
$
NONHYDrostatic
DISCRET UPW MOM
TIMEI METH EXPL 0.2 0.5
$
$*********OUTPUT REQUESTS************************
$
POINts 'data1' 5000. 0.
POINts 'data2' 4900. 0.
POINts 'data3' 3000. 0.
TABLE 'data1' NOHEAD 'Table_point_1_50_1D_gr1_H8_L1200_coastline.tbl' TSEC WATL VEL BRKP OUTPUT 000000.000 1 SEC
TABLE 'data2' NOHEAD 'Table_point_1_50_1D_gr1_H8_L1200_100m_offshore.tbl' TSEC WATL VEL BRKP OUTPUT 000000.000 1 SEC
TABLE 'data3' NOHEAD 'Table_point_1_50_1D_gr1_H8_L1200_2000m_offshore.tbl' TSEC WATL VEL BRKP OUTPUT 000000.000 1 SEC
GROUP 'data4'  1 7500 1 1
QUANTity HRUN depth=100
BLOCK 'COMPGRID' NOHEAD 'Table_section_1_50_1D_gr1_H8_L1200_WATL.mat' WATL OUTPUT 000000.000 1 SEC
BLOCK 'COMPGRID' NOHEAD 'Table_section_1_50_1D_gr1_H8_L1200_VEL.mat' VEL OUTPUT 000000.000 1 SEC
BLOCK 'COMPGRID' NOHEAD 'Table_section_1_50_1D_gr1_H8_L1200_BRKP.mat' BRKP OUTPUT 000000.000 1 SEC
$TABLE 'data4' NOHEAD 'Table_section_1_50_1D_gr1_H8_L1200.tbl' TSEC WATL VEL BRKP OUTPUT 000000.000 1 SEC
$
COMPute 000000.000 0.001 SEC 003300.000
STOP
************************************************
```

Figure B.2: Input file 1D nearshore model SWASH

```
$*************HEADING***************************
$
PROJect  'Test_5000'  '1'
$
$ Tsuanmi propagation in the bay
$
$*********MODEL INPUT*************************
SET depmin = 0.01 maxerr=5
MODE DYNamic TWODimensional
COORDINATES CARTesian
CGRID CURVilinear 640 62
READgrid COORdinates 1. 'XYgrid_5000_3000_2500_gr1_curvi_500m.txt' 1 0 1 FREE
VERTical 1
$
INPgrid BOTtom CURVilinear STAGgered EXCeption -50
READinp BOTtom 1. 'bottomfile_5000_3000_2500_gr1_curvi_500m.bot' 1 0 FREE
$
$*********CONDITIONS****************************
$
INITial ZERO
$
BOUndcond SEGMent XY 1 100 1 3000 BTYPe WEAKrefl CONstant SERIes 'timeserie_bc_H6_T600.txt'
$
FRICtion MANNing
$
BREaking 0.6 0.3
$
NONHYDrostatic
DISCRET UPW MOM
TIMEI METH EXPLicit 0.4 0.8
$
$*********OUTPUT REQUESTS************************
$
POINts 'data1' 5000. 1550.
POINts 'data2' 4900. 1550.
POINts 'data3' 3000. 1550.
TABLE 'data1' NOHEAD 'Table_point_5000_3000_2500_H6_L600_coastline.tbl' TSEC WATL VEL BRKP OUTPUT 000000.000 1 SEC
TABLE 'data2' NOHEAD 'Table_point_5000_3000_2500_H6_L600_100m_offshore.tbl' TSEC WATL VEL BRKP OUTPUT 000000.000 1 SEC
TABLE 'data3' NOHEAD 'Table_point_5000_3000_2500_H6_L600_2000m_offshore.tbl' TSEC WATL VEL BRKP OUTPUT 000000.000 1 SEC
CURve 'data' 1. 1550. 7499 7500. 1550.
QUANTity HRUN depth=100
$TABle 'data' NOHEAD 'Table_curve_5000_3000_1500_H6_T600_WATL.tbl' WATL OUTPUT 000000.000 1 SEC
$TABle 'data' NOHEAD 'Table_curve_5000_3000_1500_H6_T600_BRKP.tbl' BRKP OUTPUT 000000.000 1 SEC
$TABle 'data' NOHEAD 'Table_curve_5000_3000_1500_H6_T600_VEL.tbl' VEL OUTPUT 000000.000 1 SEC
$
COMPute 000000.000 0.01 SEC 001000.000
STOP
************************************************
```

Figure B.3: Input file 2DH nearshore model SWASH

C

Background of SWASH

C.1. Different models

Numerical models can be distinguished in two main categories: phase-resolving models (SWASH) and phase-averaged models (SWAN). The phase-resolving models are based on vertically integrated, time-dependent mass and momentum balance equations and the phase-averaged models are based on a spectral energy balance equation. The SWASH phase-resolving model stands out in its ability to simulate complex nearshore processes, including wave breaking, nonlinear interaction, wave run-up and wave-induced circulation. A further distinguishing feature is the numerical implementation of momentum conservation, which is a prerequisite for a plausible representation of hydraulic jumps and bores and is therefore important in this research. Finally, the SWASH model requires just one tuning parameter for wave breaking, which in practice is relatively easy to estimate. (Zijlema et al., 2011)

Volume-of-Fluid (VOF) and Smoothed Particle Hydrodynamics (SPH) are well-known methods to treat the free surface motion. However, to simulate large-scale wave evolution and shallow water flows in an efficient and feasible way, an approach is adopted where the free-surface motion is tracked using a single-valued function of the horizontal plane. Most of the models that uses this technique are non-hydrostatic of nature and therefore consist of the nonlinear shallow water (NLSW) equations with the addition of a vertical momentum equation and non-hydrostatic pressure in horizontal momentum equations. The amount of grid cells in the vertical are much less in these models compared to the VOF and SPH models. In addition, the NLWS equations are able to deal accurately with large gradients or discontinuities in the flow, such as tsunami inundation. (Zijlema et al., 2011)

C.2. Derivation of the Shallow Water Equations

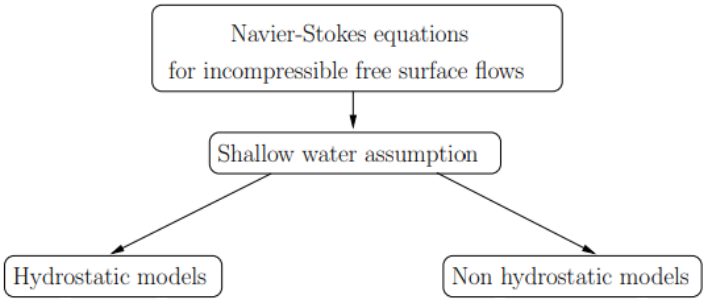

Figure C.1: Averaged models derived from Navier-Stokes equations (Sainte-Marie and Bristeau, 2008)

The Navier Stokes equations (C.1), derived from the physical conservation of mass and momentum, are used as a starting point. The first equation in C.1 is the mass balance equation and the second, third and fourth

equations are the momentum balance equations in x-, y- and z-direction respectively. Navier-Stokes describes the relation between the density, pressure, temperature and velocity of a moving fluid. For problems in which the vertical dynamics can be neglected compared to the horizontal effect (most of the tsunami problems), the shallow water equations (SWE) are valid (Hansen, 1949). These SWE can be derived from the incompressible 3D Navier-Stokes equations by depth averaging. The SWASH model uses these SWE equations to calculate the propagation of waves in which the pressure is assumed to be hydrostatic or non-hydrostatic. The equations in this chapter are outlined in terms of Cartesian notation.

$$\begin{aligned}
\frac{\partial \rho}{\partial t}+\frac{\partial \rho u}{\partial x}+\frac{\partial \rho v}{\partial y}+\frac{\partial \rho w}{\partial z} &= 0 \\
\frac{\partial \rho u}{\partial t}+\frac{\partial \rho u^2}{\partial x}+\frac{\partial \rho uv}{\partial y}+\frac{\partial \rho uw}{\partial z}+\frac{\partial p}{\partial x}-\frac{\partial \tau_{xx}}{\partial x}-\frac{\partial \tau_{xy}}{\partial y}-\frac{\partial \tau_{xz}}{\partial z} &= \rho f_1 \\
\frac{\partial \rho v}{\partial t}+\frac{\partial \rho vu}{\partial x}+\frac{\partial \rho v^2}{\partial y}+\frac{\partial \rho vw}{\partial z}+\frac{\partial p}{\partial y}-\frac{\partial \tau_{yx}}{\partial x}-\frac{\partial \tau_{yy}}{\partial y}-\frac{\partial \tau_{yz}}{\partial z} &= \rho f_2 \\
\frac{\partial \rho w}{\partial t}+\frac{\partial \rho wu}{\partial x}+\frac{\partial \rho wv}{\partial y}+\frac{\partial \rho w^2}{\partial z}+\frac{\partial p}{\partial z}-\frac{\partial \tau_{zx}}{\partial x}-\frac{\partial \tau_{zy}}{\partial y}-\frac{\partial \tau_{zz}}{\partial z} &= \rho f_3
\end{aligned} \tag{C.1}$$

Where ρ is the density and u, v and w are in the velocities in x-, y- and z-direction respectively. The forces described by the Navier-Stokes equations can be divided in body forces and surface forces. The surface forces are the pressure gradient (p) and the frictional forces (τ_{xx}, τ_{xy}, τ_{yx} and τ_{yy}). The body forces are gravity, Coriolis and tidal forces which are given as one combined symbol f in the formula. The Coriolis force and tidal force is neglected in the simulation of tsunami propagation. The only body force is than the gravity force and is given by $F = \rho g$.

Two assumptions are made about the fluid (sea water). The first assumption is that the fluid is incompressible, which means that ρ does not depend on p. This does not mean that the density is constant, since ρ depends on temperature and salinity. But if the assumption is made that salinity and temperature are constant throughout the domain, ρ can be taken as a constant. Since the mass density is constant, the mass balance equation reduces to the continuity equation:

$$\begin{aligned}
\frac{D\rho}{Dt} = \frac{\partial \rho}{\partial t}+u\frac{\partial \rho}{\partial x}+v\frac{\partial \rho}{\partial y}+w\frac{\partial \rho}{\partial z} &= 0 \\
\Rightarrow \quad \frac{\partial u}{\partial x}+\frac{\partial v}{\partial y}+\frac{\partial w}{\partial z} &= 0
\end{aligned} \tag{C.2}$$

The Navier-Stokes equations can be rewritten after the assumption that the Coriolis and tidal forces are neglected and the assumption of incompressibility and constant density.

$$\begin{aligned}
\frac{\partial u}{\partial x}+\frac{\partial v}{\partial y}+\frac{\partial w}{\partial z} &= 0 \\
\frac{\partial \rho u}{\partial t}+\frac{\partial \rho u^2}{\partial x}+\frac{\partial \rho uv}{\partial y}+\frac{\partial \rho uw}{\partial z}+\frac{\partial p}{\partial x} &= \frac{\partial \tau_{xx}}{\partial x}+\frac{\partial \tau_{xy}}{\partial y}+\frac{\partial \tau_{xz}}{\partial z} \\
\frac{\partial \rho v}{\partial t}+\frac{\partial \rho vu}{\partial x}+\frac{\partial \rho v^2}{\partial y}+\frac{\partial \rho vw}{\partial z}+\frac{\partial p}{\partial y} &= \frac{\partial \tau_{yx}}{\partial x}+\frac{\partial \tau_{yy}}{\partial y}+\frac{\partial \tau_{yz}}{\partial z} \\
\frac{\partial \rho w}{\partial t}+\frac{\partial \rho wu}{\partial x}+\frac{\partial \rho wv}{\partial y}+\frac{\partial \rho w^2}{\partial z}+\frac{\partial p}{\partial z} &= -\rho g+\frac{\partial \tau_{zx}}{\partial x}+\frac{\partial \tau_{zy}}{\partial y}+\frac{\partial \tau_{zz}}{\partial z}
\end{aligned} \tag{C.3}$$

If the depth is much smaller than the wavelength, which is the case for most of the tsunamis, the vertical velocity terms are small and a hydrostatic pressure assumption can be made (Proudman, 1953). By a scaling argument, the z-momentum equation reduces to only the pressure gradient and the gravity term. Hydrostatic pressure is associated with pressure variation in the vertical, which results from the pull of gravity on the fluid. The vertical variation is a function of height or elevation. From this reduced z-momentum equation, the hydrostatic pressure distribution is obtained for the x- and y-momentum equations.

$$\frac{\partial p}{\partial z} = -\rho g \quad \Rightarrow \quad p = \rho g(\zeta - z) \quad \Rightarrow \quad \frac{\partial p}{\partial x} = \rho g \frac{\partial \zeta}{\partial x} \quad where \quad \zeta = free\ surface\ elevation \tag{C.4}$$

The final step is to integrate from the bottom to the free surface elevation ζ. The depth-averaged, hydrostatic, free-surface flow can be described by the 2DH SWE equations:

$$\begin{aligned}
&\frac{\partial \zeta}{\partial t} + \frac{\partial hu}{\partial x} + \frac{\partial hv}{\partial y} = 0 \\
&\frac{\partial u}{\partial t} + u\frac{\partial u}{\partial x} + v\frac{\partial u}{\partial y} - \nu_h(\frac{\partial^2 u}{\partial x^2} + \frac{\partial^2 u}{\partial y^2}) = -g\frac{\partial \zeta}{\partial x} - \frac{\partial \tau_{b,x}}{\partial \rho_0 h} + fv + \frac{\partial \tau_{w,x}}{\partial \rho_0 h} - \frac{1}{\rho_0}\frac{\partial p_{atm}}{\partial x} \\
&\frac{\partial v}{\partial t} + u\frac{\partial v}{\partial x} + v\frac{\partial v}{\partial y} - \nu_h(\frac{\partial^2 v}{\partial x^2} + \frac{\partial^2 v}{\partial y^2}) = -g\frac{\partial \zeta}{\partial y} - \frac{\partial \tau_{b,y}}{\partial \rho_0 h} + fu + \frac{\partial \tau_{w,y}}{\partial \rho_0 h} - \frac{1}{\rho_0}\frac{\partial p_{atm}}{\partial y}
\end{aligned} \tag{C.5}$$

When simulating long waves in the nearshore area, the wavelength can be decreased and therefore the model needs to have a non-hydrostatic assumption. The depth-averaged, non-hydrostatic, free-surface flow can be described by the nonlinear shallow water (NLSW) equations given by the SWASH Manual (TeamSWASH, 2010):

$$\begin{aligned}
&\frac{\partial \eta}{\partial t} + \frac{\partial hu}{\partial x} + \frac{\partial hv}{\partial y} = 0 \\
&\frac{\partial u}{\partial t} + u\frac{\partial u}{\partial x} + v\frac{\partial u}{\partial y} + g\frac{\partial \eta}{\partial x} + \frac{1}{h}\int_{-d}^{\eta}\frac{\partial q}{\partial x}dz + c_f\frac{u\sqrt{u^2+v^2}}{h} = \frac{1}{h}(\frac{\partial h\tau_{xx}}{\partial x} + \frac{\partial h\tau_{xy}}{\partial y}) \\
&\frac{\partial v}{\partial t} + u\frac{\partial v}{\partial x} + v\frac{\partial v}{\partial y} + g\frac{\partial \eta}{\partial y} + \frac{1}{h}\int_{-d}^{\eta}\frac{\partial q}{\partial y}dz + c_f\frac{v\sqrt{u^2+v^2}}{h} = \frac{1}{h}(\frac{\partial h\tau_{yx}}{\partial x} + \frac{\partial h\tau_{yy}}{\partial y})
\end{aligned} \tag{C.6}$$

D

1D simulations: Results

INCLUDE TIMESERIES AT THE COASTLINE TO CALCULATE FROUDE NUMBER AND MOMENTUM FLUX.

Table D.1: 1D simulations: point of breaking with corresponding breaker parameter

α_2	**Test**	L_{front} **[m]**	T_{100} **[s]**	T_{front} **[s]**	H_{100} **[m]**	**Wave type**	**BRKP [m]**	**Undular formation [m]**	$\xi_{tsunami}$ **[-]**
1/50	1	9396.2759	600	300	4	Surging	x	x	0.969473
	2	9396.2759	600	300	6	Surging	x	x	0.791572
	3	9396.2759	600	300	8	Surging	x	x	0.685521
	4	18792.552	1200	600	4	Surging	x	x	1.371042
	5	18792.552	1200	600	6	Surging	x	x	1.119451
	6	18792.552	1200	600	8	Surging	x	x	0.969473
1/75	7	9396.2759	600	300	4	Surging	x	x	0.646268
	8	9396.2759	600	300	6	Breaking front	34	x	0.527675
	9	9396.2759	600	300	8	Breaking front	74	x	0.45698
	10	14094.414	900	450	4	Surging	x	x	0.791513
	11	14094.414	900	450	6	Surging	x	x	0.646268
	12	14094.414	900	450	8	Surging	x	x	0.559684
	13	18792.552	1200	600	4	Surging	x	x	0.91396
	14	18792.552	1200	600	6	Surging	x	x	0.746246
	15	18792.552	1200	600	8	Surging	x	x	0.646268
1/100	16	9396.2759	600	300	4	Breaking front	62	x	0.484688
	17	9396.2759	600	300	6	Breaking front	170	x	0.395746
	18	9396.2759	600	300	8	Breaking front	290	x	0.342726
	19	14094.414	900	450	4	Surging	x	x	0.593619
	20	14094.414	900	450	6	Breaking front	15	x	0.484688
	21	14094.414	900	450	8	Breaking front	51	x	0.419752
	22	18792.552	1200	600	4	Surging	x	x	0.685452
	23	18792.552	1200	600	6	Surging	x	x	0.55967
	24	18792.552	1200	600	8	Breaking front	0	x	0.484688
1/150	25	9396.2759	600	300	4	Breaking front	440	x	0.323119
	26	9396.2759	600	300	6	Undular breaking	810	920	0.263826
	27	9396.2759	600	300	8	Undular breaking	1180	1340	0.22848
	28	18792.552	1200	600	4	Breaking front	5	x	0.45696
	29	18792.552	1200	600	6	Breaking front	55	x	0.373106
	30	18792.552	1200	600	8	Breaking front	135	x	0.323119
1/200	31	9396.2759	600	300	4	Undular breaking	1100	1250	0.242338
	32	9396.2759	600	300	6	Undular breaking	1850	2100	0.197868
	33	9396.2759	600	300	8	Undular breaking	3000	2400	0.171359
	34	18792.552	1200	600	4	Breaking front	120	x	0.342718
	35	18792.552	1200	600	6	Breaking front	320	x	0.279828
	36	18792.552	1200	600	8	Undular breaking	1100	1280	0.242338
1/300	37	9396.2759	600	300	4	Undular breaking	3050	4000	0.161558
	38	9396.2759	600	300	6	Undular breaking	4080	6000	0.131911
	39	9396.2759	600	300	8	Undular breaking	5840	7750	0.114239
	40	18792.552	1200	600	4	Undular breaking	800	880	0.228477
	41	18792.552	1200	600	6	Undular breaking	1550	1750	0.186551
	42	18792.552	1200	600	8	Undular breaking	2380	2650	0.161558
1/500	43	9396.2759	600	300	4	Undular breaking	5000	12500	0.096935
	44	9396.2759	600	300	6	Undular breaking	10700	17200	0.079147
	45	9396.2759	600	300	8	Undular breaking	11400	20750	0.068543
	46	18792.552	1200	600	4	Undular breaking	3970	4670	0.137086
	47	18792.552	1200	600	6	Undular breaking	5530	7700	0.11193
	48	18792.552	1200	600	8	Undular breaking	7180	10500	0.096935

Table D.2: 1D simulations: characteristics tsunami wavefront with corresponding Froude numbers.

α_2	**Test**	L_{front} **[m]**	T_{front} **[s]**	H_{100} **[m]**	**Wave type**	H_{coast} **[m]**	$V_{coast,max}$ **[m]**	Fr_{coast} **[-]**	$(hu^2)_{max}$ $[m^3/s^2]$
1/50	1	9396.2759	300	4	Surging	5.71	2.87	0.383468	63.88
	2	9396.2759	300	6	Surging	6.93	3.99	0.483918	167.31
	3	9396.2759	300	8	Surging	9.26	4.99	0.523553	320.4
	4	18792.552	600	4	Surging	4.66	1.36	0.201146	10.85
	5	18792.552	600	6	Surging	6.7	1.95	0.240526	35.36
	6	18792.552	600	8	Surging	9.2	2.51	0.264208	81.26
1/75	7	9396.2759	300	4	Surging	5.35	3.92	0.541096	102.61
	8	9396.2759	300	6	Breaking front	0.73	6.51	2.43268	257.15
	9	9396.2759	300	8	Breaking front	1.2	8.75	2.550251	491.56
	10	14094.414	450	4	Surging	5.73	2.72	0.362791	55.32
	11	14094.414	450	6	Surging	7.79	3.77	0.431259	142.62
	12	14094.414	450	8	Surging	10.06	4.7	0.473112	270.85
	13	18792.552	600	4	Surging	5.45	2.06	0.281731	31.96
	14	18792.552	600	6	Surging	7.71	2.87	0.330005	92.48
	15	18792.552	600	8	Surging	10.29	3.63	0.361297	191.11
1/100	16	9396.2759	300	4	Breaking front	0.47	6.86	3.194778	146.09
	17	9396.2759	300	6	Breaking front	1.11	11.19	3.391049	399.74
	18	9396.2759	300	8	Breaking front	2.2	12.77	2.748812	789.67
	19	14094.414	450	4	Surging	5.48	3.39	0.462354	78
	20	14094.414	450	6	Breaking front	7.19	4.64	0.552483	199.19
	21	14094.414	450	8	Breaking front	0.96	6.55	2.134377	382.03
	22	18792.552	600	4	Surging	5.88	2.6	0.342334	49.18
	23	18792.552	600	6	Surging	7.99	3.6	0.406625	125.38
	24	18792.552	600	8	Breaking front	10.23	4.5	0.4492	248.1
1/150	25	9396.2759	300	4	Breaking front	1.22	11.86	3.428233	275.68
	26	9396.2759	300	6	Undular breaking	2.18	14.17	3.064129	638.24
	27	9396.2759	300	8	Undular breaking	3.05	16.41	3.00002	1102.7
	28	18792.552	600	4	Breaking front	5.5	3.42	0.465597	81.05
	29	18792.552	600	6	Breaking front	0.63	5.82	2.341091	211.13
	30	18792.552	600	8	Breaking front	1.15	8.3	2.471125	409.7
1/200	31	9396.2759	300	4	Undular breaking	1.77	11.93	2.862987	314.98
	32	9396.2759	300	6	Undular breaking	1.81	16.23	3.851631	692.58
	33	9396.2759	300	8	Undular breaking	2.77	17.71	3.39738	1190.2
	34	18792.552	600	4	Breaking front	0.65	6.5	2.574081	110.02
	35	18792.552	600	6	Breaking front	1.03	10.73	3.375566	298.39
	36	18792.552	600	8	Undular breaking	1.28	14.02	3.956476	627.4
1/300	37	9396.2759	300	4	Undular breaking	1.7328	12.7659	3.096298	311.03
	38	9396.2759	300	6	Undular breaking	1.7309	12.7656	3.097924	680.26
	39	9396.2759	300	8	Undular breaking	2.42	18.32	3.759961	1299.7
	40	18792.552	600	4	Undular breaking	0.93	10.48	3.469647	205.41
	41	18792.552	600	6	Undular breaking	1.79	13.31	3.176267	516.69
	42	18792.552	600	8	Undular breaking	1.4887	17.2245	4.507218	929.13
1/500	43	9396.2759	300	4	Undular breaking	0.92	10.96	3.648229	215.42
	44	9396.2759	300	6	Undular breaking	0.95	14.35	4.700625	433.8
	45	9396.2759	300	8	Undular breaking	1.44	16.54	4.40068	757.03
	46	18792.552	600	4	Undular breaking	0.92	11.32	3.768062	219.16
	47	18792.552	600	6	Undular breaking	2.55	13.87	2.77314	628.95
	48	18792.552	600	8	Undular breaking	1.2	17.81	5.190854	1105.1

E

2DH simulations: Results

Table E.1: 2DH simulations: Slope continental shelf, wave characteristics, bay dimensions, wave type and the tsunami breaker parameters for each simulation. *Test 1,4,7,20,23 and 25 are 1D simulations to compare

α_2	**Test**	L_{front} **[m]**	T_{front} **[s]**	H_{100} **[m]**	W_b **[m]**	W_h **[m]**	W_b/W_h **[m]**	**Wave type**	$\xi_{tsunami}$	$\xi_{tsunami,2DH}$
	1	9396.276	300	6	1	1	1	Surging	0.791572	0.791572
	2	9396.276	300	6	3000	1500	2	Surging	0.791572	0.559726
1/50	3	9396.276	300	6	3000	2500	1.2	Surging	0.791572	0.722603
	4	9396.276	300	8	1	1	1	Surging	0.685521	0.685521
	5	9396.276	300	8	3000	1500	2	Surging	0.685521	0.484737
	6	9396.276	300	4	1	1	1	Surging	0.646268	0.646268
	7	9396.276	300	4	3000	1500	2	Breaking front	0.646268	0.45698
	8	9396.276	300	6	1	1	1	Breaking front	0.527675	0.527675
	9	9396.276	300	6	3000	2000	1.5	Breaking front	0.527675	0.430845
	10	9396.276	300	6	2000	1500	1.333333	Breaking front	0.527675	0.45698
	11	9396.276	300	6	3000	1500	2	Breaking front	0.527675	0.373123
	12	9396.276	300	6	4000	1500	2.666667	Breaking front	0.527675	0.323134
	13	9396.276	300	6	3000	1000	3	Breaking front	0.527675	0.304653
1/75	14	9396.276	300	6	3000	500	6	Breaking front	0.527675	0.215423
	15	9396.276	300	6	4000	2000	2	Breaking front	0.527675	0.373123
	16	9396.276	300	6	5000	2500	2	Breaking front	0.527675	0.373123
	17	9396.276	300	6	5000	3000	1.666667	Breaking front	0.527675	0.408735
	18	9396.276	300	6	6000	3000	2	Breaking front	0.527675	0.373123
	19	14094.41	450	6	3000	1500	2	Surging	0.646268	0.45698
	20	18792.55	600	6	3000	1500	2	Surging	0.746246	0.527675
	21	9396.276	300	8	1	1	1	Breaking front	0.45698	0.45698
	22	9396.276	300	8	3000	1500	2	Breaking front	0.45698	0.323134
	23	9396.276	300	4	3000	1500	2	Breaking front	0.484688	0.342726
1/100	24	9396.276	300	6	1	1	1	Breaking front	0.395746	0.395746
	25	9396.276	300	6	3000	1500	2	Breaking front	0.395746	0.279835
	26	9396.276	300	8	1	1	1	Breaking front	0.342726	0.342726

Table E.2: 2DH simulations: point of breaking, Froude number at the coastline and the maximum momentum flux at the coastline for all simulations. *Test 1,4,7,20,23 and 25 are 1D simulations to compare

α_2	**Test**	W_b/W_h **[-]**	**Wave type**	**BRKP wavefront [m]**	H_{coast} **[m]**	$V_{coast,max}$ **[m/s]**	Fr_{coast} **[-]**	$(hu^2)_{max}$ $[m^3/s^2]$
1/50	1	1	Surging	x	6.93	3.99	0.483918	167.31
	2	2	Surging	x	2.69	6.63	1.290633	332.95
	3	1.2	Surging	x	2.41	5.75	1.182564	254.23
	4	1	Surging	x	9.26	4.99	0.523553	320.4
	5	2	Surging	x	3.64	7.51	1.256767	317.17
1/75	6	1	Surging	x	5.35	3.92	0.5411	102.61
	7	2	Breaking front	60	2.64	6.52	1.281183	142.12
	8	1	Breaking front	34	0.73	6.51	2.43268	257.15
	9	1.5	Breaking front	61	3.49	7.97	1.362107	387.1
	10	1.333333	Breaking front	58	4.03	7.46	1.186456	332.05
	11	2	Breaking front	85	4.66	9.17	1.356257	490.87
	12	2.666667	Breaking front	88	4.78	8.4	1.226679	654.05
	13	3	Breaking front	105	4.23	9.02	1.400238	675.55
	14	6	Breaking front	125	5.41	9.99	1.3713	678.19
	15	2	Breaking front	75	3.79	8.43	1.382527	488.05
	16	2	Breaking front	80	4.42	7.96	1.208836	613.51
	17	1.666667	Breaking front	68	3.6	8.16	1.373107	405.97
	18	2	Breaking front	80-85	3.8	8.4	1.375793	475.91
	19	2	Surging	x	5.55	5.71	0.773847	344.09
	20	2	Surging	x	0.76	2.14	0.783741	178.91
	21	1	Breaking front	74	1.2	8.75	2.550251	491.56
	22	2	Breaking front	150	5.12	10.17	1.434999	961.45
1/100	23	2	Breaking front	14.5	8.56	5.28	0.57619	240.85
	24	1	Breaking front	170	1.11	11.19	3.391049	399.74
	25	2	Breaking front	280	4.63	10.53	1.56244	870.94
	26	1	Breaking front	290	2.2	12.17	2.619659	789.69

F

Extra Tsunami Theory Details

Some of the used equations in the report are given here in more detail. Or some extra theory is given that is not directly related to the research objective but gives more insight in the background of the topic.

F.1. Green's law

According to the linear wave theory, for small wave amplitudes (H/d«1), the wave energy per wavelength per unit crest length is:

$$E = \frac{1}{8}\rho g H^2 L \tag{F.1}$$

If energy conservation yields:

$$E_1 = E_2 \rightarrow (\frac{1}{8}\rho g H^2 L)_1 = (\frac{1}{8}\rho g H^2 L)_2 \rightarrow \frac{H_1}{H_2} = \sqrt{\frac{L_1}{L_2}}$$

In the linear wave theory, dispersion effects are neglected for shallow water waves like a tsunami and therefore the wave period T stays constant. The wavelength is $L = cT$, so the wavelength only depends on the water depth since $c = \sqrt{gd}$. The change in wave height becomes:

$$\frac{H_1}{H_2} = (\frac{d_1}{d_2})^{\frac{1}{4}} \tag{F.2}$$

F.2. N-waves

By analysing tsunamis in the past, a large drawback of water can be observed preceding the massive tsunami crest arrives. These tsunami waves can not be described by a solitary wave since they have a component below mean sea level. Tadepalli and Synolakis (1994) proposed the idea to replace the solitary wave input with a N-wave, which is a mathematically manipulated solitary wave (equation F.3) to make it look like a tsunami wave. The N-wave could be either a leading depression N-wave (LDN) or a leading elevation N-wave (LEN). N-waves are more likely to be generated close to the shore because the critical distance of propagation is not long enough to generate a wave with a leading crest like a solitary wave. They observed that LDN waves run-up higher than LEN waves, suggesting that solitary wave modelling is not able to predict the right run-up values for nearshore generated tsunamis.

$$\eta(x,0) = \alpha H(x-x_2)sech^2(K_s(x-x_1)); \qquad K_s = \frac{1}{h}\sqrt{\frac{3}{4}\frac{H}{h}} \tag{F.3}$$

where $\alpha < 0$ is a scaling parameter to ensure the N-crest represents the wave height H.

F.3. Run-up and Inundation

Tsunami waves can have dramatically run-up height, commonly greater than two times the height of the tsunami approaching the shore (Bryant, 2014). The highest run-up was measured at Aneyoshi Bay south of Miyako City (Mori and Takahashi, 2012). The approximated run-up height for a solitary wave (Synolakis, 1987) and the N-wave (Tadepalli and Synolakis, 1994) is given by equation F.4.

$$\begin{aligned} Solitary\ wave: \quad & H_{rmax} = 2.83(cot\beta)^{0.5} H_t^{1.25} \\ N-wave: \quad & H_{rmax} = 3.86(cot\beta)^{0.5} H_t^{1.25} \end{aligned} \tag{F.4}$$

where H_{rmax} is the maximum run-up height of a tsunami above sea level and H_t the wave height at shore or the toe of a beach in meters. β is the slope of the seabed in degrees.

Experimental studies in the past showed that the run-up height depends on whether breaking waves or non-breaking waves run-up the coast. For breaking waves, the run-up height for a given wave condition increases with bed slope. For non-breaking waves the analytical solutions suggest the opposite dependency (Shimozono et al., 2012).

F.4. Inland penetration and velocity

The volume of water under the tsunami wave crest near the coastline equals the volume of the inundation area by a rule of thumb. The longer the wave period (L), the greater the volume of flooding is. The maximum run-up distance (x_{max}) depends on the wave height at the coastline (H_{FL}), the friction Manning's coefficient n, a constant k (0.06) and the slope of the land surface (α) (Pignatelli et al., 2009):

$$x_{max} = H_{FL}^{1.33} n^{-2} k cos\alpha \tag{F.5}$$

Through preliminary tests, the typical Manning's n is 0.02 for the seafloor and 0.05 for dense populated areas (Shimozono et al., 2014).

The tsunami velocity (c) in the deep sea is given by equation 2.4 and is only a function of the water depth. During tsunami run-up the velocity equates with water depth:

$$v_r = 2\sqrt{gH_t}; \qquad H_t = d \tag{F.6}$$

where v_r is the velocity of run-up (m/s) and d is the depth of water flow over land (m) (Bryant, 2014).

F.5. Resonance and Mach-Stem waves

The ria coast consists of several bays. Tsunamis have a period of 10 minutes to an hour, which can match with the natural resonance of a bay or harbour. When resonance occurs, the tsunami wave height can be amplified significantly. Resonance can be the cause of a more destructive tsunami at the coast of Japan.

The part of the wave near the cliff continues to grow in amplitude. This is called a Match-Stem wave and it can increase ocean swell by a factor four. This can also have a large effect on the inundation and run-up height of a tsunami wave in ria coastal areas. Resonance and Mach-Stem waves are beyond the scope of this research.

G

Extra figures

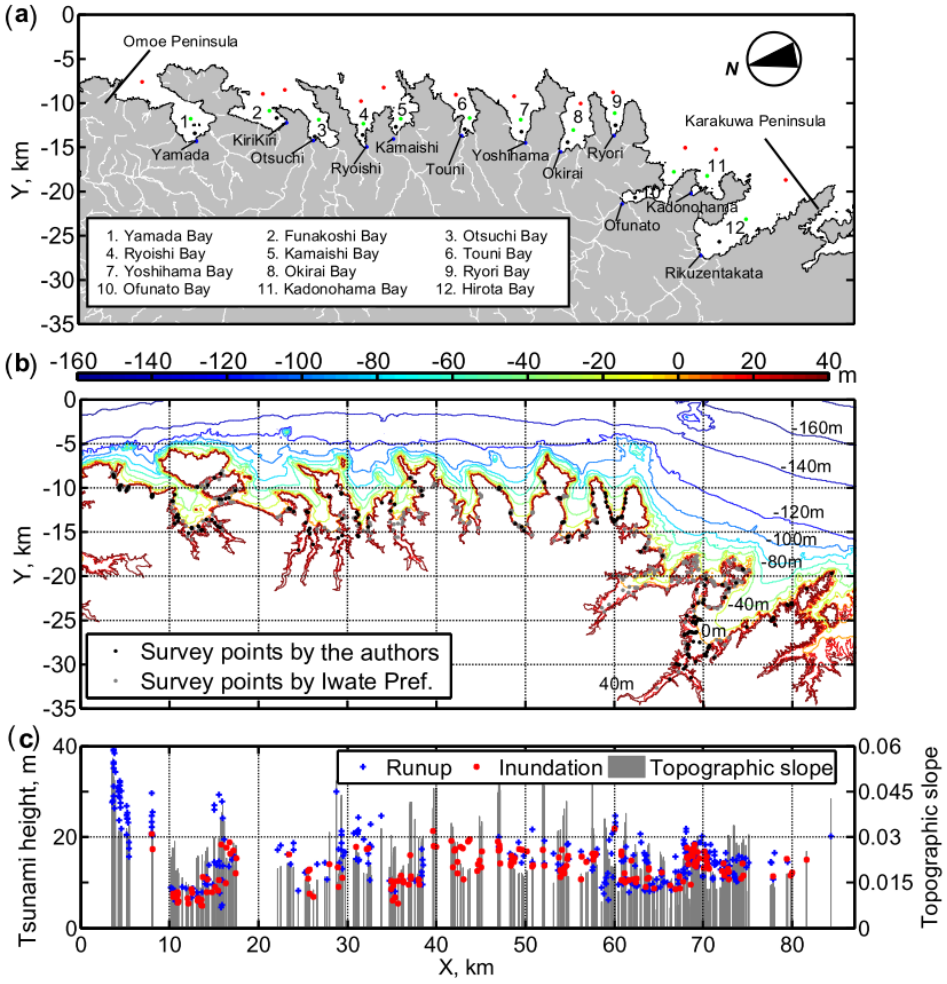

Figure G.1: (a) Map of the study area along the central Sanriku coast. (b) Topography and bathymetry of the study area. (c) Distribution of the measured tsunami heights and topographic slopes along the x-axis. (Shimozono et al., 2012)